BRAIN TUMOR GLIOMA ANALYSIS THROUGH COMPUTATIONAL INTELLIGENCE

Thesis submitted to Alliance University

for the Award of

DOCTOR OF PHILOSOPHY

by

MRS.DISHA SUSHANT WANKHEDE

Registration No.: 19030145CSE001

DEPARTMENT OF COMPUTER SCIENCE AND ENGINEERING

ALLIANCE COLLEGE OF ENGINEERING AND DESIGN

ALLIANCE UNIVERSITY

2024

BRAIN TUMOR GLIOMA ANALYSIS THROUGH COMPUTATIONAL INTELLIGENCE

Thesis submitted to Alliance University

for the Award of

DOCTOR OF PHILOSOPHY

by

MRS.DISHA SUSHANT WANKHEDE

Registration No.: 19030145CSE001

DEPARTMENT OF COMPUTER SCIENCE AND ENGINEERING

ALLIANCE COLLEGE OF ENGINEERING AND DESIGN

ALLIANCE UNIVERSITY

2024

DECLARATION

I declare that the thesis entitled Brain tumor glioma analysis through computational intelligence has been prepared by me under the guidance of Dr. Chetan J. Shelke Professor, Dept. of Computer Science and Engineering, Alliance college of engineering, Alliance University Campus, Anekal, Karnataka. No part of this thesis has formed the basis for the award of any degree in any University or fellowship previously.
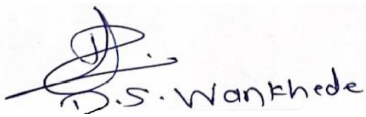
MRS. DISHA SUSHANT WANKHEDE

Registration No.: 19030145CSE001

Department of Computer Science and Engineering

Alliance College of engineering, Alliance University Chikkahagade Cross,

Chandapura-Anekal Main Road, Anekal,

Bangalore, Karnataka - 562106

D.S. Wankhede

_____
Signature

DATE: 31/7/2024

CERTIFICATE

I certify that **MRS.DISHA SUSHANT WANKHEDE** has prepared her thesis entitled **BRAIN TUMOR GLIOMA ANALYSIS THROUGH COMPUTATIONAL INTELLIGENCE,** for the award of PhD degree of Alliance University, under my guidance. She has carried out the work at Alliance College of engineering, Alliance University.

Dr. Chetan J. Shelke

Associate Professor

Department of Computer Science and Engineering

Alliance College of Engineering, Alliance University

Chikkahagade Cross, Chandapura-Anekal Main Road,

Anekal, Bangalore, Karnataka - 562106

_____

Signature

DATE:

DEDICATION

My Parents, Spouse, Friends, Relatives, Well-wishers, Mentors

and My Dear Lovely Daughter Anvita

ACKNOWLEDGEMENT

LIST OF TABLES

LIST OF FIGURES

LIST OF ABBREVIATION

WHO - World Health Organization

GBM - Glioblastoma

MRI - Magnetic Resonance Imaging

ML - Machine Learning

DL - Deep learning

CNN - Convolutional Neural Network

CE - Contrast-Enhanced

GM - Gray-Matter

FLAIR - Fluid-attenuated inversion recovery

GBMs - Glioblastoma Multiformes

IQ - Intelligence Quotient

CSF - Cerebro Spinal Fluid

GRE - Gradient Echo

TE - Echo Time

TR - Repeating Time

HOG - Histogram of Oriented Gradient

PCA - Principal Component Analysis

BraTS - Brain Tumor Segmentation

GLCM - Gray-Level Co-Occurrence Matrix

SVM - Support Vector Machine

TPMSVM - Twins Parameterized Support Vector Machine

CMI - Confocal Microwave Imaging

SOM - Self-Organizing Map

GWO - Grey Wolf Optimization

RPN - Regions Proposal Network

MSDnet - Multi-Scale Dense Network

PSNR - Peak signal-to-noise ratio

MSE - Mean Squared Error

MLP - Multi-Layer Perceptron

VEGF - Vascular Endothelial Growth Factor

ROC - Receiver Operating Characteristic

MR - Miss Rate

TPR - True Positive Rate

FPR - False Positive Rate

SUV - Standardised Up take Value

TABLE OF CONTENTS

ABSTRACT

The field of image processing offers distinctive features and is useful in medical diagnostics and imaging system. For the radiologists, manually identifying and classifying the Tumor has become a demanding and frantic process. Brain Magnetic resonance (MR) images must be extracted from malignant Tumor areas, which is a laborious and time-consuming task carried out by radiology experts or healthcare professionals. Current studies now heavily rely on medical imaging mainly to the continuous progress in automated brain Tumor classification and segmentation. This aids in quick decision as well as clear vision, diagnosis, and easier medication progression for the professionals. A dynamically Deep Learning technique for Glioblastoma brain cancer survival prediction rate was put out to address the aforementioned problems.

In this research thesis, we present two approaches for detecting the brain tumor, risk prediction and measure the survival rate of patient. In the first approach, we developed the computer-aided tumor diagnosis techniques based on CNN that have demonstrated to be effective and have contributed considerable strides in computer vision. The deep learning method for predicting the prognosis of glioma brain tumors is covered in this research. Glioma prediction has been determined using MRI brain tumor imaging. Data pre-processing is the initial phase. The MRI brain images were improved by intensities normalization using histogram normalization, de-noising via bilateral filtering, and the removal of information contaminants. Probabilistic noise salted and peppers distortion was also taken out. Secondly, radiomic features segmentation was completed using the MFCM clustering approach. Then, Rough Set Theory-based Grey Wolf Optimization was used to choose the most important and instructive aspects from the obtained characteristics. Then, using FR-

CNN, the overall survival predictions categorization is performed to the important feature selection in MRI brain images. The proposed MFCM-RSGWO-FRCNN approach is tested against state-of-arts FCM, OTSUS, NB, and SVM approaches. Evaluation parameters like Specificity, Sensitivity, PSNR, Mean Square Error (MSE), Segmentation Time, and Prediction Accuracy were used to examine the technique. The proposed MFCM-RSGWO-FRCNN has the advantages of less converging and the corresponding characteristics.

In the second approach, machine learning technique of the Random Forest model and Deep Neural Network method is proposed to predict the glioblastoma recurrence risk. Initially, Resampling and Z-Score Normalization are the image pre-processing techniques that are used to remove the outlier in MRI brain image data. After the pre-processing brain images are then segmented using the Recurrent Neural Network-Generative Adversarial Network (RNN-GAN), which mitigates the impact of imbalanced pixel labels. Subsequently, the Wavelet Band-Pass Filtering technique is presented to extract the texture features and the CE-T1WI model predicts PFS and ORR in recurrent GBM patients treated with the combination of Nivolumab and Bevacizumab. Accordingly, Random Forest and DNN techniques are proposed for patients' recurrence risk prediction.

After analyzing both models, the second RNN+GAN Model gives a better result as compared to the first MFCM RSGWO-FRCNN Model. The RNN+GAN Model achieves a 95.11% accuracy score; Sensitivity is also 95.11% and Specificity is 98%. The RNN+GAN Model increase the survival rate which is 2.47% after diagnosis and overall treatment of patients. And finally, RNN+GAN Model is compared with existing state-of-art methods.

CHAPTER 1
INTRODUCTION

1.1 Overview

A brain tumor is caused by the formation of aberrant tissue in the brain. It plays a significant role in the rising death rate among adults and adolescents. According to the tumor's aggressiveness and rate of growth. A primary tumor starts inside or outside the brain, whereas a secondary tumor develops when the malignant cells of the original tumor spread to body suggested by Gaur L. et al., (2020). According to WHO, brain tumors are divided into normal (less harmful) and malignancy (dangerous) categories based on the source and behavior of cells (dangerous). Glioblastoma (GBM) is a prevalent and dangerous type of brain tumor. The expectancy for GBM is typically terrible, and final treatments that include maximal surgical removal, radiotherapy, and chemotherapeutic mentioned by Martinez E. et al., (2020). Diagnosis and treatment of Glioblastoma recurrence were inevitable even though both therapies are unable to eradicate this fatal malignancy. The brain MRI is utilized in the identification, prognosis assessment, and medication or even other medication decisions of people with GBM as a quasi-radiological image processing approach. Structural, operational, and physiological data are extracted using MRI. As a powerful diagnostic image processing technique, MRI uses this data to produce real-time multidimensional images of GBM. Brain tumors in MRI are almost the definitive arm, guiding many therapy decisions, other surgical management, and survival rate estimates as discussed by Ke, Qiao. et al., (2019).

Basic predictive methods for brain tumor survival assessment were well at the collective scale, but improved survival prediction remained a difficulty, probably due

to the well-documented biological variability of the illness and treatments. Various survival investigations have employed the Cox proportional hazards (Cox PH) approach mentioned by Baek, E.T. et al., (2021), a common survival method in statistics, to find significant medical variables for the building, which visually depicts a statistical method to forecast customized cancer prediction. Simple multiple regression approaches, on the other hand, are inadequate at detecting unique meaningful features in information, hence machine learning (ML) techniques were rapidly becoming investigated in brain tumor survival assessments Wu, Jiewei et al., (2020).

Deep learning has been utilized to find a pattern in massive amounts of complicated data that are within normal vision, and then utilize those patterns to produce data-driven forecasts. The advancement and utilization of deep learning for clinical image processing, particularly radiomics assessment for a brain tumor, has resulted from advancements in image research and computing research working together suggested by Giger ML. et al.,(2018). Radiomics, a constantly emerging subject, allows for a statistical examination of tumor characteristics on a macroscopic level. Radiomics is the process of extracting, analyzing, and interpreting massive collections of visible and semi-visible image data for the identification and categorization of malignancies at the tissue stage. High-Level glioma is still a deadly and severe cancer, but because of recent improvements in tumor genomes and the hopeful beginnings of targeted therapies, researchers may be able to profit even more from developments in ML approaches deployed to the brain tumor recognition system.

Another difficulty in clinical image analysis is that producing such datasets is time-consuming and the information is varied. This exposes an overfitting problem on the training dataset and is not beneficial as a serious issue for deep learning techniques explained by Erickson BJ.et al.,(2018). To interact with a small amount of data, such as those experienced in clinical image analysis, numerous strategies can be used, such as time series analysis mentioned by Han, Changhee, et al.(2022), data augmentation Kayalibay B. et al.,(2017)., histogram analysis mentioned by Xi YB, Guo F, Xu ZL.(2018) , Hemanth G. et al.,(2022).

BT can be assumed as a issue that determines if a particular region corresponds to the healthy tissue, glioblastoma, or edoema categories. Custom characteristics and classification approach such as Linear regression, Adaboost, RF, Knn, and decision tree suggested by Tian Q.,et al.,(2018). Deep learning in this subject has increased its popularity, particularly image segmentation. Several of the existing prominent CNNs for segmentation issues utilize a patch-wise method discussed by Bisdas S.et al.(2018). , in which smaller patches of the images around each pixel are evaluated and a cascade of progressively complicated and generalized aspects of nonlinear characterizations of the information is extracted as mentioned by Avşar, Ercan, and Kerem Salçin. (2019). Moreover, CNN models are utilized to separate the tumor and sub-regions to obtain information such as size, local binary patterns, and geometrical data.   Then, for average survival prediction rate discussed by Hang Chen (2019).   are suggested with maximum resolutions of residual convolutional networks based on fully connected, connected neural model on 4 predetermined characteristics.

A range of radionics features is beneficial for grade had mentioned by Bakas S. et al.,(2018), genotyping categorization done by Rathore S. et al.(2018), and result from forecasting was discussed by Beig N. et al.,(2018) in the setting of glioblastoma. Rathore found a subgroup of eleven radionics peritumoral variables from pretreatment MRI to be diagnostic of total survival in individuals with glioblastoma, involving severity, variability, and texture characteristics. Deep learning has been used in several current attempts to investigate deeper and high-order characteristics that might enhance the predicted effectiveness of existing radiomics algorithms for brain tumors was mentioned by Rathore, S. et al.,(2018).

Regarding survival rate prognosis and molecular features categorization, DL based radionics approaches for brain cancers were suggested Liu, L. et al.,(2019). Nie used MRI to construct a CNN-based radiomics system to predict survival rates in glioblastoma patients. The constructed approach can predict the average survival rate better than conventional approaches after selecting six deep characteristics from pertained CNN explained by Sun, L., Zhang, S., & Luo, L. (2018). It's vital to remember that such approaches have drawbacks, and considerable obstacles remain.

1.2 Brain Tumour

The human nervous system is made up of this sensitive, vascular tissue. A finely structured system of nerves carries signals to the human brain. The nervous system is in charge of most of its organs. Currently, theories as to whether gliomas develop are constantly being discussed. Cells typically develop, die, and are restored. Occasionally, though, this regular process is flawed, and human cells continue to develop even if no additional cells are required. Healthy cells eventually pass away

due to aging or injury, whereas cancer cells don't. As a result, continue to develop rapidly.

Basic brain cancer may be malignant (cancerous) or benign (Normal). A malignant tumor is harmful because it develops spontaneously and swiftly moves to the various organs and nervous systems of the human body. It is simple to remove benign brain cancer from the body since they are well-defined and don't penetrate the normal tissue severely. Usually, cancers receive a grading (Grade I to IV). The grading given is a representation of how the tissues look under a microscope. Normally benign grade-I cells have a modest pace of development and resemble healthy brain neurons in appearance. Grading II denotes cancerous cells; however, the form is much less resemblance to healthy brain cells. In Grade III, the cells diverge from normal cells in appearance, which is a sign of malignancies. Grade IV denotes extremely abnormal-looking and aggressively growing cancerous body cells.

1.2.1 Brain Tumour Types

As per the World Health Organization, there seem to be 125 predicted tumor variants. Depending on the tumor's severity in the brain cortex, suprasellar area, posterior fossa, and ventricle systems, are categorized. Cancer develops from glial cells like a flame and is derived from neural cells via their support. The area in which cancer develops determines the name given to it. As an example, since they develop inside the anterior-posterior, pituitary cancers are also known as cerebral adenomas. Meningiomas are cancers that develop from the tissue area which surrounds the brain and is known as the central nervous system. Benign growths are cancers that develop from the nerves that pass through the membrane. Acoustics neuromas are tumors that develop on the nerves that regulate hearing. Most cancers were categorized mainly as:

5

- Benign (Normal)

- Malignant (Dangerous)

The cells in a normal brain's cancer are not malignant. These cancers were removed with surgical, radiation, or chemotherapeutic, and never develop back as mentioned by Saba, T., Khan, M. S., Mehmood, Z., Tariq, U., & Ayesha, N. (2021). A cancerous lump might, therefore, obstruct the brain's abundant blood circulatory system. In almost any case, benign cancers that continue to have this impact on the brain's critical regions will indeed be exceedingly harmful to the person's condition. A benign cancer diagnosis seldom develops into a cancerous one.

Significant changes in proliferative tissue divisions occur in malignant brain cancers discussed by Karayegen, G., & Aksahin, M. F. (2021). The tissue area, which is made up of a thick shell of enzymes and fats, creates serious cancerous cells. Malignant brain cancers spread typically in the lungs, kidneys, or testicles part of the human body suggested by Sahaai, M.B. and Jothilakshmi, G.R. (2021). Thereafter, aberrant cells enter the cerebral layers via the neural nerve and extract cellular components, which has an impact on the internal functioning of the brain and the nerve structure. As per the tumor's thickness, form, and position, the cells that make up the cancer are dispersed throughout the human brain. The WHO states that a tumor's volume and structure can be utilized to determine whether it is malignant or not. Figure 1.1 following depicts the locations of the various types of brain tumor's inside an adolescent.
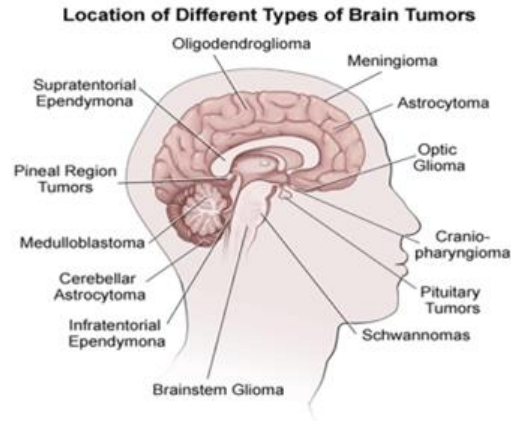
Figure. 1.1 Various Types of Brain Tumours Inside an Adolescent

Source: Health Library/ Brain Tumor,
https://demo.staywellhealthlibrary.com/Content/cancer-source-v1/types-of-brain-tumors/

In both adolescents and youngsters, oligodendrogliomas, meningiomas, and astrocytomas had discussed by Divya, S., Padmapriya, K. and Ezhumalai, P., (2021) Although gliomas typically develop in the cerebral hemispheres, they can also develop in the spinal cord, brain cells of the cerebellar, and nervous system. The source of the astrocyte cells determines the subtypes of glioblastoma. "Astro" in Greek is a star-shaped object. The meninges are the layer that acts as a guardian for the Central Nervous System (CNS) through this tissue, the tumor present in these meninges is called the Meningioma the brain that develops from the meninges was suggested by Pei, L., Vidyaratne, L., Rahman, M.M. and Iftekharuddin, K.M., (2020).

1.2.2 Radiologic Image Classification

Instead of using the tumors' pathology, four groups of brain cancers can be distinguished only by their radiologic appearances on contrast-enhanced T1-weighted imaging. The four categories are as described in the following: ring-enhanced tumors, full-boosted tumors with no edema, and full-boosted tumors with edema was discussed by Naser, M.A. and Deen, M.J., (2020).

1.2.2.1 Non-Enhanced tumors

During contrast-enhanced (CE) T1-weight imaging, these tumors look hypoechoic (darkened as Gray-Matter (GM)) and therefore do not absorb imaging techniques. T1-weight radiographs are displayed in Figure 1.2, as seen here. These were often full, either with or without edema. These show hyperintense in T2-weight imaging. The highest prevalent types of this tumor are oligodendrogliomas, gangliogliomas, and low-grade gliomas.

(a)   (b)   (c)
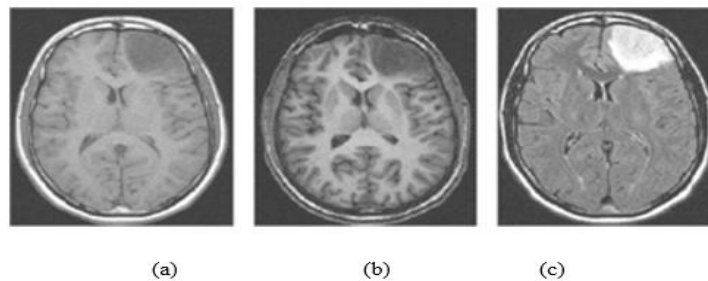
Figure 1.2: A tumor that is not increased. T1-weight axial slice (a). The identical T1-weight slice with contrast enhancement. b) The FLAIR image

Source: https://www.nimh.nih.gov/research/research-conducted-at-nimh/research-areas/clinics-and-labs/etpb/nnu/fellows-0

1.2.2.2 Fully-Enhanced tumors without edema

Almost most of the tumor's data points show hyperintense in contrast-enhanced T1 weight images, as illustrated in Figure 1.3, and cancers improved with contrasting medication in T1-weight images.
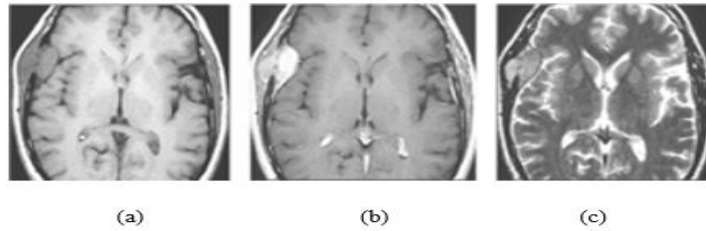
Figure 1.3: A completely developed tumour devoid of edema. a) T1-weighted image's axial slice. b) The identical T1-weighted image slice that has been increased with contrast. c) A T2-weighted picture

Source: http://www.neuroradiologycases.com/2012/09/ischemic-stroke-and-vascular.html

Such cancers don't have edema and look hyperintense on T2-weight and FLAIR imaging but hypointense on T1-weight brain images. Tumors in this category are Meningiomas (some types), lymphomas, ependymomas, pituitary adenomas, and craniopharyngiomas.

1.2.2.3 Fully-Enhanced tumours with edema

The edema as well as the core portions of such cancers are divided into two divisions. As shown in Figure 1.4, the edema appears the solid area that follows the contrast agent appears hyperintense in both T1-weight brain image and contrast-enhanced T1-weight brain image. In FLAIR and T2 -weight brain images, the tumor in both areas is seen as being hypoechoic. This group comprises benign growths of several forms as well as high-grade oligodendrogliomas, adenoma astrocytomas (highly-graded Primitive Neuroectodermal Tumours), and others.
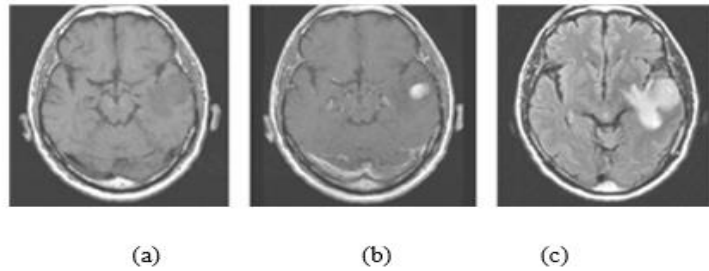
Figure 1.4: A tumour with edema and complete enhancement. a) An axial slice of the T1-weight brain image b) An identical slice of the T1-weight brain image enhanced by contrast. c) The FLAIR picture

Source: https://radiopaedia.org/cases/glioblastoma-nos-mimics-parafalcine-meningioma

1.2.2.4 Tumors with ring enhancement

Such tumors are divided into three parts. Both T1-weight brain images and contrast-enhanced T1-weight brain images show that the core region has necrotic and hypoechoic. The compact region, which covers the necrotic and absorbs the contrasting agent, T1-weight brain imaging and hyperintense in T1-weight imaging, as illustrated in Figure 1.5. Edema is the term for the third portion that encircles the core part. The edema shows hyperintense in both T1-weight and contrast-enhanced T1-weight brain imaging. The necrotic is brighter than its remaining parts in T1-weight brain imaging, whereas the solid region, edema, and necrotic were hypoechoic. In FLAIR imaging, the necrotic shows as just a hypoechoic sign, but the edema and solid portions show as just a hyperintense signal. Such features are shared by Glioblastoma Multiformes (GBMs) and highly-graded oligodendrogliomas.
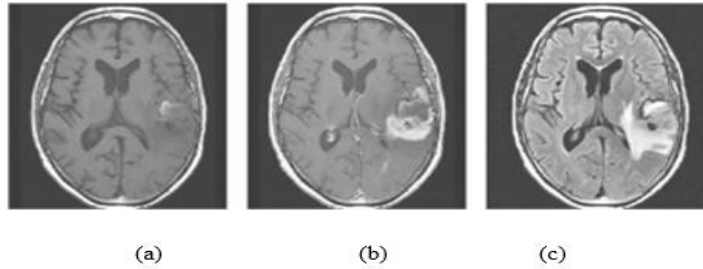
Figure 1.5 A tumor with ring enhancement. a) Axial brain imaging slice using T1-weight. b) The identical T1-weight brain imaging slice boosted by contrast. c) FLAIR cerebral imaging

Source: https://onlinelibrary.wiley.com/doi/epdf/10.1111/j.1750-3639.2007.00076_3.x

1.2.3 Symptoms of Brain Tumour

The primary and secondary indications of brain lesions change for the tumor location, size, and type tumor. When the brain tumor puts pressure on a nerve, chokes the blood supply path around the vicinity of the brain, resulting from the swell of the internal organ, in the region of the brain because of the accumulation of fluids is the onset of the symptoms of a brain tumor.

Hallucination, intense, headaches, frequent vomiting, speech disorder, blur vision, and hearing impairment are some of these symptoms. There is also the presence of mood swings or personality changes. There have also been reports of inability to concentrate, bad memory, numbness, or tickling in the arms or legs mentioned by Yogananda, C.G.B. et al.,(2020). The aforementioned symptoms of a brain tumor make it easy for the physician to predict the illness if the symptoms are clearly stated by the patient.

1.2.4 Diagnosis

Many CAD tests are undertaken to analyze the changes in the brain to aid in the diagnosis of tumors, some of which include CT scans, angiograms, MRIs, and biopsies. There are, however, other neurological examinations, such as hearing loss tests with an audiometer, muscle endurance, eye check-up, and intelligence Quotient (IQ) test. All these tests are done by the physician to properly understand the situation.

In MRI, a patient is tested with a large machine attached to a computer, which is equipped with a strong magnet. These machines act as CAD and frames of various slices of the human brain are produced in 3D which includes three axes such as axial, coronal, and sagittal view. These help in computing the internal voxel regions of the patient's head. The victim or tumor-affected patient is normally diagnosed using a contrast agent or special dye, which is intromitted into the blood vessels through injection. The computation results are based on the internal functional changes in the brain. This sophisticated analysis is skewed toward functional MRI (fMRI) and PET scan, to analyze abnormal tissues such as tumor or any other foreign objects in the human body mentioned by Tang, Z. et al.,(2020).

CT scan uses x-ray radiation for analyzing internal regions and does not have the potency or functionality of reconstructing images, but it takes a series of slices of the head which help in diagnosis.

A procedure called angiography involves injecting a tracer into the circulation, that causes the brain's blood arteries to appear on X-ray images. When a tumor is

developed, the X-ray might reveal the tumor or the blood arteries sustaining it explained by Xia, W. et al.,(2021).

1.2.5 Treatment

People with brain tumors undergo a sequence of surgery, involving radiotherapy-like laser radiation applied in the tumor incision area and chemotherapy applied with chemical drug agents to destroy the tumor cell regions. Often these treatments are administered simultaneously, which is dependent on the size, grading, and type of tumor.

Surgery is the usual treatment for a brain tumor. In this, the surgeon opens the skull and removes as much of the tumor tissues as possible. However, if the tumor is in the brain stem, surgery is not possible. In such cases, radiotherapy is the next suitable option. Radiation therapy usually happens after surgery. It destroys cancer cells through high-energy X-rays and lasers.

Chemotherapy involves the use of drugs or chemotherapeutic agents which functions as cytotoxic to destroy the cancer cells. These drugs are intromitted into the body through the mouth or vein. When the drug enters the bloodstream, it spreads throughout the body to kill tumor cells. These drugs can also be placed into the brain in the form of wafers. Usually, this is done for adults, in which the wafers are implanted into the brain. After a few weeks, the wafers dissolve and kill cancer cells.

1.3 MRI Imaging

Protons and neutrons make up the nuclei in the cells of the individual body. Because protons are positively charged but neutron is negative, the nucleus has positively

charged. A high-speed spin produces a vertical magnetic moment when a charged nucleus spins on its axis. This phenomenon is described by the law of electromagnetic induction. The nucleus could be separated into two categories: magnetic nucleus and non-magnetic nucleus, depending on the various spinning nature. The earlier designates the nucleus that can produce a magnetic moment due to its spin, whereas the latter designates neutrons that are unable to do so. A nucleus is classified as a magnetized nucleus if it contains protons or neutrons in an odd ratio else, it is classified as a non-magnetic nucleus. That is true when and just when an atomic nucleus has an equal amount of protons and neutrons. MRI can only be performed on the magnetic nucleus mentioned by Zaw, H., Maneerat, N., & Win, K. T. (2019).

However, in the existing image modality, mainly hydrogen nuclei only with single neutrons and single protons were primarily utilized. Theoretically, the magnetic nucleus among all components could be utilized for MRI scanning. The primary magnet, gradients technologies, RF mechanisms, computer devices, as well as other ancillary devices make up the majority of the five components that make up a traditional MRI scanning device as shown in Figure 1.6.
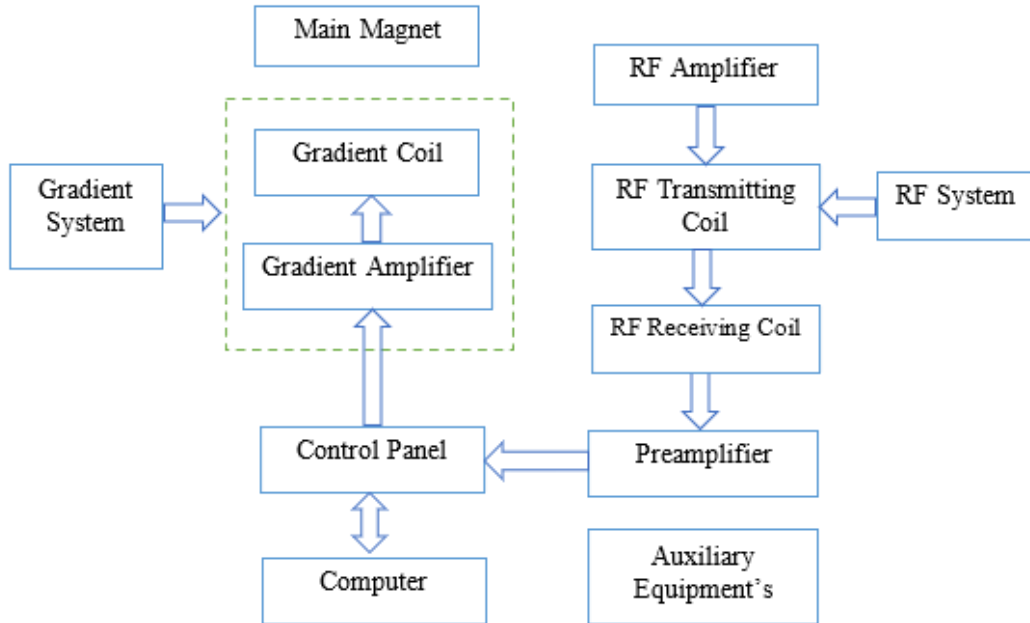
Figure 1.6: MRI Scanning system

The main magnet comes in two forms: An electromagnetic magnet (twined by coils) and a permanent magnet (made of permanent magnet material). The linear gradient magnetic field is generated by the gradient system. The MR echoing is produced by the regular switching of the area of the gradient and spatial orientations of the MRI signals. The radio frequency circuits that make up the majority of an RF device are employed to pick up the produced MRI echoes. The whole MRI scanning system's processing, involving pulse excitation, signal gathering, data processes, and imaging displaying, is managed by a computing device. This computing software could add extra advanced skills, such as data analysis, and three-dimensional simulation, as well as other things, with the help of certain multi-functional programs. The term "auxiliary system" mostly referred to the supporting technology which keeps the MRI scanning structure running normally.

The MRI imaging process is described below:

The human body generates magnetization phenomena when fed to a strong magnetic field. The amount of hydrogen nucleus in cells is a factor in the macro-magnetic properties of various organs. The macro-magnetic moment vectors would be entirely immersed in the major magnetic fields as the contents are more. Ever more powerful the transverse macro-magnetic energy generated, the greater the pulse signals discharged from the nucleus with transverse magnetic moments. Although both are pointing similarly, the magnitude of the macro-magnetic moment vectors remains significantly lower than those of the primary magnetic field. These are extremely faint when overlapped to be picked up by Radiofrequency coils. Therefore, it's not possible to differentiate between various cells based on the various macro vector values brought on by the various hydrogen nucleus concentrations.

The scanning device applies Radiofrequency impulses to the individual body in the primary magnetic fields in an attempt to differentiate various cells. The pulsed' power will be transferred to the hydrogen atoms when they are at a low-energy level, causing it to change to a higher level by soaking up the power. All these so computed tomography phenomena are just one. The incoming pulses cause the macro-magnetic energy vectors to deviate. The degree of deflection increases as Radiofrequency pulse frequency increases. The power of the nucleus is large and variable upon assimilation. The power would naturally be dissipated when the radiofrequency signal was stopped, and the hydrogen atoms will resume their previous stable level. An electromagnetic pulse would be released during the procedure of restoration and would be picked up by the Radiofrequency coils for brain image.

There seem to be two types of relaxation: transverse and longitudinal relaxation. These relaxation processes result from the disappearance of the RF pulses, while the macro-magnetic vector tries to rebuild. T1 and T2 describe the characteristics of the tissues. Different tissues with different characteristics would have corresponding T1 and T2 mentioned by Fu, J. et al., (2021). Figure 1.7 displays a schematic diagram of MRI equipment.

Figure 1.7 The MRI machinery and inspection's schematic view.

Source- https://medicalxpress.com/news/2017-12-fda-issues-tougher-mri-dye.html

Restricted water movement is used to detect an abnormality. Perfusion-weighted MRI is used to examine the vascularity of the tissue, permitting the detection of alteration in the blood volume or circulation. MRI imaging is completely non-invasive because there is no medication injected into the body and no medical instrument is inserted into the body. This makes the process completely safe.

Additionally, because of its high resolution, precise placement of soft cells, and sensitivity to illness features, MRI scanning is particularly well suited for the detection of brain abnormalities mentioned by Amin, J. et al.,(2020) – Jakola, A. et al.,(2020).

In radiation therapy and surgical scenarios, when acquiring MRI data, the physicians must accurately assess the patient's health by the pertinent image data and thoroughly plan for the illness treatments depending on relevant clinical data. In general, doctors can perform the subjective segment approach of brain images based on the acquired MRI imaging and the physician's expertise and skill to properly determine the volume, shape, position, structural dispersion, and other abnormalities of the tumor areas explained by Sharif M. et al.,(2020). Figure 1.8 displays the numerous MRI imaging forms, and Figure 1.9 displays the numerous weighted MRI brain image forms.
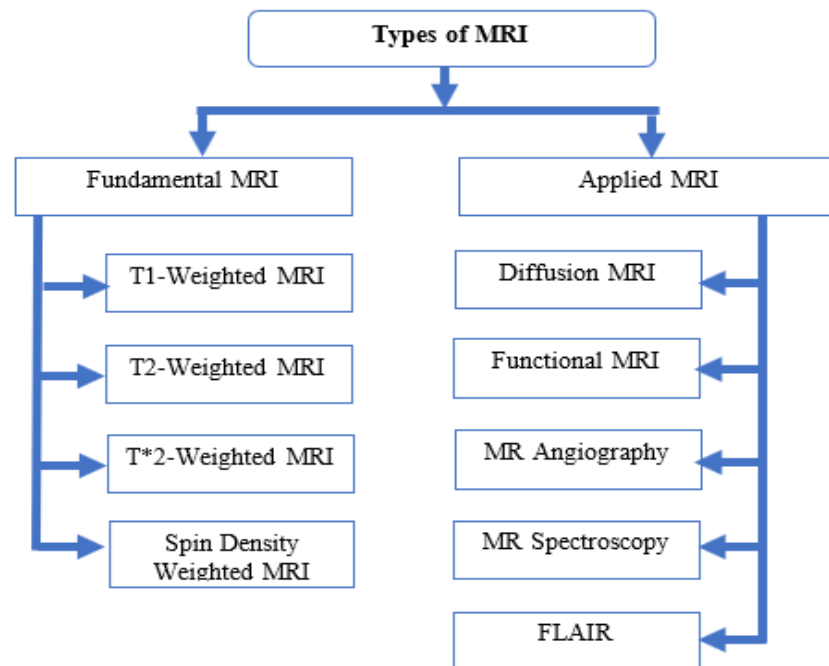
Figure 1.8: Magnetic Resonance Imaging Types

1.3.1 T1 Weighted Image

The directional relaxing duration is T1. That shows the amount of period needed for a substance to become magnetic upon already becoming exposed to a magnetic force or the amount of period needed to restore longitudinal magnetization following the application of a Radiofrequency pulsed. The resonant protons' thermodynamic reactions with the other charged particles, and the magnetic nucleus in the magnetic field, define T1.

All the molecules move naturally because of rotation, vibration, and translation. Smaller molecules move faster and larger molecules move slowly. The primary magnetic field of the MRI scanner affects the molecule movement frequencies and resonant frequencies, which are both represented by the T1 relaxing period.

1.3.2   T2 Weighted MRI

The longitudinal relaxation period (T2) measures the duration of longitudinal magnetism in an externally applied magnetic field that is entirely consistent. Magnetic interaction among rotating protons causes T2 release. T2 interactions just change phases, not power, which results in a lack of coherence.

The occurrence of static intrinsic forces within the material is necessary for T2 relaxation. Protons on large molecules were typically to blame for them. the protons are aligned together or against the primary magnetic force, such stationery or gradually changing magnetic energies produce local zones with enhanced or diminished magnetic fields.
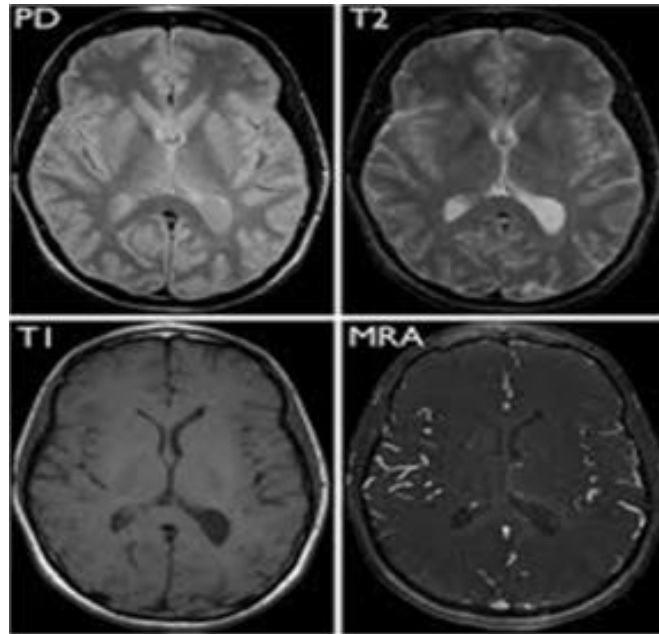
Figure 1.9 Different weighted MRI image

Source: https://radiopaedia.org/cases/neurofibromatosis-type-1-with-optic-pathway-glioma-1

1.3.3 T2* Weighted MRI

Gradient Echo (GRE) sequencing is very susceptible to T2* decline in T2* dependent cinematography, which is achieved by appropriately adjusting user-selectable variables including echo time (TE), flipping angle, and repeating time (TR). The lesions, structure, and regions of de-phasing were visible as dark places on such T2* weight sequences, allowing for its identification or characterization.

1.3.4 Spin Density Weighted MRI

In MRI images, brain tissues are categorized into normal and abnormal tissues. Normal tissue includes GM, WM, and CSF. The abnormal tissues usually contain tumors, and may also contain necrosis, cystic degeneration, and edema. Distinguishing normal and abnormal tissues is very difficult since they overlap with

each other. Table 1.1 displays the pattern of grey contrast on cells overlaid by tissues in various MRI brain images.

Table 1.1 *The Gray Dissemination of the Various Tissues*

	Gray	*White*	*CFS*	*Tumor*	*Edema*
T1 weighted	- +	- -	- - -	-	- -
T2 weighted	+ -	- -	+ + +	+	+ +
PD	+ -	- -	- -	+ +	-

The positive symbol in Table 1.1 suggests a high grey value, whereas the negative symbol indicates a low grey value. The dark areas correspond to the number of negative indications. The related area is brighter if there are additional positive indications present. The strength pattern in the tumor region is often unequal since that contains a range of aberrant cells. Additionally, this serves as one of the requirements for classifying the interior cells of the cancer area.

1.3.5 FLAIRE Images

The Flair sequential method has a much longer TE, and TR duration when compared to T2-weighted imaging. As a result, anomalies are kept visible, while the normal CSF liquid is reduced.
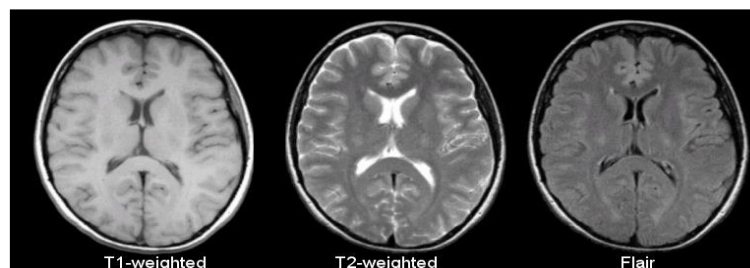
Figure 1.10: Assessment between T1, T2 and Flair brain images

Source:https://www.researchgate.net/publication/344539928_A_survey_on_Brain_Tumor

1.4 Image Preprocessing

The image preprocessing comprises various methods and techniques to geometrically correct the MRI brain image, and enhance the quality to make it easier for quantitative and qualitative interpretation. The noise and fluctuations are suppressed in the process. Some of the basic methods that take place during preprocessing include transformation, rotation, and filtration.

1.4.1 Noise Reduction Techniques

Based on the histogram's and probability density function's structure, the disturbance is categorized. Uneven noise, Poisson distortion, salt-and-pepper interference, gamma noise, and Rayleigh distributions are typical concepts of image distortion. The salts and speckle noise are a result of incorrect memory places, damaged camera sensors, and time issues during brain image digitization. Gamma distortion is a result of brain images' low pass filter. Filters can eliminate all of those disturbances. A modified brain image with improved edge recognition is created once the disturbance has been removed, and that aids in extracting the precise position of the cancer region.

1.4.2 Contrast Enhancement

Enhancing brain image contrast is crucial to image recognition, particularly for biological imaging systems. The basic objective of image contrast improvement is to raise quality to a level superior to it which the actual reference images. The image device quality, the user's lack of shooting experience, and the bad weather factors were to blame for the photographs' low resolution.

If these conditions were satisfied, the resulting photos will lack various elements and have low quality. The pictures could appear washed away. The above-mentioned issues are addressed through contrast improvement technologies, which also enhance an image's graphical fidelity.

Direct and indirect image improvement techniques are two categories. The direct approach of image improvement aims to achieve a contrast measurement that is expressly defined. By taking advantage of the dynamic range's underutilized areas while expressly establishing any metric, indirect approaches increase contrast. Among all these techniques, the technique based on histograms is widely used, because of its straightforward implementation abilities explained by Tandel G.et al., (2020)

1.5 Image Segmentation

The object of interest is found by the segmentation technique. It involves dividing the image into several regions or objects. The contours of an image are extracted using edge detection techniques. This procedure helps in locating the tumor, or abnormal tissue growth. A pre-process image enhances the image segmentation process. The segmentation process can be divided into two groupings: advanced and basic segmentation techniques. Advanced segmentation involves probabilistic methods, clustering, and model fitting. The basic segmentation technique involves morphological watershed, region growing, line and edge detection, point, thresholding, and region growing.

1.5.1 Threshold-based based Segmentation

The basic segmentation technique. It involves partitioning an image according to a predefined criterion into respective regions. They are global techniques, local techniques, and split, merge, and growing techniques. Local techniques involve using the neighbourhood of the pixels and local properties of an image. Global techniques involve segmenting an image based on the global information that is gleaned from the image. For effective segmentation, splitting, merging, and growth procedures make utilization of the ideas of homogeneous and geometrical approximation.

A threshold can be either local or global. A binary image can be generated by selecting the grey level image using an appropriate threshold 'T'. This is to make the process of recognition and classification easier, thereby reducing the complexity.

1.5.2 Region Expanding Technique

One of the basic techniques for area-based picture segmentation is area expansion. Since it chooses the first initial centroids, it can also be referred to as the pixel-based picture segmentation technique. The neighbouring pixel of the initial seed pixel is inspected to ascertain its inclusion in the region. This process is very identical to various clustering techniques.

The selection of a group of initial centroids is the first step in the region's growth. This decision may be made using properly spread pixels on the grids that fall within a particular grey level. The first region starts approximately where such seeds are now. According to the region membership conditions, which might be image pixel intensities, grey-level texture, or color, the region is expanded from such initial

centroids to nearby spots. The divide and combine method goes through the following stages:

- Specify homogeneity criteria. The image is divided into four equal-sized segments.

- Whether any resulting square is not evenly divided into quadrants, it is also classified into four categories.

- Combine the two or several surrounding areas that meet the requirement of uniformity at every stage.

- Continue splitting and merging the area until this is impossible to do so any longer.
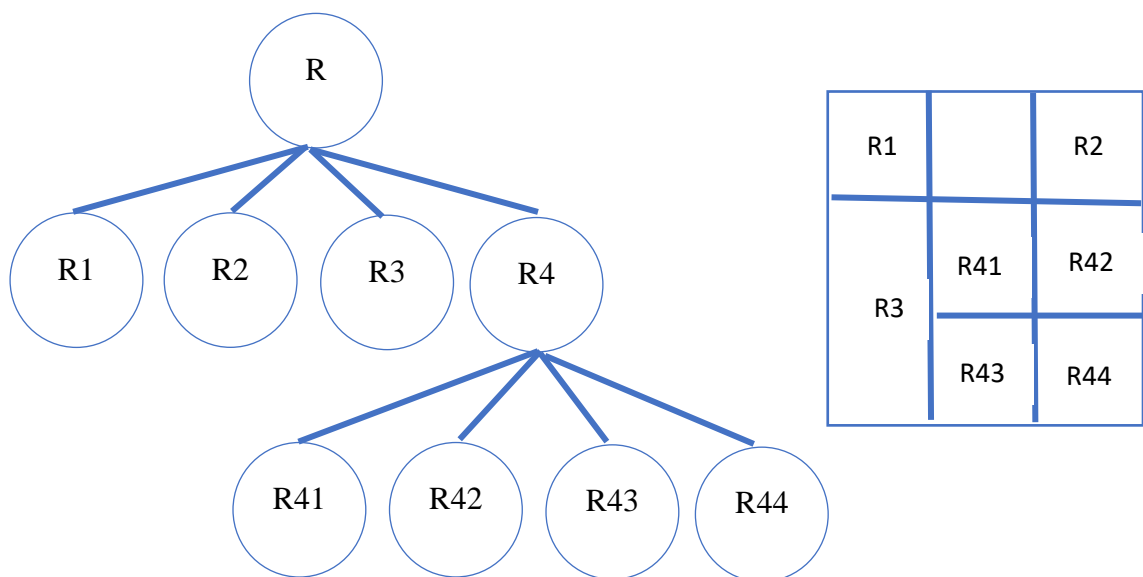
Figure 1.11: Quad-tree layout, (a) with R standing for the complete image area and (b) with the associated segmented image

Advantages:

The image could be split progressively according to the resolution demanded or wanted. The mean and variance of the segmented pixel value can be determined based on the criteria of the image. However, the splitting criteria can be different from the merging criteria.

Disadvantage

It may result in block image segmentation.

1.5.3 Watershed Segmentation

In image segmentation, the watershed is one of the powerful methods used. This method is popular for its speed, simplicity, and complete division of an image. The watershed algorithm is a precedent for grey-scale morphology. In the presence of weak boundaries and low contrasts, the algorithm still provides closed contours.

The "watershed basin" is the area wherever holes have been cut into the local bedrock while the environment is submerged under a reservoir. Reservoirs would be constructed, water will be topped off at such initial local minimum value, and the spots when water from several watersheds would converge. The procedure comes to an end whenever the water level approaches the highest point in the surrounding area. For an outcome, watershed boundaries are the divisions of the terrain among basins or areas that are divided from one another by reservoirs mentioned by Suter, Y.et al., (2020).

There are primarily two groups of watershed techniques focused on watershed transformations. Conventional approaches are found in the first category, which

includes flooding-based watershed techniques, and the second category, which includes rain-falling-based watershed techniques. Across both categories, numerous techniques have been suggested, however, the linked components-based watershed approach outperforms them all in terms of efficiency. This falls underneath the technique of the rain-falling-based watershed technique. It produces quite effective segmentation outcomes and satisfies the requirement for hardware implementations with minimal computational costs.

1.6 Feature Extraction Techniques

The technique of constructing representations or modifications from the source information is called feature extraction. These are techniques that are both machine- and human-centered. An appropriate numerical approximation is chosen for perception-based elements like texture using the human-centered method. To extract specific features, a unified computational technique is chosen in the machine-centered strategy explained by Wijethilake N.et al.,(2020).

1.6.1 Texture-Based Feature Extraction

A primary characteristic utilized in image analysis to describe the surface and organization of a given area is texturing. A collection of image pixels or an object made up of linked pixels is known as a texture. The "texture primitives" defines that collection of image pixels. Texturing is a numerical representation of the distribution of intensities in a space.

Therefore, there are two groups of texture characterization techniques. These are both structural and statistical. The statistical distributions of the pixel intensities

are used by statistical techniques to describe image texture. One of the characteristics that distinguish textures is the spatial arrangement of grey levels. Statistical techniques are used to analyze the spatial distribution of grey levels.

These are accomplished by calculating local features at every location of an image, and then deriving a collection of statistics from the distributions of feature points. By recognizing structural primitives and related positioning guidelines, structural techniques depict texture conveyed by Shree, N. V., & Kumar, T. K. S. (2018).

1.6.2 Histogram-Based Feature Extraction

The core idea of the Histogram of Oriented Gradient (HOG) descriptors would be a certain distribution of pixel intensity variations or information that can be used to characterize the appearances and structure of local elements inside images. A histogram of the gradient's orientations again for image pixels inside every cell could be built to incorporate these descriptors by breaking the images across small interconnected sections, known as pixels.

The descriptors are therefore represented by the sum of such histograms. Every pixel inside the image block is normalized, and the localized histograms could be contrast-normalized for increased precision.

Improved inversion to depict variations in luminance or shadows is produced by such a normalization technique. Among alternative descriptor techniques, the HOG descriptor still has a few significant benefits. The approach maintains normalization to geometric and photographic modifications, except for object direction, because the

HOG descriptor works on isolated pixels. Especially bigger spatial areas can experience such alterations. The HOG descriptor is therefore very well adapted for detecting humans in images.

1.6.3 Intensity-based Histogram Features

The histogram is a graphical representation that displays the total pixels in images at various degrees of its intensity. About approximately 256 different intensity ranges can be used for 8-bit, or 16-bit grayscale images. First-order statistical data describe the features of the intensities of the histogram. Four features are extracted from the histogram once it is displayed in the images. Through the use of intensity histogram graphs, the four features, homogeneity, third instant, and fractal dimension computed.

1.6.4 Second-Order Statistical Features

Whereas the Region of Interest distributions of gray-level is described by the first-order empirical features, those features never provide data on how the different grey-level are distributed spatially within the Region of Interest. These kinds of details can be gleaned from the run-length and co-occurrence matrices.

Features depending on histograms are regional in scope. Such attributes don't take into account spatial data. The combined conditional probability of image pixels paired pairings serves as the foundation for these properties. The combined probability distribution among pixels is calculated using the neighbourhood's issued distance and angles. Regarding calculations, d=1, 2 and θ = 0, 450, 900, and 1350 degrees are typically employed was confirmed by Sun, L., Zhang, S., & Luo, L. (2018b).

1.6.5 Feature Selection Algorithms

The strategies for feature selection are described in the following: according to the pre-designed selection criterion, the least crucial characteristics of the provided input information are chosen by the optimum procedures underneath the predefined condition, and the other aspects are deleted from the input to lower the quantity of information. Due to the unavoidable signal loss and discovered intervention during the device's obtaining, image processing environment, information transmission, and converting processes, even though the implemented categorization domains are distinct, the final acquired signal is intertwined with a huge amount of distortion and interference in the particular pattern identification and categorization issues. In contrast to the conventional de-noising methods, feature extraction and selection is a crucial pre-processing step that affects the image data significantly.

Feature selection helps in eliminating interference, less important data, and noise from the input. This gets rid of all the data that are not relevant to the classification at hand thereby reducing the input data and consequently the processing time.

To improve the classifier's accuracy through the removal of non-relevant data which may be replete with interference, thereby leaving only the needed data for training and classification, which improves the model and its capability to solve the problem. Higher accuracy is achieved as a result.

The operational efficiency is also improved. Since all redundant and unwanted data are removed, the computational time is reduced as well, because the complexity is reduced.

Given its significance in pattern recognition issues, the selection of features has been a contentious and challenging subject in image processing. The key problem to be resolved is how to choose the proper feature selection method, retrieve the crucial features from available data, and use experimentation to confirm the accuracy, consistency, application, durability, and computational complexity of the requirements. Figure 1.13 displays a typical feature selection architecture.
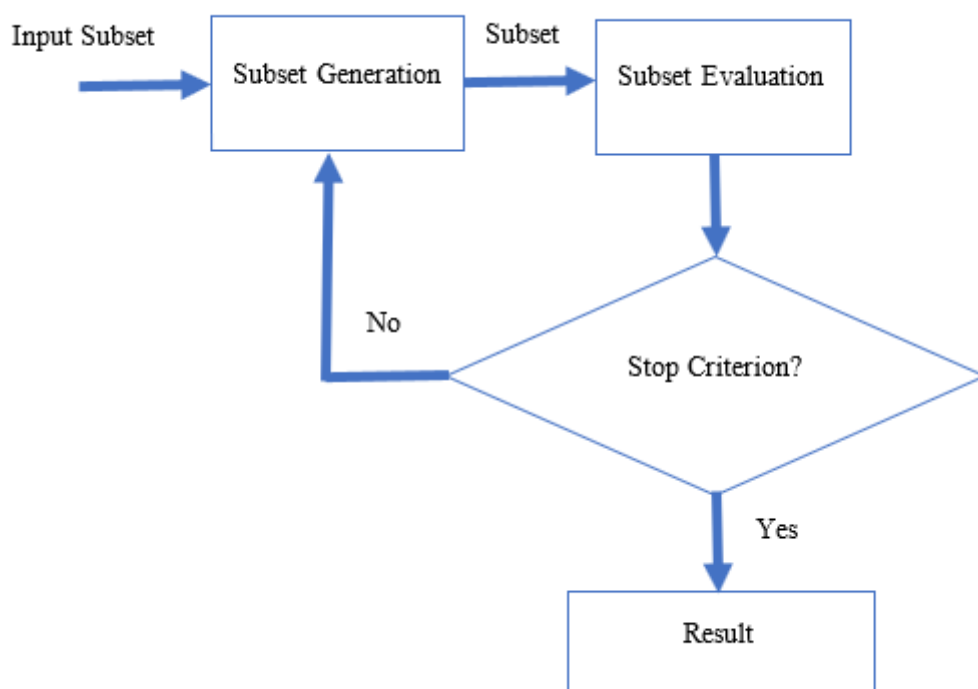
Figure.1.12: General Structure for feature selection

The following stages make up a basic features assessment procedure.

1. Subset formation: It is a procedure of selectively obtaining a set of features subset from the trained features vector matrix that has been created for the classifiers to evaluate or from a single features vector by specific conditions. The features subgroup

will be taken into account as the outcome of one level of the features extraction procedure to assess how well it performed.

2. Subset Assessment: The feature selection approach can be carried out in one of two ways: starting with an attribute subgroup that only includes one attribute and expanding it one at a time; or starting with a universal set that contains all the elements of the feature subgroup and contracting it by one at a time. Whatever method is employed for selecting features, it is necessary to assess the performance of the existing subset whenever it is changed throughout time. The pre-set condition must be used to finish the feature extraction assessment procedure.

3. Establishing the stopping condition: Every feature is a subset that must be evaluated and then its attributes must be checked against the stopping condition to see whether they meet a predetermined threshold. If that's so, feature extraction would immediately halt as well as the currently selected subgroup will be taken into consideration as the completed image. If not, this procedure will keep repeating itself till a features subgroup that satisfies the stopping requirement is found. According to the limitations of the feature-choosing requirements and the stopping conditions, the technique in this optimization problem occasionally fails to autonomously converge. Consequently, explicitly specifying the halting conditions could be necessary. This suggests therefore the effectiveness, accuracy, and precision of the feature selection operations will be strongly impacted by the feature-selecting criterion and the halting conditions.

The PCA is used as a traditional FS approach, the input datasets from the existing domain into the new space using the projections transform. Diagonalization

transformation of the raw data provides information on the projection direction. The energy of the data corresponds to the value of each new axis, for which the sum of all the energies should tally with the original data. The first n values, when the data is arranged in a descending order tally up to 95% of the total energy and the remaining can be removed.

The power proportion, that's always variable and ranges between 85% to 99%, could be explicitly changed. The higher Eigenvectors were maintained in the modified diagonal matrix, the little ones were eliminated, and the aggregate of the maintained Eigenvector achieves the percentage of the overall value, which is represented in the predicted value. The new space has only a few axes, even though there are a vast majority of energy reserves, and those axes correspond to the principal axis. To accomplish the goal of dimension reduction via projected transformations, PCA heavily relies on the concept of power concentrations.

The SVM classification decomposed, whose important component is obtaining the spatially projected transform, is frequently used to execute PCA. The eigenvalues of the matrix following the projections are represented by every row in the matrix.

1.7 Classification Algorithms

Investigators create procedures and automated systems considering sample data or prior knowledge, some learning methodologies attempt to optimize a performing objective in such a situation elaborated by Nogay H. S. et al., (2020). - Rosati, R. et al.,(2020). When training is being done under supervision, learning techniques are chosen depending on such instances (i.e., the training stage), which also comprises correct output. That type of learning activity is referred to as categorization whenever

the predicted values show the various classes to which the instances belong. These are commonly referred to as train data because the classifier's characteristics are derived from the sample dataset. The real classifiers and the classifying techniques vary significantly from one another validated by Parthasarathy, G. et al.,(2019).

1.8 Research Problem Statement

A deep convolutional layer efficiently extracts significant and reliable the features are evaluated across the entire MRI dataset. Additionally, overfitting problems occur from the classifications phase based on the entire MRI analysis in every direction, and features are not chosen depending on the precision of data obtained from the grouping. Due to the distributed nature of the training dataset in this situation, there is a significant decision-making latency. Deep learning algorithms do not optimize the usage of several levels in the training and classification procedure. Higher computing cost is the outcome of this. A predetermined conceptual framework is utilized to decide after limiting the segmentation to edge portions. Unfortunately, these procedures are laborious, time-consuming, and subject to human mistakes. Hence, the requirement for automated classification and mortality predictions occurs.

1.9 Motivation of Research

The third-highest percentage of brain tumor deaths worldwide has been reported from India. Glioblastoma Cancer is among the worst malignancies, with an average and maximum life expectancy of 15-to-16 months for individuals who obtain appropriate medication. An accurate assessment is essential for determining the condition and developing the best possible medication strategy. A Brain tumor can be quickly diagnosed with the aid of computer vision, which has been done in the past. The

learning cost and accuracy rate of traditional machine learning approaches are its limitations. This encourages the creation of novel computer vision algorithms for MRI tumor identification that are simpler and have better efficiency, as traditional machine learning approaches have limitations on training speed and identification precision. In the past few decades, dynamic prediction using a contemporary deep framework has generated a lot of innovative research issues and attracted a lot of research attention. Nevertheless, deep neural models need additional layers for training. This encourages the development of innovative CNN modelling for glioma tumor prediction based on adaptive networks.

1.10 Objectives of the Research

The major objective is further divided into sub-objectives as stated below:

- To develop DL models for supporting the diagnosis of radiologists and automated detection of glioblastoma brain tumor in MRI Images

- To identify feature extraction and feature selection techniques that support in identification of glioblastoma brain tumor.

- To predict the total survival rate of patients suffering from a glioblastoma brain tumor

1.11 Unique key Contribution of this Study

A hybrid deep learning model has been presented in our suggested research work to classify the glioblastoma brain tumor from MRI images. The suggested deep learning method for predicting the prognosis of glioma brain tumor. Glioma recognition was

determined using MRI brain tumor imaging. A dynamic Deep Learning technique for

Glioblastoma brain cancer survival prediction rate was put out to address the

aforementioned problems.
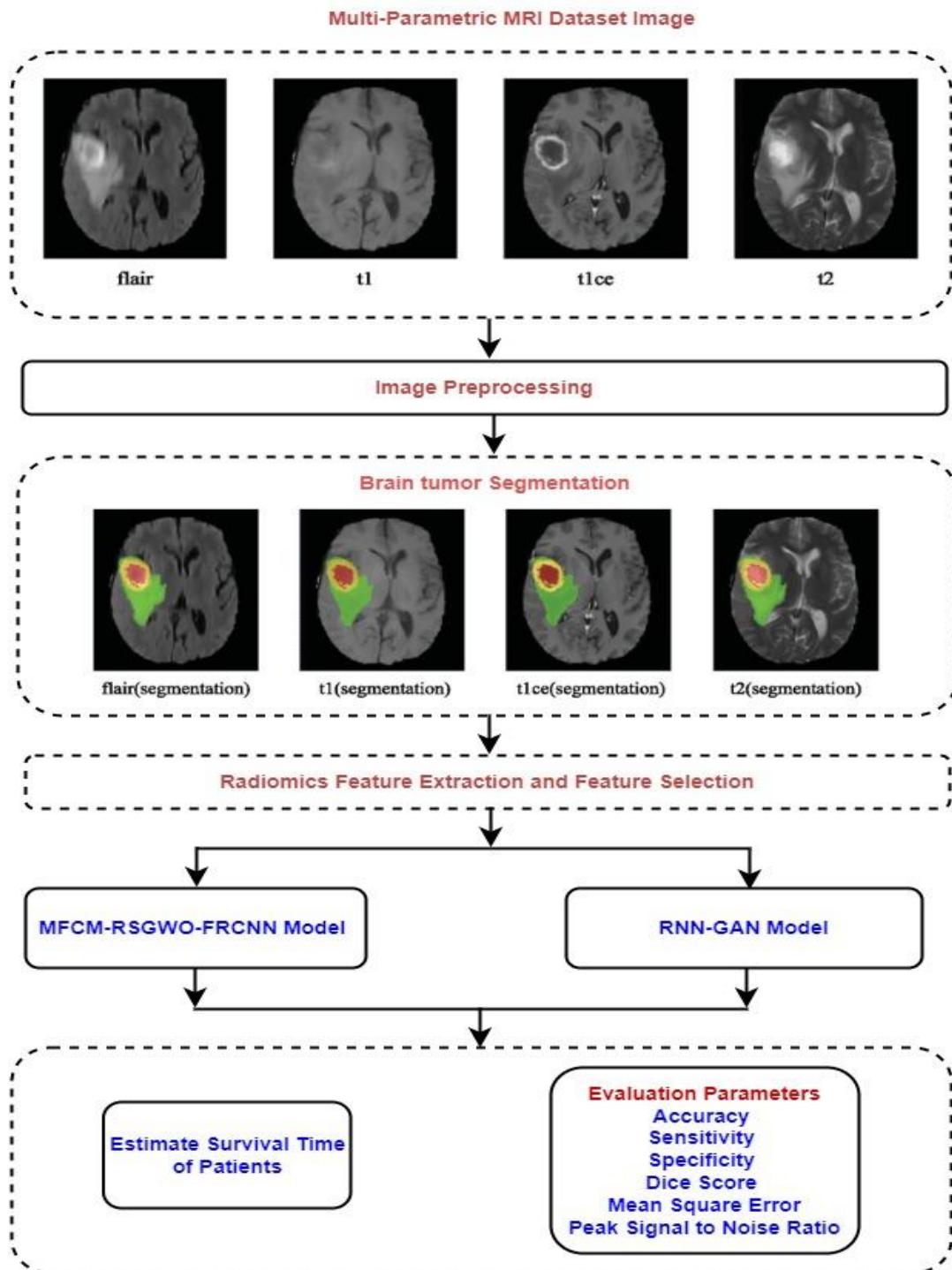
Figure 1.13: Complete Architecture of Proposed System.

Contribution 1:

In a summary, the contributions are as follows.

In this study, we have developed two deep learning models for predicting the glioblastoma brain tumor segmentation and classification from human brain MRI images, which will help to accurately diagnose and classify the MRI images. In the First model, a unique and dynamic network-based faster R-CNN modelling strategy was developed. The MFCM classification technique is then used for segmentation utilizing radiomic characteristic data. The categorization for overall survival rate estimation is then completed to features chosen in MRI brain images using a FR-CNN technique. As a result, the suggested classifier improves accuracy while requiring shorter training time and a faster-converging rate. In the second model, the Hybrid deep learning approach has been used in each step of the proposed model.

After observing the results of both models, found that the second model gives better results and the efficiency of the suggested approach is improved by 3%.

1.12 Dataset

```
                    ┌─────────────────────┐
                    │       Dataset        │
                    └──────────┬──────────┘
             ┌─────────────────┴─────────────────┐
    ┌────────────────────┐          ┌────────────────────┐
    │  Benchmark Data set │          │  Real Time Dataset  │
    │      ( Kaggle)      │          │                     │
    └────────────────────┘          └────────────────────┘
```
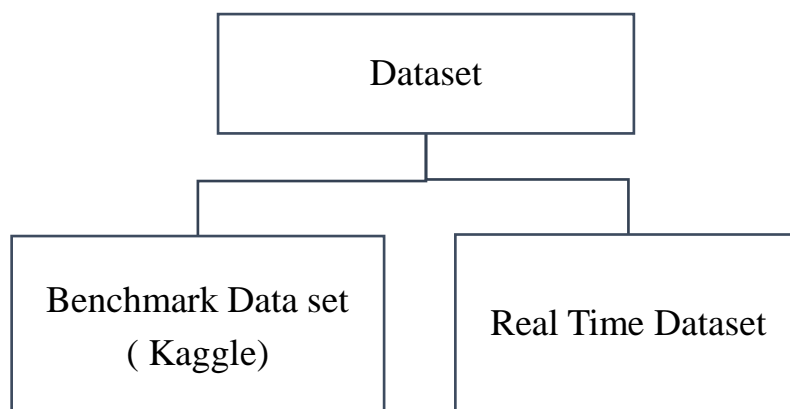
Benchmark Dataset

The standard benchmarking dataset aims to establish a common assessment criterion to assess the effectiveness and reliability of brain tumor identification and categorization. This dataset includes,

Table 1.2 *Details Regarding Benchmark Dataset*

	Controlled	**Patients with Tumor**
Adult Group	73	180

Real Time Dataset

Real Time Data Collected from Tata Memorial Hospital Hospital, Mumbai, Maharashtra (80 Patient Data Set Shared From TMC)

Table 1.3 *Details Regarding Real-time Dataset*

	Controlled	**Patients with Tumour**
Adult Group	528	1232

Table 1.4 Details of real time patient's dataset

Patients	**No of Images**	**Patients**	**No of Images**
Patient 1	22	Patient 41	20
Patient 2	20	Patient 42	20
Patient 3	22	Patient 43	20
Patient 4	20	Patient 44	20
Patient 5	20	Patient 45	22
Patient 6	20	Patient 46	20
Patient 7	20	Patient 47	20
Patient 8	20	Patient 48	20
Patient 9	20	Patient 49	22

Patient 10	22	Patient 50	20
Patient 11	20	Patient 51	20
Patient 12	20	Patient 52	20
Patient 13	24	Patient 53	20
Patient 14	20	Patient 54	20
Patient 15	23	Patient 55	20
Patient 16	20	Patient 56	24
Patient 17	22	Patient 57	22
Patient 18	20	Patient 58	20
Patient 19	20	Patient 59	20
Patient 20	20	Patient 60	20
Patient 21	20	Patient 61	20
Patient 22	20	Patient 62	20
Patient 23	20	Patient 63	20
Patient 24	22	Patient 64	20
Patient 25	20	Patient 65	20
Patient 26	20	Patient 66	20
Patient 27	20	Patient 67	22
Patient 28	20	Patient 68	20
Patient 29	22	Patient 69	22
Patient 30	20	Patient 70	20
Patient 31	20	Patient 71	20
Patient 32	22	Patient 72	22
Patient 33	20	Patient 73	20
Patient 34	20	Patient 74	20
Patient 35	22	Patient 75	22
Patient 36	20	Patient 76	20
Patient 37	20	Patient 77	22
Patient 38	22	Patient 78	22
Patient 39	20	Patient 79	20
Patient 40	20	Patient 80	22

MRI Scan

- T1-Weighted ,T2-Weighted ,FLAIR

- Kaggle Data Set (T1,FLAIR) (253 Case Data Available)

- Real-Time Data Collected from Tata Memorial Hospital Hospital, Mumbai, Maharashtra (80 Patient Data Set Shared From TMC)

Inclusion and Exclusion Criteria

- Previous research was considered when researchers created or approved a technique for MRI-based adult brain tumour segmentation or recognition.

- Inclusion Criteria- Pre-operative and Post-operative CE T1, FLAIR adult group images consider.

- Exclusion- Inadequate Image quality, subsection or biopsy result.

1.13 Permission Letter

Real-Time Data Collected from Tata Memorial Hospital, Mumbai, Maharashtra (80 Patient Data Set Shared From TMC)

Non-Disclosure Agreement - VL 183254

1.14 Layout of the Thesis

The thesis is divided into six chapters, each of which covers MRI scans utilized to forecast the glioblastoma subtype of brain tumors and the prediction of the survival of the patient. Details of each chapter are given below:

Chapter 1 – This Chapter provides a comprehensive overview of brain tumours and the various sorts of them. This chapter also covers the topic of exposing problems with state-of-the-art techniques, research goals, and the framework of the overall model that is suggested to address such problems. This chapter describes the rationale, the problem definition, and our contribution to the problem based on the existing circumstances.

Chapter 2 – The comprehensive literature review in this chapter is divided into three sections: segmentation, feature extraction, and brain tumour prediction. The section is wrapped up with a summary table. This chapter recalls and compares prior work's findings according to criteria of accuracy, sensitivity, specificity, and precision. The proper objectives of the current work and its ultimate conclusion are outlined in light of the literature.

Chapter 3 – This chapter discusses the history of MRI image processing. The first section of the chapter goes over the research on brain cancer characteristics and imaging-based methods for their identification. In order to emphasize the study being carried to provide a methodology for the automated diagnosis of a brain tumor, significant methodologies are then identified. Additionally, it provides a survey of the research on several image processing methods, including those for segmentation, relevant feature extraction, categorization, the immunological approach, and three-dimensional reconstructions.

Chapter 4 – This chapter describes the research on glioblastoma imaging techniques including its operational applications in section 4.1. The experimental result and

discussions are discussed in section 4.3, the proposed technique is detailed in section 4.2, and the research is concluded in section 4.4, respectively.

Chapter 5- In this chapter, conclusion and suggested methods for strengthening differences to bring the research to a close and summarize the contributions of the dissertation. There are also recommendations for further improvement.

CHAPTER 2
LITERATURE REVIEW

This chapter discusses the history of MRI image processing. The first section of the chapter goes over the research on brain cancer characteristics and imaging-based methods for their identification. To emphasize the study being done to provide a methodology for the automated detection, significant methodologies are then identified. Additionally, it provides a survey of the research on several image processing methods, including those for segmentation, relevant feature extraction, categorization, the immunological approach, and three-dimensional reconstructions.

2.1 Overview

The completed analysis was considered. The next sections provide a thorough review of earlier studies and projects that dealt with extracting the features, segmentation, and classifications using different techniques. MRI imaging can show specifics of various traits and offer a crucial foundation for the identification and treatment of sickness in individuals. Moreover, there are also a few limitations in the computer-based assessment of MRI healthcare images, including variations in images devices, images systems, and image variables between patients, duplication, interference, as well as other intervention parameters from image acquisition, the massive portion of image datasets from numerous sequence data to be interacted to, the homogeneous patient situations between many persons, the absence of previous awareness, and the complicated MRI system. Because of the invasiveness of glioblastoma, the internal and external parts of the tumor often contain various cells, and the tumor borders are often unclear.

The aforementioned limitations on the level of automation in MRI-based healthcare imaging systems make it nearly difficult to create an efficient and effective fully automated system efficient and effective fully automated systems. The problem is now at the centre of study as well as being a critical and challenging one in the worldwide, combined domains of healthcare and data. Many efforts are made to address this problem, and numerous novel or better techniques are used to provide it.

Currently, an effective approach is to create a semi-automatic system with mixing of human involvement. This can both increase the system levels of automation and minimize the amount of unnecessary engagement. The system can fully utilize the multi-modality brain MRI sequencing data and effectively tune the classifier to increase classifying performance and reliability by using additional methods (pre-or post-processing procedures).

2.2 Image Segmentation

The images are divided into several interconnected sections after the image segmentation. Segmentation aims to divide an image into various sections for additional processing before changing the representations of an image for easier evaluation. According to the problem, multiple image segmentation techniques are used. The various methods for image segmentation include edge, threshold, region, and cluster-based. Depending on distinct strategies, there are two categories of segmentation techniques. These are identifying differences and resemblances. In order to segment an image using sudden variations in brightness, discontinuity must be detected. It covers edge identification as an example of an image segmentation technique.

Conventional MRI imaging processing may operate directly on the pictures as a standard image analysis task, ignoring any associated health information. To separate the areas having identical and comparable properties for every two-dimensional brain MRI segment, various image-handling techniques are used. Areas can be made up of blocks rather than being sequential and still have consistent properties. For the finish, of the two-dimensional segments' preliminary investigation, more sections with distinct properties were separated from other areas. The conventional challenge of cancer identification in brain MRI images is one of image processing.

Regional algorithms make utilization of the estimated properties (correlation) of consecutive frames, whereas bounding techniques make utilization of the properties of the vastly different pixels surrounding the border, such as the jumping density, complicated contour, grey gradient, level of the frequency spectrum, etc. According to Parthasarathy G. et al., (2019), many edge identification operators, including the Canny operator, Sobel operator, and others, provide the foundation of widely employed border recognition techniques. These operators have the same value as discrete rectangular patterns of varying shapes, such as 3 * 3, 5 * 5, etc. The appropriate border is made up of a combination of the core pixels of the patterns that correlate to the convolutional outcome over the complete image as the patterns travel pixel by pixel. Edge recognition usually yields single contour points, and thus needs to employ several connection strategies to retrieve the entire border's shape. Different edge recognition algorithms have various benefits and drawbacks, but they are all often noise-sensitive and not failed.

Massive volumes of input image data, the computing complexity of the fundamental processes, and computational time restrictions make image processing jobs

computationally demanding. The objectivity of the problem Just about all organizations make extensive use of digital image analysis. Utilizing it frequently enables the industry to achieve newer technical heights. The most challenging query here is automated data retrieval and pattern analysis, which form the cornerstone of decision-making in the control of manufacturing operations. Real images are challenging for an automated approach and have several characteristics that are defined not just by the circumstances of the formation of the image but also by its methodologies and consequent preparation, and a combination of extracted data. Actual images are used in manufacturing vision processes, monitoring, supervising procedures, etc.

It is typically used to describe particular formal aspects of images. Furthermore, considering the range of characteristics of the real image, discussing the network characteristics would be the more correct way to describe it and, subsequently, make the greatest utilization of the data it contains. The consistency of the intricate, multi-level arrangement of several feature sets that characterize the examined image in all facets of expression of its qualities is the primary prerequisite of this approach. A huge set of modifications is one example of an operator creating a succession of images. It should not alter the geometric features of the image while having an impact on almost any feature groupings. Throughout this instance, a single feature may appear in a variety of ways across various images in the multi-sequence, always altering. Therefore, as an outcome of such modifications, it can either vanish or alter to the point where it needs to be regarded as a different autonomous characteristic or feature.

2.1.1 Unsupervised Segmentation Methods

The process of segmenting an image entails breaking it up into homogenous areas. To do this, heterogeneity must be measured objectively. In contrast to techniques that utilize an image-based objective assessment, the image segmentation job addressed in this study utilizes a morphological objective assessment to evaluate the segmentation performance. In contrast to areas with identical intensities or textures, the objective is to segment the brain images into areas that have homogenous (and well-known) morphological features. However, Section 2.1 will mainly concentrate on unsupervised strategies that attempt to segment the MRI brain images into two significant areas, that is tumor or edema. Section 2.2 will describe numerous techniques suggested for brain tumor segmentation that uses an image-based objective assessment.

2.1.1.1 Unsupervised segmentation with an anatomic objective measured

Abdel-Gawad et al., (2020) suggested an unsupervised method for segmenting cancer pixels from T1-weight post-contrast brain MRI images. An individually chosen region of interest was subjected to an intensity threshold in such an approach, which was followed by a region-growing technique that expanded the threshold regions to the edges indicated by a Sobel edge detection filter. During several rounds of dilatation (which made the specified cancer area develop) and erosion, the area development results were improved (tumor region shrink). These two processes, which are also known as morphological operations, modify the labels provided to certain pixels by looking at the label of the pixel location.

Miao J. et al., (2020) suggested the same approach for MRI image objects whose intensities differ from those of their surroundings. Whereas one drawback of these approaches is the need for manually sliced or region of interest selections, a more serious drawback is that do not adequately account for the existence of hyperintense pixels, which reflect typical structure in T1 post-contrast Images . In addition to normal tissues that might absorb the contrast substance, such false positives have included non-tumor structures with short T1 durations. The expectation that the whole border will have a significant intensity differential between its neighbouring tissue, which is not necessarily the situation, is yet another significant drawback of these approaches.

Biswas A. et al., (2021) presented an ANN strategy. The initial stage is to create an ANN model to identify brain tumor and extract the relevant features using K-Means and FCM Clustering. The retrieved features are sent through a correlation analysis selection procedure, with the finest features being chosen as the result. For experimentation and verification, 3 BraTS databases from 2015, 2017, and 2018 were used, with an accuracy of 98.32, 96.97, and 92.67 percent, accordingly.

Vijh, S., et al., (2020) demonstrated brain tumor based on the OTSU Embedded Adaptive PSO Method and CNN. This approach was effectively employed to determine the particular tumor area and measurements such as size, thickness, and length, and images are exhibited in various dimensions such as coronal, frontal, and axial. In regards to tumor diagnosis, the assessment findings of semantic segmentation performed based on the GLCM approach are extremely encouraging.

Ye J. et al., (2021) suggested the VNet frame for predicting the glioma tumor grade based on the radiomics feature extraction from tumor images .To classify and extract information from brain images, the VNet technique leverages the framework. Such VNet variants are compact and can be installed on Edge equipment as required. The grade is localized using the shape and statistics of the tumor. Just after the tumor has been localized, the segmentation procedure takes place inside the detector area, increasing the likelihood that the segmentation will be done correctly. The suggested approach provides an effective rate of 90% during the identification phase, and better results can be obtained with additional training images.

Deepak S. et al., (2021) proposed the sophisticated architecture for predicting the types of brain tumor of Radiomics images. Fivefold cross-validation and CNN and, the accuracy score of the suggested models is 95% .

Veeramuthu A. et al., (2022) projected a deep CNN for tumor images based on tumor segmentation taking into account the ambiguity of the image feature in the radiography MRI imaging sub-areas. Additionally, to obtain tumor subtype categorization, implement a deep CNN to the tumor segmentation.

2.1.1.2 Unsupervised segmentation with an image-based objective measure

Numerous studies have focused on methods for unsupervised brain cancer segmentation in MRI brain images without using an anatomically precise metric. Such techniques partition images into homogeneity sections utilizing image-based features like intensities or textures instead of across anatomically relevant divisions. Because this strategy has significant drawbacks, such techniques won't be discussed for a significant duration.

The need for manual interference to select (and maybe split, combine, or process) the tumor sections which are to be utilized for statistical research makes such concerns particularly clear when addressing heterogeneity tumours. Although not directly applicable to quantitative analysis, these techniques are often appropriate for enhanced visualizations.

Brindha, P. G. et al., (2021) suggested the three techniques such as Hopfield Neural Networks, Boltzmann Machines, and ISODATA looked at to do unsupervised brain cancer segmentation with an image-based objective assessment. This kind of strategy was introduced more recently by S. L. Bangare et al., (2018). The utilization of a Markov Random Field framework that statistically significant utilizes impacts that adjacent pixel values should also have over each other's labels, obviating necessity anatomical processes, and a fully automated "brain masking" preprocessing procedure gives one such technique an edge over equivalent technique . This research developed the Markov Random Field using the Classifier Conditional Modes technique on the assumption that the tissue classifications. Wu, W. et. al., (2021), presented an alternative method, to Glioblastoma which also utilized a Gaussian Mixture Framework (learned utilizing an Expectation-Maximization strategy), however, and utilized an Evidence Theory preparation instead of a Markov Random Field to account for image pixels dependencies in nearby pixels.

2.1.1.3 Summary of unsupervised segmentation

Whereas supervised segmentation approaches would be ideal because these do not include the humanistic variation of manual train datasets, unsupervised segmentation techniques using morphological quantitative assessments have only had little success.

This is partly because it is challenging to translate human professionals' visual interpretation and anatomical expertise into procedures that provide the necessary outcomes. Unsupervised segmentation techniques that utilize an objective assessment depending on intensity or texture can manage more complex instances and are helpful in improving visualizations, but the outcomes are frequently inappropriate for automatic quantitative analysis because intensities and texture differences frequently don't relate to the proper morphologic differences.

2.1.2 Supervised Segmentation

In order to effectively construct a segmentation framework based on the supervised approaches for images, segmentation differs from unsupervised approaches by using tagged train data. Data-driven methodologies, like classifiers, have the advantages that pertinent patterns in the dataset are found automatically instead of through manual trial and interpretation. A well-liked technique for carrying out brain image segmentation with a supervised learning technique is the design of the categorization problems. The goal of classifying is to classify an object based on a collection of attributes into one of the definite class labels. In the supervised approach, there are two phases: the training and testing, which employs labeled data to create a framework that mappings of characteristics to labels, and the testing stage, which utilizes evaluated relevant features to assign labels to unlabeled data. These 2 steps are used by numerous unsupervised techniques as well, but the use of the labeled data training stage of supervised techniques encourages the models to concentrate on producing discriminations in the feature set which match the specific semantic discriminations.

Using the terms normally and malignancy as categories and the intensities in the various brain MRI images as the relevant feature is an easy way to formulate the brain cancer segmentation problem like a supervised classifying issue. According to this concept, the learning step would involve developing a classifier that distinguishes between tumor and normal regions using the brain MRI image intensities. Using this framework to divide unlabeled image pixels into one of the 2 categories according to respective pixel intensities would constitute the test phase.

Utilizing supervised formulations has many benefits, including the ability to execute a variety of operations by simply altering the training dataset. It was demonstrated in recent research that compared supervised segmentation methods to the unsupervised knowledge-based approach covered in the earlier part.

2.2 Feature Extraction Approach

Certain image processing techniques have it that the tumor area is extracted and passed to the next level. It is crucial for analyses and categorization to define a collection of features that properly describe the data. This procedure is known as feature extraction. Usually, gray values contribute a small portion of the information contents. Image information is normally spatial by nature.

In spectral data, most of the information is repeated from image to image and this complicates the process of analysis and categorization. The key objective of feature extraction is to simplify and make the process of analysis and classification effective. The above-mentioned statement can be made true only when the following points hold; the redundancy of image data has to be eliminated, the variability of the image data has to be eliminated and finally, the data need to be restructured to

optimize the effectiveness of the classifiers. This is followed by the extraction of spatial information. When a spatial pattern is taken into consideration, shape, size, orientation, texture, and position are given importance. Among all these, texture is the primary feature of interest. Some of the main crucial aspects of pattern identification are textures. The texture is an attribute that plays a vital role in photo interpretation. Qualitative terms such as smooth, uniform, flat, coarse, grainy, even, uneven, regular, irregular, periodic, and random describe the term texture.

Chato L. et al., (2021) proposed a ML framework ,the texture in this project has had brain image preprocessing performed on it, and the counts are calculated by splitting the texture area with that window's area. The window is read from the pre-processed image while using the statistical window approach, and the OTSU thresholding features are then determined at various volumes. If the total exceeds the number, the classification method is then used to classify the data. Whenever the count exceeds the number, the process comes to an end.

Shim, K. Y. et al., (2021) proposed a ML model, the Radiomics feature extraction method was used for extracting the relevant features based on local and distant recurrence. Fivefold cross-validation was performed on both local and distant recurrence features of glioblastoma tumor.

Priya S. et al., (2021) proposed image is segmented into pixel blocks of size 2×2, each pixel with an RGB component, in that work. Using this block, a training vector of dimension 12 is created. The aggregate of this training vector is called the training set. The various machine algorithm is applied over the training set.

Zuo S. et al., (2019) glioblastoma tumor patients based on RNA sequencing using six gene signatures. Effective RNA sequence discrimination is achieved with this simple feature set. The wavelet sub-band, discrete cosine transforms, and spatial partition was used to retrieve the sub-band frequency feature sets. impacts of changing trained class sizes, trained classes count, discriminating space size, and several frequency measures utilized for categorization.

Hajianfar G. et al., (2019) analyzed univariate and multivariate radiogenomics features based on magnetic resonance imaging radiomics features of glioblastoma tumor patients. The feature extracting algorithm applies components from both models and region growing techniques. Incorporation of prior operational knowledge of shape and location can be used in this case, which contributes to an accurate volume and asymmetry.

Hashemzehi R. et al., (2020) proposed a unique computer method based on multi-resolution decomposition to retrieve important information from MRI images and minimize the distortion in images. Multi-resolution from the median through the Starck-Murtagh-Bijaoui wavelet Transform is used for noise suppression.

Lee, M. et al., (2019) proposed status in glioblastoma brain tumor. The quantitative radiomic data-based approach was used to obtain statistical features. The radiomic methods can be utilized to retrieve a variety of attributes. Therefore, in the study, four second-order features including entropy, inverse differential moment, correlations, and circular second moment are evaluated, demonstrating the system's ability to deliver the high discriminating efficiency needed for moving image prediction.

Amin J. et al., (2018) proposed fusion features from MRI brain images. This study introduced a unique feature extracting technique for the categorization of images. This work fusion of feature approach to extract numerous local descriptors. This method is developed upon the Probability Density Function formed by those descriptors. The features of fusion are extracted with the gradients. It is suitable for all kinds of work associated with classification because it does not impose any specific assumption on the target. zyurt F. et al., (2019) suggested Expert Maximum Fuzzy Sure Entropy. The PCA based feature extraction .The sampling approach is not crucial when the size of data images is to select relatively large as postulated.

Thakur T. et al., (2021) suggested innovative approaches based on RPCA and RPCA+LDA for cancer identification utilizing gene expression data. Firstly, RPCA is utilized to draw attention to the distinctive genes linked to a certain biological mechanism. The feature selection process is then carried out utilizing RPCA and RPCA+LDA. SVM is also employed to classify tumor. The findings show that the suggested approaches for tumor categorization are efficient and workable.

Deepa, B. et al., (2021) the Transform and Wavelet feature extraction analysis used in the process of extracting the texture feature. A novel computational algorithm to extract segments and detect regularity is discussed in this work. This method uses both speed and precision to retrieve and classify texture features of MRI images.

Shim Ka et al., (2020) proposed to use of locating the tumor, the new methods extract the main features in brain images. To adequately describe the feature in DSC-MRI images the coordinates framework is constructed. By combining region growing and edge detection, a tumor is detected.

55

K, K. K., T, M. D., & Maheswaran, S. K. (2018) proposed two methodologies, one based on tree-structured wavelet transform and the other based on GLCM. This work concludes that the wavelet provides better feature discrimination in terms of memory space and computation cost between the classes than the GLCM.

A. Keerthana et al., (2021) proposed methods that use classification between non-adults and adults using SVM. There are the six descriptors, including dominant hue, structural, design, edges histogram, homogeneous texturing, and area shape, are used to accomplish that. For every descriptor, additional data is produced to retrieve the required features and go on to classification tasks.

2.3 Image Classification Techniques

There are two broad categories of image classification techniques that can be distinguished. These are non-parametric classifiers and training and learning learners. The categorization variables must undergo a thorough training stage for learning-based suggested classifiers. Some of the known parametric methods are boosting, parametric generative models, decision trees, fragments, and object parts. These are the leading image classifiers, in particular SVM-based methods.

Non-parametric classifiers do not require any training of parameters. Such a classifier decides what to classify based solely on the brain input image data. The decides popular parametric classifications, often known as Neural network-based classifiers, use Nearest Neighbour distance estimates. However, it renders inferior performances when compared with learning-based classifiers.

Non-parametric classifications have the benefit of handling a large number of classes organically. It prevents the over-fitting of variables, a major problem with learning-based methods. These classifiers do not require any training phase. Two image categorization techniques greatly lower the effectiveness of non-parametric brain MRI image classifiers. Image-to-image separation and quantized are the terms used to characterize them.

To get compressed image interpretations, local image descriptors are used to characterize brain images. Such descriptors are quantization to provide a smaller bag - of - words.

Quantization reduces complexity and weakens the effectiveness of descriptions. Several learning-based classifications require this kind of dimensionality reduction. Whenever a non-parametric classification lacks a training step to make up for the data losses, it is unneeded and destructive. Kernel-based techniques require image-to-image separation. Usually, if the query image is comparable to one of the dataset brains images can KNN classifiers deliver accurate image categorization. It only really generalizes to the labelled brain MRI images. For several classes with a high variety controlled, this restriction is extremely harsh. The Naive Bayes Nearest Neighbour classifier computes the direct images that are the closest distance without quantizing the descriptor.

Lotan, E. et al., (2019) suggested model greatly when the application of such function in a neural network for unsupervised classification of images for mapping function is used. If the classification is done in a high dimensional space, then it can be separable linearly when compared to that in a low dimensional space.

In challenging image categorization tasks when the sole features are high-dimensional histograms, the Support Vector Machine generalizes effectively and different wavelet transform. Some type of discrete intensity or color histogram is used as the input in this case. The Support Vector Machine which was motivated by Gurbina, M. et al., (2019), has a stronger generalization ability, which accounts for the extremely better results.

Krishna T. Gopi et al., (2018) In this study, particle swarm optimization and SVM are two well-liked methods investigated for classification learning. Classification performance is increased by utilizing covariance matrices, decomposition-based number of pixels, and textural data on the collection of features.

The probabilistic neural network classifiers with the utilization of innovative morphological filtering show robust advancement to various MRI data sets. The probabilistic neural network approach structure and the feature can be chosen quickly using GLCM method. The study concludes that Varuna Shree et al., (2018) proposed that classifiers require careful consideration when choosing input MRI data.

Li Z. et al., (2018), suggested the model for an improved categorization method that uses the association of kernels with support vector machines to detect tumors in MRI images. GSDM and Tamura's techniques were used to retrieve the texture and Tamura characteristics. For feature identification, a genetic approach with combined probability was used. Support vector machines were used to classify data along with different kernels, and the effectiveness was verified.

Elshaikh, B. G. et al., (2021) proposed, Linear discriminant analysis of the texture classification model built from conceptual component pieces. Depending on how well they can distinguish between different textures, a best-fit collection of six operations is chosen. The results are transformed into a conventional deviation matrix that is calculated over a moving window. Zonal sampling characteristics are computed using this matrix. The collection of unique features is utilized for texture categorization once a feature selection method has been performed. This method renders accurate classification. The developed algorithm can be applied to different types of classification problems.

Almalki, Y.E. et al., (2022) provided the parameters of novel non-linear hybrid feature vector techniques that combine the use of structural data and spatially ranking methods in image analysis. Thus, a vector comprising the recorded sample data in both spatial and ranking order is used by the Invariant Clustered approach. The classical machine learning architecture was used for classifying the MRI brain image material which may be categorized based on the brightness patterns in the filtered images and determines the wavelet coefficients. In various cases, including picture de-blocking, impulse noise removal, and image extrapolation, the classification-based hybrid filtering outperforms linear filtering and order statistical filtering.

Murali, E., & Meena, K. (2020) suggested Adaptive Thresholding and Histogram based techniques for detecting brain images. The multi-resolution histograms' feature groups were mapped using the novel, quick kernel functions, which also calculated a weighting histogram overlap in each area. The pyramids matching process detects correspondence automatically depending on the highest

resolutions of histogram cells, in which a matching pair shows first, and is linear in the number of features.

Zhao J. et al., (2019) suggested the classifications technique creates a 2-D hidden supervised network for brain MRI images to enhance categorization by gradient and context sensitive features. It takes into context sensitive feature vectors for supervised brain tumor segmentation that are statistically reliant on a fundamental state mechanism with conditional probabilities based on the values of the nearby block within both horizontal and vertical dimensions.

Gu X. et al. (2021) suggested an efficient coding technique called Locality-constrained Linear Coding using Convolutional Dictionary Learning., and the projection coordinates are then combined using maximum pooled to get the final representations. The accuracy is achieved in two clinically relevant multi-class classification tasks using this method with a CNN algorithm, which works better than the conventional non-linear SPM methods.

Choi K. S. et al. (2019) proposed the suggested framework is a unique learning strategy that incorporates the advantages of sharp and RNN classification, in contrast to previous methods. The fundamental architectural aspect of the suggested approach is how to ascertain the clusters' architecture in the multidimensional feature space. By the use of 5 test scenarios, the efficiency of the suggested technique was assessed.

Choi Y. S. (2021) suggested a hybrid technique for predicting based on radiomics features using deep learning. The suggested technique is used in this instance for a collection of training data, whereby the input data are parameters that

are assessed online and the output data are qualitative factors that are categorized by human analysts. The suggested approach creates a robust deep neural model, that deduces that various features that can be precisely evaluated differ in value. The technique's usefulness is dependent on the absence of intricate repetitions in the training phase.

Zhao Y. X. (2019) employing Multi-view Semi-Supervised 3-D Self-ensemble Network using MRI brain images for healthcare image processing systems for tumor segmentation. The Self-ensemble classifier combined with several kernel space features is the suggested approach. The kernel class specifies the selection conditions. To create a comprehensive and systematic approach, the feature selection technique is combined with Self-ensemble classification. The suggested strategy greatly improves outcomes and uses less time than experimentation without feature selection and adaptable train the model.

Bakas S. et al., (2018) developed various ML techniques for Identifying the ML algorithms for segmentation and measuring the average Survival rate of the patient over the BRATS challenges. In general, machine learning classifiers find the separation hyper-plane by using two non-parallel descriptive margins. This classifier is appropriate in a variety of situations, particularly whenever the data have an incorrect pattern and the input values have a significant impact on the distortion. comparable to the various machine learning classifiers with a parametric margin.

Hemanth, G. et al., (2019) examined a technique since it can be determined directly from the deciding functions of a CNN without any mathematically time-consuming oversampling, the approach is computationally significantly more

effective than the leave-one-out approach. Investigations on synthetic data and a well-known handwriting digits identification set demonstrate the generalization effectiveness of CNN for novel identification, which makes techniques better.

Lu C. F. (2018) suggested a multi-level machine learning model for the diagnosis and monitoring. They suggested a system for choosing trained three levels of machine learning classifier. It takes advantage of a training level of machine learning feature that only employs the classification of sub-type of gliomas tumor from points that are located outside the distribution of the dataset. The produced models preserve the generalization power to the levels of a trained network on the entire trained dataset, but utilizes three level of classifiers and displays faster-training speed, according to analytical outcomes, which show that the suggested approach can minimize the training set significantly.

2.4 Brain Tumour Classification Techniques

Brain tumor are small malignant tissues that are developed in the human body. Primary brain tumor typically develop in the cerebellum and remain there. Tumor first appears elsewhere in the tissue before spreading to the brain in metastasis brain tumor. Due to the advancement in technology, knowledge about brain tumor has been enriched, because of the high-resolution techniques such as in medical imaging systems.

Among all the above-mentioned techniques, MRI is the technique for lesion detection, tumor extent definition, tumor spread detection, and evaluation of residual and recurrent disease.

To use the fact that tumor occupy the space where normal cells would be, and that their severity features differ from those of normal cells, a system for detecting tumors from MRI brain images has been developed by Han W. (2020) based on deep transfer learning. In this procedure, the brain was retrieved by excising undesirable brain-related tissues such as the skull, forehead, fat, and muscle. CSF resembles tumor intensity characteristics in T2 scans. As a result, the symmetrical properties of the CSF categories are examined across the middle continuous line. The images with the CSF classes are further segmented into the CSF and tumor classes utilizing the expanded maximum transformation if the symmetric is not obtained. The tumor area and the usual CSF area are divided by this transformation.

2.4.1 CNN Inception-V3

Convolutional layer factorization is utilised in the InceptionV3 model to minimise the number of parameters. reducing processing without compromising network speed by switching from 55 Convolutional filters to two 33-filter combinations.

Inception's 42 layers, 24M parameters, and 1–1, 3–3, and 5–5 filter sizes allowed for the largest amount of pooling while still extracting features at different scales. Calculations are sped up by using 11 filters.

2.4.2 VGG16 Neural Network

The deep neural network containing 16 layers is called VGG-16. A series of pre-trained parameters from ImageNet is loaded into the network. In the highest five tests, the model performs 92.8% accurately in ImageNet, a database of over large brain tumor images divided into two categories.

The RGB image has three channels and a preset input size of 224 x 224 pixels for the VGG16 framework. It has maxpool layers of 2x2 filters with stride 2 and 3x3 convolutional layers with stride 1.

2.4.3 CNN- AlexNet

A brain image is modified via the technique of convolutional, which involves putting filtering it. Poling is a discretization technique depending on samples. The input dimension should be decreased as the major justification. enabling speculation regarding the characteristics present in the binned sub-regions.

The CNN Network is a collection of unique layers that, through the aid of a differentiable function, convert input brain images into the final output. AlexNet is made up of numerous inception models with convolutional kernels (CKs) ranging in size from 1 by 1 to 5 by 5, each with its own set of features. The crucial characteristic was retrieved at the start of the procedure.

Melam, Nagaraju. (2018) suggested a new approach for detecting the bounding region of brain tissue. It also binds the peculiar abnormal tissue regions in the segmentation phase. In this work time, and complexity was reduced considerably.

Younis A. et al., (2022) proposed a DL approach to analyze BT from MRI brain images. Faster CNN and VGG16 classifiers were used to diagnose the brain tumor and classify it to yield tumor region. This approach is in line with the techniques used by radiologists to diagnose and prognosticate brain tumors utilizing several MRI images, which is not the scenario with various other approaches and

training stages. The following is a description of the phase which was noted in that research.

Ranjbarzadeh R. et al., (2021), suggested an innovative technique for tumor categorization in brain images T1, T1c, T2, and FLAIR was investigated. In two distinct ways, the suggested deep C-CNN network extracts. Images from Proton Magnetic Resonance Spectrometry are used for this categorization. The outcomes of using this technique demonstrate how precise, quick, and reliable it is.

Chen H. et al., (2021) suggested a DL approach, this study sought to diagnose glioma tumor and detects and localizes low and high tumors in three dimensions with numerical models, which involved a planar antenna array and synthetic cylindrical. The development of an image creation method improved tumor responses and decreased earlier than usual time interference. Prior information is not required for the reconstruction algorithm. Both the cylindrical configuration and the plane detect tumor and in addition to that accurate identification of the tumor region.

Fang, B.et al., (2019) presented that the 3-D structure of hyperspectral imaging (HSIs) data provides a chance for 3-D systems to effectively collect spectral and spatial features from image data. During HSI categorization, an innovative end-to-end 3-D densely convolutional neural model with spectral-wise attentiveness strategy was used.

Khosravanian A. et al., (2020) designed a model for Two phases are involved in the segmentation process using the fast level set. The first phase comprises the film artifact and the noise involved in that image is removed, after acquiring the image. In

the second phase of the image, the prime tissue structures are identified in the image volume.

Moradmand, H. et al., (2020) examined the influence the automation algorithm by employing symmetric analysis for detecting brain tumor. The tumor area is calculated after the tumor has been detected and segmented. A modular and multi-step approach was used to resolve the problem of segmentation.

Carré, A. et al., (2020) suggested a standardized machine and protocols for predicting the brain tumor across MR images using the radiomics features. A fully automatic algorithm that is fast and robust, which does not require any prior information about the training process is used. In addition, to identify the seeding sites, both the homogeneous texture properties and the spatial aspects of the MRI brain images were brought into consideration. The segmentation results obtained are accurate.

Yaqub M. et al., (2020) presented, the segmentation is done in two phases. MRI brain image acquisition is the first stage. Artifacts and noise of any kind have been eliminated. The optimized convolutional neural network with vectors quantized can achieve a higher value of tumor pixels and computational performance at the least number of weighted sums.

Cho, H., Lee, S. H., Kim, J., & Park, H. (2018) builds the radiomics features were measured for classifying the grade of tumor and tumor region. The brain tumor at different grades by using the radiomics method. The tumor is detected based on a threshold set. This work superimposes the healthy area with the tumor affected area.

Bae S. et al., (2018) investigates radiomic characteristics from MRI with medical and biological factors that enhance survival rate prediction in people having glioblastoma tumor.

Amin J. et al., (2020) proposed to consider the size, texture, and severity of the brain tumor. such a feature set is selected for each patient lesion. For additional statistical analysis, the goal is to localize and customize various forms of structure in brain. This study discusses the use of adaptive heuristics along with a generalized flexible-based segmentation technique to build a hybrid technique. Also, with increasing improvement and comprehension of pattern detection algorithms, tries to adjust offered benefits by changing the parametric settings of patterns by relevant data and using time-dependent considerations.

Feng X. et al., (2020) presented a new Ensemble 3-D U-Nets model to forecast patient survival rates, a linear framework was implemented. The improvements were evaluated and found to have a high level of predictive performance in patients with both low-grade gliomas and glioblastomas. Utilizing recognized brain mapping as a prototype for a normal brain, researchers initially look for aberrant areas. Set geographical and geometrical limitations to the areas of identified tumor.

Qian Z. et al., (2021) determines the best machine learning techniques for gliosarcoma and glioblastoma differentiating using radiomics features. According to a radiomics feature analysis predicated on the characteristics of the tumor volume is to use the technique LASSO in combination with the SVM classifiers. In comparison to all segmentations that met the requirements, the obtained outcomes exhibited the greatest combination of area characteristics and border characteristics. The tumor

volume and peritoneal edema were used to retrieve radiomic characteristics. The effectiveness of three feature extraction and classification approaches in differentiating between GSM and GBM was examined.

Sotoudeh, H. et al., (2019) new AI methods have been designed to automate the diagnosis from histopathological, forecast grading and genomes from MR imaging, and offer information into gliomas prognosis. For physicians without computer expertise, a concise explanation of the fundamental ideas behind AI techniques and their applicability to medical training is introduced. To examine cutting-edge AI methods for glioma detection and treatment. It is suggested to employ a learning processing technique to create the classifier model within the rendering-related optical parameter functionality. The categorization of high-resolution computerized tomography is a difficult issue for classification models, but experimental results show that it was greatly enhanced by additional learning stages and modifications.

Korte J. C. (2021) examine the effects of an HNC radiation response model with non-reproducible radiomics properties. While limiting the system to credible features utilizing a correlation threshold technique, it is entirely feasible to categorize identical patient categories utilizing radiomic features from computing software. This is significant because it offers a methodology for evaluating the repeatability of observed radiomic patterns from previous experiments, which is pertinent for medical diagnostic validating studies. In contrast to an IBSI-compatible software suite, this research examined the consistency of radiomics features computed with two popular radiomics software products such as IBEX and MaZda. From 336 diffusion-weighted

MR images of 58 patients with head and necks cancer from the radiotherapy research, intensity histogram, size, and textural features were retrieved.

Kobayashi K. et al., (2021) proposed the deep learning model to automatically selected radiomics features and classify the glioma tumor grades. The pixel intensity value of such a technique is unaffected by the form of cancer. It helps to improve the computer's potential to automatically estimate, allowing for a thorough examination of the essential surgical, chemotherapeutic, and radiation operations.

2.5 Brain Tumour Classification System in Multiple MRI Sequences

Mohsen H. et al., (2018) proposed a DL approach the discrete wavelet transforms and principal components analysis was used effectively combined data in the input layer and decision for making the layer to retrieve relevant feature for tumor identification. Whereas data fusion will add additional distortion, duplication, and computing effort, adequate data can minimize the classification's randomness and arbitrary nature to enhance the effectiveness of tumor identification.

Suter Y. et al., (2020) suggested the ML model for analyzing the glioblastoma survival rate based on the radiomics feature extraction method. The choice of class boundaries is where this approach becomes challenging.

Kim D. et al., (2019) analyze the study's design elements to determine how well artificial intelligence techniques performed in the diagnostic examination of clinical images. Instead of using internal verification, this research utilized external validation; in the terms of external validation, was data obtained for validation. However, almost all of the research findings which have been published during the

study duration and assessed the effectiveness of AI techniques for early diagnosis in image analysis have been actual evidence of detailed feasibility investigations and lacked the architecture elements necessary for reliable verification of the medical effectiveness of AI techniques in real-world settings.

Chen G. et al., (2020) proposed a framework to handle large dataset images. it employs the optimized probability maps and statistical features approach for extracting the relevant features. Using hierarchical learning of the cascaded random forests is optimized the weight error values and the difficulty of the local spirited system, where the source is identified as the average distance between the feature vector and its respective MRI input images and the labels as the number of active neural in the systems.

Jalalifar A.et al. (2020) predicated on abnormality identification utilizing a one-class SVM approach, suggested a technique .Two outliers masks are produced by the approach using separate one-class support vector machines. Moreover, the model's effectiveness varies widely, making it not very reliable. It employed an approach made up of probabilistic models and active contour frameworks. The technique is based on the retrieval of multi-dimensional features and a detailed summary of future natural data, however several of the underlying concepts may not hold for every case.

Iqbal S. et al., (2019) In this publically available MICCAI BRATS 2015 dataset was used. This dataset contains four modalities T1, T2, T1c, and FLAIR of MRI images. CNN and LSTM networks are two distinct deep models that are trained on the same dataset and integrated to create ensembles to enhance the outcomes.

Haarburger C. et al., (2020) reported the repeatability of radiomics the first stage involves manual MRI image segmentations from 4 specialist users, and the second stage involves a probabilistic automatic segmentation method utilizing created neural network. discover reliable findings for both manual and automatic MRI image segmentations across all three different datasets, demonstrating that some radiomic characteristics are resistant to segmentation variation while others are vulnerable to poor repeatability under various segmentation approaches.

Ranjbarzadeh R. et al., (2020) presented contacting, and the variability of the organ. In the rapid identification of cancers cells, the segmentation of the initial input grey images is changed into the segmentation of the likelihood mapping after the probability mapping of MRI brain images will be first determined using the pattern recognition underneath the adjacent neighbouring factor The concave and convex endpoints were then determined after the Kirsch filter was used to retrieve the organs borders. The images were uniformized along the boundaries of the organ using the mean-shift method. Lastly, the tumor were divided using the FCM method.

Shboul Z. A. et al., (2019) presented the DL approach for predicting the Glioblastoma Patient Survival rate based on Radiomics features. In this study, proposed a model for glioblastoma and aberrant tissues classification and segmentation and also survival prediction of patients using brain MR images. The suggested framework contains techniques for segmenting tumor tissue utilizing radiomics characteristics-guided deep neural networks and along with surviving regression and classification utilizing these aberrant tumor tissue sections as well as other pertinent medical variables.

Patel M. et al., (2021) predicated on merging medical, radiomic, and cellular to distinguish the tPD and psPD in patients having glioma. The machine learning random forest approach was used for relevant feature selection under bootstrap sample cross-validated sequential backward removal. The resultant models were validated using naive Bayes with a five-fold cross-validation procedure.

Mahmoud A. et al.,(2023) proposed and examines the value of CNN models by using various measures on a dataset of brain tumor. The models in use had their accuracy, sensitivity, and specificity measured and compared.

Tandel G.S. et al., (2023) Five convolutional neural networks were used in the proposed ensemble strategy.

Table 2.1: Summary of Some Literature Review in the field of brain tumor detection

Authors	Techniques/ Methods	Classifier/ Algorithms	Benefits	Problem Identified
Abdel-Gawad et al., (2020)	Sobel Edge Detection Technique	Classical Genetic algorithms	Correct ROI (Region of Interest) identification is made possible by using neural networks to operate at varied intensities.	Changes in intensity when acquiring the images
Miao J.et al., (2020)	Adaptive Dictionary Learning	Fuzzy C-means clustering algorithm	The relationship between compression and intracranial structure deformation in order to detect the progression of brain tumors on T1 post-contrast images.	Suggested approach cannot produce the ideal segmentation output with intensity inhomogeneity
Biswas A. et al., (2021)	K-Means and FCM Clustering	ANN	Seven potential designs for categorising MRI brain tumour of MRI mages.	Accuracy of reconstruction was less
Vijh, S. et al., (2020)	Embedded Adaptive PSO	CNN	To designed the deep model with a self-defined framework on an MRI dataset for brain tumours detection and finally result is compared.	Work only on binary class so it difficult to predict another tumor.
Ye J. et al., (2021)	Radiomic feature	VNet	Seven potential designs for	Accuracy of reconstruction was

	Extraction, LLG, HOG		categorising MRI brain tumour of MRI mages.	less
Deepak S. et al., (2021)	Fivefold Cross-Validation	CNN-VGG16, SVM		The size of the tumour determines. Whereas if tumor is smaller than 3 mm in diameter, it is challenging to locate the tumour.
Veeramuthu A. (2022)	Image-based classifier	Deep CNN	Seven potential designs for categorising MRI brain tumour of MRI mages.	Accuracy of reconstruction was less
Brindha P.G.et al., (2021)	NA	ANN CNN	To designed the deep model with a self-defined framework on an MRI dataset for brain tumours detection and finally result is compared.	Work only on binary class so it difficult to predict another tumor.
S. L. Bangare et al , (2021)	Sobel Edge Detection	OTSU's	Predict 2-D view of all stages of tumor	Only grey MRI with limited dataset used.
Chato, L. et al., (2021)	Radiomic Features	KNN, SVM, VGG16, NN	Developed a ML model for predict the survival rate for glioblastoma patients and analyze the aggressiveness of	if the dataset contains a mixture of high- and low-grade tumours. then results may vary.

			tumor	
Priya, S. et al., (2021)	Six Spatial Scale Filters, Fivefold Cross-Validation	Neural Network	To analyse the texture based T1 contrast-enhanced images for examining the effectiveness of MRTA for glioma survival rate of patients.	color space is shows to vary the final outcomes.
Panwar S. et al., (2021)	NA	AlexNet	Effectively categorize the different forms of brain tumours.	Very small dataset was utilized to pretrained the network
Rani S et al., (2022)	Cellular Logic Array Processing	3D-AlexNet	Proposed a framework to identify the specific pattern to detect the brain tumor from medical image	Computational time is more for pattern recognition

2.6 Research Gaps from Previous Research Work

Table 2.2: Summary of various filters for feature extractions used in previous Work

Filters Name	Working	Advantages	Disadvantages
Median	Depending on the average Pixel intensity of brain Image	effective at lowering speckle noise and salt and pepper distortion.	Comparing to a mean filter, difficult and time consuming.
Wiener	Depending on frequency-domain and inverted filtration process	effective at reducing the effects of distortion from images.	Its modest performance is a result of operating in the frequency domains. fails to

			produce satisfactory outcomes for additive noises.
Hybrid	It is combination of two filters such as median and wiener	Removes the effects of blurring, impulsive distortion, and speckling from MRI images	Complex and time consuming
Gaussian	It serves as low-pass filtration for frequencies	Effect is to remove high spatial frequency components from an image.	Sometimes used distort MRI images and eliminate details
Average	It is depending on values of pixel intensities	Reduces Gaussian noise. Response time is fast, Boundaries and edges are Preserved	The average pixel value replaces the actual value

Table 2.3: Summary of Various Image segmentation methods

Various Techniques	*Advantages*	*Disadvantages*
Threshold Method	Pixels are partitioned depending in their intensity value	The edges that can be seen are made up of individual pixel and could be absent entirely. computationally costly
Watersheds Method	improve the capture range, capture weak edges	Over segmentation
K-mean	Computationally faster than other methods, if k-value is small	Difficult to predict k-value, doesn't work with different size and different density,

		accuracy depends on the predicted k-value
Active contour method	Utilize designs with active contours. effectively maintains the universal line forms.	For the contouring, locate powerful image gradient. poor MRI image borders, poor precision, and image distortion
Region growing	Establish the initial centroids and effectively distinguish the areas with the similar characteristics.	To get suitable location, only manual effort was needed.

2.7 Contribution of this chapter

- The vast amount of historical information on MRI brain images is covered in this chapter. The background data on brain tumor and their identification was discussed before moving on to the previous research.

- The fundamental methods used by multiple investigators and the system they had discovered using automated identification methods were then discussed.

- Additionally, the chapter analyses the literature on categorization, feature extraction approaches, optimization, and three-dimensional reconstructing approaches.

- This chapter also discussed and used in image segmentation and feature extraction.

CHAPTER 3

Glioblastoma Brain Tumour Survival Prediction Using Deep Learning

This chapter presents the research on glioblastoma imaging techniques including its operational applications in section 3.1. Section 3.2 presented the complete methodology deep learning model. Section 3.3 mentioned the experimental result analysis, and the research is concluded in section 3.4.

3.1 Overview

Whenever abnormal brain cells multiply, brain tumor form. The death rate is significantly increased in adolescents and adults with cancers than in people without. Depending on their severity and development rate. Whenever harmful cells proliferate from the initial tumor, secondary tumor develop in different regions of the human body highlighted by Xia, W. et al.,(2021). Initial tumor appear in the brain. According to the WHO, the source and activity of cells determine whether a brain cancer is normal or malignant. Older patients with an initial stage of brain tumor are more likely to develop GBM, a very prevalent and dangerous type of tumor. The diagnosis for GBM is poor investigated by Zaw, H. et al., (2019) even though it is managed with chemotherapeutic, radiotherapy treatment, and maximal surgeries. Medicinal response and GBM regrowth were inevitable even though these multifunctional therapies are inadequate to cure this terrible sickness. As MRI is a non-invasive clinical diagnostic technique, it is frequently utilized in the diagnostic, prognostic prediction, treatment, and other therapeutic strategies of individuals having GBM. MRI uses the image to gather physiological, structural, operational, and

compositional data. Among the more effective approaches for diagnosing GBMs is MRI since it can capture real-time multimodal imaging of the disease. In brain tumor segmentation, MRI segments were primarily used for labelling. This affects several therapy choices, additional therapeutic strategies, and total survival predictions indicated by Fu, J. et al., (2021). The basis for the collaborative decision is that glioma patients require reliable predictions to make smart selections before receiving therapy confirmed by Amin, J. et al., (2020).

3.1.1 Methods for Imaging Glioblastoma and Related Functional Issues

Nowadays, X-ray, MRI, and computerized tomography (CT) scans are among the methods utilized to monitor brain development, and the resulting images by such methods have improved over time conveyed by Sharif, M. et al.,(2020). for determining neurological development is MRI, which is effective for classifying and identifying different types and grading tumor in the clinical analysis explored by Tandel, G. M. et al.,(2020). It can be used to identify dangerous tumor and locate affected cells inside the brain. This technique can reveal tumor characteristics that the unaided eye would have missed. These custom-made clauses are selected for either conventional facts approaches or deep learning computations observed by Fan, C. et al., (2017).Brain cancer survival rates using a deep learning-based radiomics framework have been suggested by Suter, Y.et al.,(2020). Nie created a Convolution neural radiomics model employing a combination of MRI data from 75 patients (train data) and 38 individuals to determine the total patient survival rate with glioblastoma. The developed approach outperformed conventional approaches to predicting total survival if seven deep characteristics were chosen from the relevant CNN investigated by Wijethilake, N. et al.,(2020). Such methods can radically alter how neuroimaging

is utilized to enhance diagnosis and treatment for patients with traumatic brain injury, which is a distinctive benefit. It's crucial to remember that these methods have constraints, and there are still big problems to solve. In the chapters, a unique framework for glioma in relationship to radionics was developed using CNN characteristics for survival rate prediction. It contributes to increasing the prediction system accuracy in the environment of autonomous care and decision.

3.1.2 Survival Prediction for Glioblastoma Brain Tumor

Research in the field has shifted to ml algorithms throughout the last ten years. From standpoint of machine learning, the MRI image segmentation of brain tumor can be seen as a pixel problem to determine whether such a specific voxel corresponds to healthy tissue, glioblastoma, or edema category. Artificial characteristics and techniques depending on traditional machine learning, including AdaBoost, linear regression, and support vector machines are groups of techniques used to produce these features highlighted by Shree, N. V., & Kumar, T. K. S. (2018). Therefore, in the sector, deep learning has rapidly gained popularity, especially for image segmentation, classifying, and prediction. According to the network design, the 3 types of deep learning techniques employed for brain cancer segmentation are patch-wise, semantic information, and cascade-based.

Nowadays, a large number of well-known CNN based utilize patch-wise strategies to address segmentation issues discussed by Sun L. et al.,(2018b), Smaller areas of the image encompassing every pixel are examined to use a sequence of more intricate and simplified aspects of nonlinear interpretations of the dataset elaborated by Nogay, H. S., & Adeli, H. (2020). Additionally, the tumor is segmented using

CNN models, and features like form, entropy, and geometrical attributes are extracted from this. One of the biggest hurdles for investigators is finding malignancies in low-complexity systems. Benign growths, glioblastoma, and pancreatic tumor, as per current research, can be reliably diagnosed, although their method necessitates a large amount of convolutional and kernel, which raises the computing cost. The malignant brain tumor test image was found using a subsequent expansion of the models. Despite the study focused on non-medical purposes, it provides insights into how Faster-R CNN might be applied to diagnostic imaging defined by Rosati, R. et al.,(2020). To forecast the survival rate of glioma tumor, the research suggests a deep-learning technique.

The neurological system varied collection of cancers that can develop close. The position of the tumor within the brain has a significant impact on the symptoms of these victims, and clear diagnostic and major remedial alternatives were determined, which may have a detrimental effect on the patient's condition life. Brain tumor are typically only identified through neuroimaging just after the onset of neurological problems. Numerous studies have used this methodology, and the approach has failed as a result of coefficients overhead, overfitting, and inefficient extraction of features. A deep learning approach does not optimize the utilization of several layers in the training and classifying systems. The computational cost rises as an outcome. Additionally, overfitting problems arise from the classification procedure that is based on the complete MRI analysis in each direction. According to the obstinate edge regions, segmenting images using a standard architecture is difficult. The learning latency and recognition effectiveness of traditional ML approaches are limited. Consequently, the time consuming, incorrect, and inefficient technique

creates a requirement for an enhanced deep learning model. To forecast glioma tumor in MRI diagnosis, a unique and dynamic network-based faster R-CNN modelling strategy was developed and published by Wankhede, D. S., & Rangasamy, S. (2022).

3.2 Proposed MFCM-RSGWO-FRCNN Model

Considering healthy tissue or large size overlap intensity, brain tumor were challenging to model and produce patterns for. Better precise diagnoses are produced, and there are several benefits to using MRI brain imaging data and computer based medical image analysis. Computer-aided tumor diagnosis techniques and CNN have been demonstrated to be effective and have contributed considerable strides in computer vision. Glioma recognition was determined using MRI brain tumor imaging. The complete architecture for the suggested deep learning model is depicted in Figure 3.1.
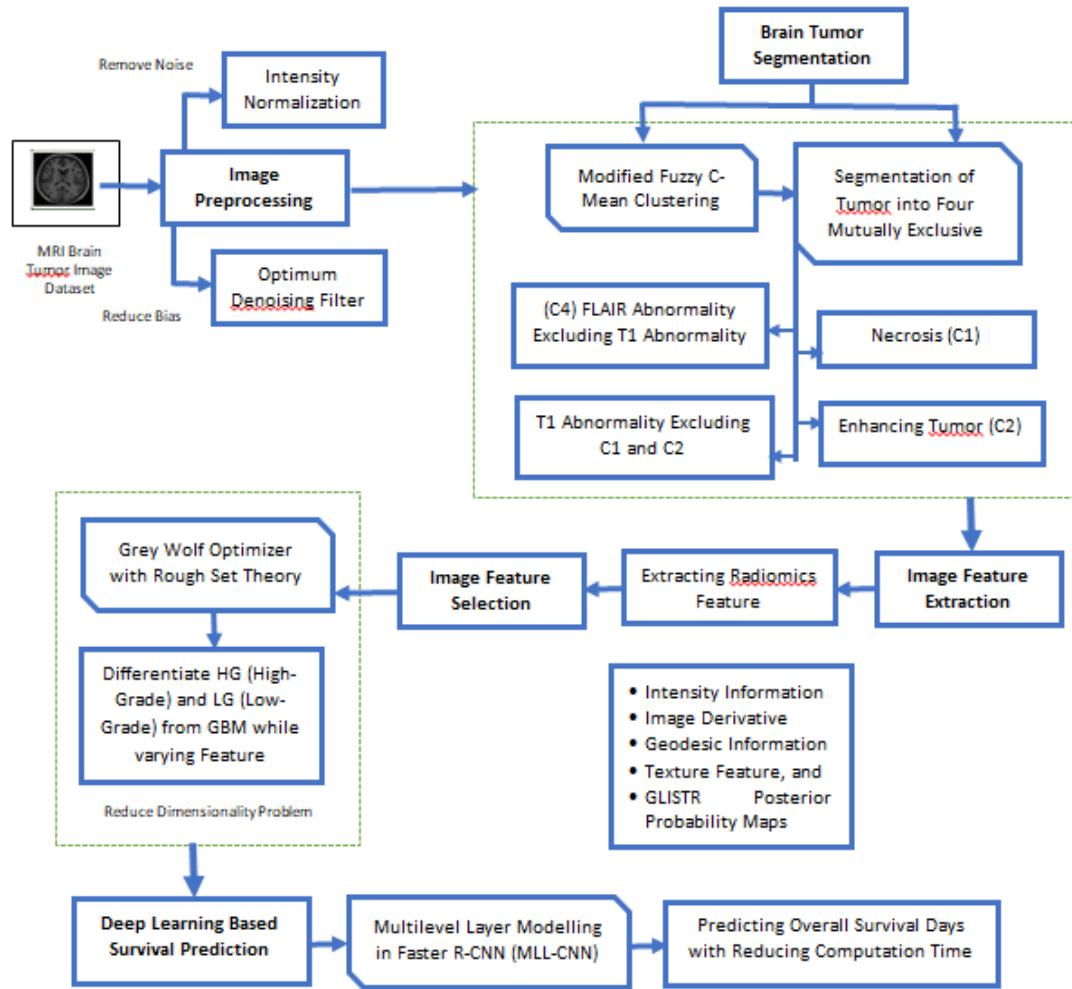
Figure 3.1: Complete Architecture of Proposed MFCM-RSGWO-FRCNN Model

The suggested method consists of four steps. The initial stage involves gathering the MRI brain data for utilization from a fixed website and preprocessing it to get rid of all the impurities. The MRI brain images also include several types of distortion, such as salted and speckle noise and Gaussian distortion. Furthermore, in certain instances, MRI images are collected using different scanning devices, and imaging intensity is used to normalize the MRI images. As a result, preprocessing includes by statistical normalizing and using filtering to improve the MRI brain images. The aim main of preprocessing is to build the database by removing unwanted data and restoring missing features from MRI images. The MFCM classification technique is then used

for segmentation utilizing radiomic characteristic data. Countless features may be retrieved from the segmented MRI brain images. The most important and instructive aspects from the retrieved important features. The categorization for overall survival rate estimation is then completed to features chosen in MRI brain images using an FR-CNN technique. As a result, the suggested classifier improves accuracy while requiring shorter training time and a faster converging rates. The following steps must be taken while using the suggested glioma brain cancer survival predictive model.

3.2.1 Data Collection

The standard benchmark MRI brain tumor sample 254 images taken from the publically available Kaggle were used to create the database. A prediction of the complete survival rate has been created from each batch of input brain images.

3.2.2 Pre-processing and Noise Removal

Improving the visual information from the brain's image using the pretreatment stage, and improving the image properties is crucial for postprocessing. The MRI scans show many types of distortion, containing salt and pepper noise and Gaussian noise. Since these brain images were taken with various scanning machines, the intensity also needed to be adjusted. Because multiple scanning devices are used to capture the images, intensity is also adjusted. To remove noises and distortions from the image in this study, symmetrical filtration and histogram normalization are used.

3.2.2.1 Image Normalization

Intensities is a fundamental preprocessing procedure in brain MRI investigation. Large intensity variations can occur when different scanners or

84

specifications are utilized for imaging the same patient at different periods throughout MRI data collection. Further, MRI preprocessing and population analyses, such as data augmentation, segmentation, and cell size estimate, would be significantly hampered by these intensities are vary. A normalization technique modifies the distribution of every follow-up scan to suit the selected standard scanning to increase imaging similarities and facilitate MR image comparison among MRI images. For intensity normalization, the histogram normalization procedure has been used without any practical assistance or previous experiences.

In an identical patient, utilizing varied acquired variables and varying field intensities were comparable for the same severity kind percentages for the identical cell types in brain MRI images. As an outcome, low-quality MRI images will be fed to the network as the inputs, while a high-quality MRI images will be utilized as the outputs. The histogram's tails are usually to blame for problems. The tailed with high intensity typically relate to abnormalities and abnormal intensity, causing large scanning oscillations. To avoid this problem, the backgrounds and outliers are first removed from the source images during preprocessing, leaving only the Intensity of Interest, which is then utilized as the reference scaling.

The T_{max} , T_{min} are the two standard scale factors with min and max intensity. The benchmark image's distribution is composed of the Low-Intensity Homogeneous subgroups LIR and HIR. The distribution was initiated from the LIR and extends all the distance to the HIR. The MRI image intensity are translated to the HIR and LIR ratios. The source MRI images distribution is moved and enlarged as illustrated underneath to accommodate of input MRI image's grayscale values.

$$h'(a,b,c) = \frac{HIR-LIR}{T_{max}-T_{min}} \left(h(a,b,c) - T_{min}\right) + LIR \qquad 3.1$$

Whereas, at T_{min} represents the initial input images of brain which is target histogram $h(a,b,c)$ and extends to T_{max} grayscale level images, scaled up between the lower boundary n_1' of brain images and n_2' is the upper boundary respectively. When the number of pixels $h'(a,b,c)$ of the new normalised brain images lie between HIR respectively. The variables n_2 and n_1 reflect the upper and bottom boundaries of the reference MRI image before scaling up. This is achieved by employing two separate linear mappings. From $[T_{1l}, \pi_l]$ to $[LIR, \pi_s]$, the first is ranges while from $[\pi_l, T_{2l}]$ to $[\pi_s, HIR]$ the second ranges. Let's define the normalising function as $O(a,b,c)$. The expression for $O(a,b,c)$ is:

$$O(a,b,c) = \begin{cases} \left\lceil \pi_s + (h(a,b,c) - \pi_i)\frac{LIR-\pi_s}{T_{1l}-\pi_s}\right\rceil, n_1' \le h(a,b,c) \le \pi_i \\ \left\lceil \pi_s + (h(a,b,c) - \pi_i)\frac{HIR-\pi_s}{T_{2l}-\pi_s}\right\rceil, \ \pi_i \le h(a,b,c) \le n_1' \end{cases} \qquad 3.2$$

where the mean values of the input MRI images histogram and reference MRI images histogram were displayed as π_i and π_s, and the functionality of the ceiling is known as $\lceil \cdot \rceil$. The pixel values of the input MRI images are denoted as T_{1l} and T_{2l}. Three important intensity factors are required for normalising the MRI images [minimum (LIR and T_{1l}), maximum (HIR and T_{2l}), and mean (π_i and π_s)], will be effectively attained without the need for the study's incorrectly supplied histogram boundaries. The recommended normalising approach therefore deviates from the current normalisation technique. When comparing the input MRI brain images to the source images, the effectiveness of histogram normalisation is evaluated utilizing the noise quantification.

3.2.2.2 MRI brain images de-noised based on bilateral filtering

Probabilistic, salt-pepper and other types of noise can be present in the MRI imaging of glioblastoma. The data remains unchanged from the inputted MRI brain data after the noise has been removed. These input MRI brain images are de-noised using bilateral filtering. The bilateral filtering technique applies the spatial weight average without employing the smoothed edge concluded by Parthasarathy, G.et al.,(2019). It is achieved by combining two Gaussian filtering methods, including one that acts in the spatial domains and another in the pixel intensity plane. Both the intensities and the spatial range are being used to calculate the weights. P is the output of each pixel location based on a bilateral filter.

$$\bar{F}(p) = \frac{1}{N} \sum_{z \in S(p)} e^{\frac{-\|q-p\|^2}{2\varepsilon_e^2}} e^{\frac{-|F(q)-F(p)|^2}{2\varepsilon_s^2}} F(q) \qquad 3.3$$

Where, $S(p)$ ε_e and ε_r are factors that control the weight in the severity and spatially domain begin to decline.

$$N = \sum_{z \in S(p)} e^{\frac{-\|q-p\|^2}{2\varepsilon_e^2}} e^{\frac{-|F(q)-F(p)|^2}{2\varepsilon_s^2}} \qquad 3.4$$

Color mappings, cubic de-noising, texture pattern elimination, as well as other applications including image de-noising have been used in bilateral filtering. The intensity of the signal is presented to the variables of the spatial state in a high-dimensional region that expresses the filtering. By implementing the bilateral filtering as two straightforward linear convolutional layers in this enhanced area, they can create straightforward parameters for down-sampling the crucial functions and attaining accelerated.

3.2.2.3 Brain Tumour Segmentation

Brain tumour segmentation determines the location and size of abnormal tumour regions and if the tumour area is perfused, swelling, or advanced fibrosis utilizing and protons densities MRI imaging. That tumour kinds are more visible in particular imaging methods can be determined by analyzing the images produced by the several diagnostic modalities. An automated segmentation of a tumor into four sections which are generally . According to the three-imaging series that are accessible, each pixel has 219 low-level features produced by the classification.

3.2.2.3.1 Modified Fuzzy C Means Clustering

The FCM approach assigns pixels to various categories based on fuzzy membership. Let $X = \{x_i, i = 1,2,\ldots,N \mid x_i \in R^d\}$ represent an N-pixel brain images that is divided up into the c number of clusters, with xi shows the tumor data features. The approach uses a continuous optimisation technique to try and reduce the optimal solution represented by

$$J_m = \sum_{k=1}^{c} \sum_{i=1}^{N} u_{ki}^m \|x_i - v_k\|^2 \qquad\qquad 3.5$$

Additionally, the optimization problem in equation 3.5 was changed right away to the following.

$$J_m = \sum_{k=1}^{c} \sum_{i=1}^{N} u_{ki}^m \|x_i - v_k\|^2 + \frac{\alpha}{N_r} \sum_{k=1}^{c} \sum_{i=1}^{N} u_{ki}^m \sum_{r \in N_i} \|x_r - v_k\|^2 \qquad 3.6$$

Where, N_i is the probability of several neighbours going through a windows in a neighbourhood x_i and N_r. The next term's alpha variable regulates the penalty's impact. In general, increasing 3.6 by two results in a spatial constraint that aims to preserve consistency on nearby image pixels x_i. The objective function J_m can be reduced utilizing an optimization technique given a restriction.

Neighbouring pixels in images are those in an MRI scanning that are close by and have similar feature qualities. To effectively describe the spatial features of pixel in images, the result is modified.

$$v'_{ij} = \frac{v_{ij}^y . s_{ij}^m}{\sum_{k=1}^n v_{kj}^y . s_{kj}^m} \qquad 3.7$$

$$s_{ij} = \sum_{k \in N(a_j)} v_{ik} \qquad 3.8$$

Where, s_{ij} indicates the probability of a pixel in space. a_j belonging to the i-th cluster. $N(a_j)$ is a pixel- or voxel-centered squares frame in the spatially space. a_j in the spatial domain and y, m are the set of parameter. While residue was unchanged by clustering, the spatially function enhances the unique membership score. The MFCM Algorithms has the following phases:

Phase-1: Set c total number of clusters and y set of parameters.

Phase-2: Evaluate membership matrix $V^b = \left[v'^b_{ij}\right]$ using Eq. 3.8,

Phase-3: Evaluate t_j based on Eq. 3.5,

Phase-4: continue phase 2 and 3, upto the last terminating criteria is met:

$\left| V^{b} - V^{(b-1)} \right| < \varepsilon$ where b indicates how many iteration stages there are $(b = 0,1,2,\ldots)$ Obtaining the radiomic features from the MRI images based on this segmentation. The radiomics characteristics included data about Pixel intensity, image derivatives, geometric data, texture-based features, and GLISTR Bayesian probabilities mappings. Such characteristics have been used to create frameworks for diagnosis, prognosis, and predicting therapy outcomes. These frameworks are incorporating medical, physiological, hereditary, and proteomics traits to increase accuracy.

3.2.2.3.2 Features Extraction

The raw pixel intensities for each pixel is included in the intensity element $I_{(v_i)}$, as well as significant variations between all four modes. The image derivatives element is made up of the intensity of the image gradients and the Probabilistic Laplacian. Before creating additional intensity-based features, the mean image intensity of the GLISTR segmentation cerebrospinal fluids were used to do intensity normalization. The geometrical distances from the grain used as the tumor origin in GLISTR, which was at the pixel, offered the geometric data at the pixel. Following are how the geometric distances among vi and vs were determined.

$$\min_{\gamma} \int_{\gamma} P(\gamma(S)) ds \qquad\qquad 3.9$$

Where, γ is a route that connects v_i to v_s. The fast march technique was used to optimize, the weight P according to the gradient's intensity at each pixel, With the first and second orders, texture-based statistical approaches are provided by a GLCM. The mean and variability of the intensity inside two coordinates of each

90

modality make up the first-order statistics for each region to 64 unique gray values, and each image sliced was then confined by a boundary box made up of 5x5 pixels.

Furthermore, patient improvement was carried out by reviewing the spatial arrangement of the present segmented labelling using a stochastic framework. To begin, the intensities distribution of each of the cell classes—white tissue, edema, necrosis, with a GLISTR posterior probability of 1 was separately filled out. The class-conditional probability densities $(\Pr(Iv_i)|Class_1)$ and $(\Pr(Iv_i)|Class_2)$ were modeled to use a variety of Gaussian methods, and every are calculated by method. The multiple couple proportions that were examined now are the edema regions compared it is projected that the earlier intensities populations will have significantly larger levels. In a conclusion, the strength of vertices for each cell category that was near to (i.e., within three coordinates of) the cell category to which they were opposed was evaluated.

3.2.2.3.3 Features Selection using Radiomic

The vast dimensionality of the input dataset may cause overfitting issues and increase computation costs for image radiomic characteristics like GLISTR probabilistic likelihood mappings, geometric data, pixel intensity data, texture-based, and image derivatives segregated from the pre-processed images.

3.2.2.4 Rough Set Theory

This part on rough set theory and RS-based features selection introduces a several fundamental ideas. Let $J = (P, T, C, G)$ be an informational system, and the representation of a definite non-empty occurrence collection is P, whereas T shows

the finite non-empty attributes set. C represent the set union of attributes, whereas $C = U_{t \in T} C_t$ represents scope of attribute $t. g: P \times T \rightarrow C$. Each occurrence of the data functions is connected with a particular magnitude for every feature in P, resulting in $g(y, t) \in C_t$ for any $t \in T$ and $y \in P$.

There is an invisible link $IR(A)$ that connected to each $P \in T$. $A_*(Y)$ and $A^*(Y)$ in eq. 3.13 and 3.14.

$$IR(A) = \{(a, b) \in P \times P | \forall_t \in q, g(y, t) = g(z, t) \} \qquad 3.10$$

The $P/IP(A)$ represents the partition of P determined by $IR(A)$ and can be measured as

$$P/IP(A) = \otimes \{T \in A: P/IP(\{t\})\} \qquad 3.11$$

$$S \otimes L = \{Y \cap z: \forall R \in Y, \ \forall L \in Z, Y \cap Z \neq \varphi\} \qquad 3.12$$

$$A_*(Y) = \{y \in P: [Y]_A \in y\} \qquad 3.13$$

$$A^*(Y) = \{y \in P: [Y]_A \cap Y \neq \varphi\} \qquad 3.14$$

The F-positive and F-negative zones are identified using equations 3.15 and 3.16 $F, X \in T$ which allow two equivalence relations to develop $IR(F)$ and $IP(X)$. region of X is stated as following, as shown in the equation 3.17.

$$POS_F(X) = \bigcup_{Y \in P/IND(X)} F_*(Y) \qquad 3.15$$

$$NEG_F(X) = P - \bigcup_{Y \in P/IND(X)} F^*(Y) \qquad 3.16$$

$$Bd_F(X) = \bigcup_{Y \in P/IND(X)} F^*(Y) - \bigcup_{Y \in P/IND(X)} F_*(Y) \qquad 3.17$$

One of the key challenges in data assessment is identifying connections between characteristics. If and only if $IR(F) \in IR(X)$, is based on X dependencies which is measured in similar way that $F, X \epsilon T, F$. From the eq. 3.18,

$$\mu_f(X) = \frac{|POS_F(F)|}{|P|} \qquad\qquad 3.18$$

$$\mu_d(E) = \mu_{sel}(E) \text{ and } \forall Q \in Sel, \mu_q(E) \neq \mu_d(E) \qquad 3.19$$

$T = D \cup E$ and $D \cap E = 0$ in an information table, $J = (P, D \cup E, C, G)$ .The decision features set is being utilized to indicate the accuracy of selections $\mu_d(E)$, how dependent are conditional and decision-making attributes. By employing feature minimization, unnecessary features can be removed while maintaining effectively classifying the reduced sets as the initial values. the equation 3.17 shows the feature that is a subgroup of the conditional feature called Sel.

3.3 Grey Wolf Optimization

The GWO technique was based on the hunting habits and social leadership of grey wolfs. The GWO approach begins with a group of arbitrarily generated wolf, much like similar metaheuristic algorithms. In order to create the social structure of the wolf when creating GW optimization techniques, the gray wolf populations are divided into five categories: (α), (β) (δ) respectively, in the formulation of the gray wolf optimization problem. Omega (ω) is considered to be some kind of optimistic alternative solution. The hunters are commanded by such three contenders α, β, and δ, and they also are preserved. The following is a presentation of the mathematical framework for changing the locations of the wolf.

$$\vec{D}_\alpha = \left|\vec{C}_1 \cdot \vec{X}_\alpha - \vec{X}\right|, \vec{D}_\beta = \left|\vec{C}_2 \cdot \vec{X}_\beta - \vec{X}\right|, \vec{D}_\delta = \left|\vec{C}_3 \cdot \vec{X}_\delta - \vec{X}\right| \text{n} \qquad 3.20$$

$$\vec{X}_1 = \vec{X}_\alpha - \vec{A}_1 \cdot \left(\vec{D}_\alpha\right) \qquad 3.21$$

$\vec{C}_1$, $\vec{C}_2$, and $\vec{C}_3$, and $\vec{A}_1$, $\vec{A}_2$ and , $\vec{A}_3$ are all randomised vector, Additionally, the location of the current solutions, and is the number of iterations. In order to numerical model encircling behaviour, the mathematical expressions 3.22 to 3.25 are applied:

$$\vec{T}(u+1) = \vec{T_p}(u) + \vec{B} \cdot \vec{E} \qquad 3.22$$

Where, eq. 3.20 and 3.21.

$$\vec{E} = \left|\vec{D} \cdot \vec{T_p}(u) - \vec{T}(u)\right| \qquad 3.23$$

$$\vec{B} = 2\vec{b} \cdot \vec{s_1} - \vec{b} \qquad 3.24$$

$$\vec{D} = 2\vec{s_2} \qquad 3.25$$

Generally, the alpha wolf is a leader to command of the pursuit. The beta and delta wolf can occasionally take participation in pursuing as well. The strongest possibility answer is alpha, whereas beta and delta are projected to have enhanced understanding regarding the likely hunting area to duplicate it statistically, the hunting movement of grey wolf. Alpha is the finest possible solution. The 3 top solutions discovered so far oblige some other searching actors to relocate them self in conformity with the locations of the top search actors. The locations of the wolf are changed as shown in following equation.

$$\vec{E_\propto} = \left|\vec{D_1} \cdot \vec{t_\propto} - \vec{Y}\right|, \vec{E_\beta} = \left|\vec{D_2} \cdot \vec{t_\beta} - \vec{Y}\right|, \vec{E_\delta} = \left|\vec{D_3} \cdot \vec{t_\delta} - \vec{Y}\right| \qquad 3.26$$

$$\vec{t_1} = \left|\vec{t_\propto} - \vec{B_1} \cdot \vec{E_\propto}\right|, \ \vec{t_2} = \left|\vec{t_\beta} - \vec{B_2} \cdot \vec{E_\beta}\right|, \ \ \vec{t_3} = \left|\vec{t_\delta} - \vec{B_3} \cdot \vec{E_\delta}\right| \qquad 3.27$$

$$\vec{t}(u+1) = \frac{\vec{t_1} + \vec{t_2} + \vec{t_3}}{3} \qquad 3.28$$

The updating of the parameter $\vec{b}$, A final word on the Grey wolves, that controls the ratio of exploitation to research. As per equation, the parameter $\vec{b}$ is linearly modified using every iterations upto the 2 to 0 rang, with u are iteration number and m_i maximum number of allowed iteration for the optimization 3.25.

$$\vec{b} = 2 - u.\frac{2}{m_i} \qquad\qquad 3.29$$

3.3.1 Evaluate Fitness Function

The Gray Wolf Optimizer examines new areas of the feature set and utilizes alternatives iteratively till it discovers a satisfactory result. The optimal result is composed of all possible feature options for the RS coupled Grey wolf, and the wolf's placements represent feature set decisions. The choice of a feature subgroup is made using the fitness value, which is shown in equation 3.30.

$$Fitness = \propto^* \gamma_S (E) + \beta^* \frac{|D-S|}{|D|} \qquad 3.30$$

Where, $|S|$ is to select the letter denotes the entire number of attributes $|D|$. $\propto \in 0, 1$ and $\beta = 1 - \propto$, are two related variables for the categorization quality and subset length of the significance parameter. The equation has varied consequences for the attribute reducing tasks depending on the size and accuracy of the feature subset. The higher makes ensuring that the optimal location is at the absolute minimum an approximate set minimization. Every position's value is evaluated by using fitness values. The objective of study is to maximize fitness levels. Relevant characteristics are recovered from the collected MRI brain images after every MRI brain image fitness score has been determined, and identical characteristics are eliminated.

3.4 Tumour Classification based on Faster-RCNN

The important features chosen using RS-GWO are categorized by FR-CNN to forecast the total survival rate. The R-CNN requires a forwarding run over the neural network to retrieve characteristics for every object proposal, adding a considerable amount of computational cost. This issue is reduced by using a faster R-CNN. Utilize the equivalent convolutional layers for both the RPN and Faster R-CNN analyzers once they achieve the maximum capability. The images are only processed over the CNN once within order to create and improve item suggestions. This suggestion is turned to a fixed-size feature space using the Region-of-Interest layers, then transferred to CNN's final convolutional layer. Furthermore, use boundary box analysis and Softmax categorization to derive the required carrying components. Figure 3.2 depicts the entire Faster R-CNN framework.
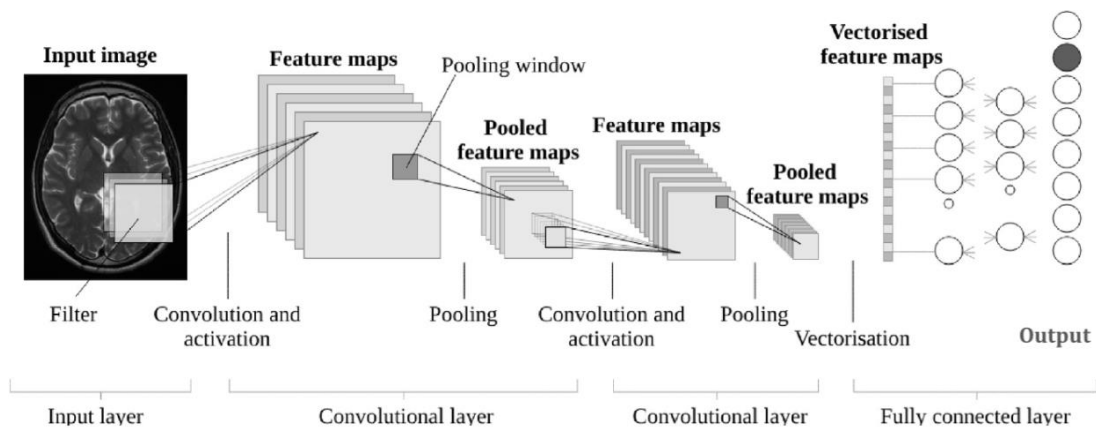

Figure 3.2: Faster-RCNN Network Model

The 3 stages of the faster R-CNN tumor diagnosis technique are the convolutional layer, regions proposal network (RPN), and boundary box forecasting. Filtration helps in extracting relevant image characteristics in the convolutional, which is accompanied by a limited system of RPNs moving over the convolutional to

forecast whether or not the cancer is identified. If the tumor is identified, the bounding box is utilized by fully - connected channels to identify the component in MRI images. In the overall process of conventional Faster R-CNN extra, the convolution layer is swapped out for a feature extraction system architecture, such as ResNet20, to increase the performance of tumor recognition.

***Convolutional Layers*:** The Four pooled levels are utilized to extract image feature mappings in addition to the 14 convolutional layers and 14 Relu levels. The feature mappings for subsequent RPN levels and full interconnectivity levels are identical.

***Region Proposal Networks (RPN)*:** This approach produces the area selections. The RPN model generates suggestions after going through 34 convolutional layers that create foreground anchoring and boundary box-regressed intervals. This area recommendation system takes a feature mapping created by convolutional from a baseline layer as feed and generates anchoring by applying sliding windows convolutional to the feature mapping.

RoI Pooling: While using network layers, obtain the proposals into the entire connection layer that followed various feature mappings. The Region-of-Interest layers, which serve the identical purpose as Fast R-CNN in turning varying RPN area offers into fixed-size features maps, get the result of the area proposals as inputs and transfer it to the next layers.

Softmax and Bounding Box Regression: In order to flatten the images, and feature mappings prior to delivering the outputs of two simultaneous fully connected layers, which are assigned a distinct task, two fully-connected layers receive the feature dimensions acquired by the Region-of-Interest pool.

In equations 3.31, the loss functions of the FRCNN are indicated. in which q_j being a thing. $u_j = \{u_a, u_b, u_c, u_d\}$ is a vector containing the 4 parametric parameters .Truth region by the affirmative anchoring u_j^*. 3.32. The logarithm loss objective and non-target are shown as in Equation 3.33 as $M_{cls}(q_j, q_j^*)$.

$$M(\{q_j\}, \{u_j\}) = \frac{1}{O_{cls}} \Sigma_j M_{cls}(q_j, q_j^*) + \delta \frac{1}{N_{reg}} \Sigma_j q_j^* M_{reg}(q_j, q_j^*) \qquad 3.31$$

$$q_j^* = \begin{cases} 0, & negative\ label \\ 1, & positive\ label \end{cases} \qquad 3.32$$

$$M_{cls}(q_j, q_j^*) = -\log[q_j^* q_j + (1 - q_j^*)(1 - q_j)] \qquad 3.33$$

$$M(u_j, u_j^*) \quad M_{reg}(u_j, u_j^*) = R(u_j - u_j^*), \quad \text{where} \quad (q_j^* = 0), \quad \text{and} \quad q_j^* M_{reg}$$

represents the only the foreground $anchor(q_j^* = 1)$ has a regression loss. The N_{cls} and N_{reg} are utilize the cls and reg of $\{q_j\}$ and $\{u_j\}$, respectively. The deep learning method's categorized outcomes are the normalized findings. This dynamic computation uses deep learning to accomplish long-tailed categorization while reducing the entire processing cost. The accuracy of categorization training performances will increase with the creation of such a Faster RCNN.

3.4.1 Multilevel Layer modelling for Survival Prediction

Depending on available data, dynamic systems can change their variables, and architecture, or select important spatial or temporal regions in the inputs. Considering that various parameters may require for preprocessing. it is typical to carry out prediction utilizing dynamic architectures based on each input. One can change the network depth and width as well as execute dynamic routing that consists of several

feasible channels. In addition to avoiding pointless computations for conventional 'easy' patterns, systems with dynamic designs also maintain overall representational capability while recognizing non-canonical 'difficult' sample data. The investigators found the total of 80 people led to enhanced performance for malignant identification on a distinct tumor through 10-fold cross-validation.

3.4.2 Multi-Scale Dense Network (MSDnet)

Interpretation with variable complexity is an easy approach to eliminate extra processing using deep neural networks to get deeper and deeper to recognize more challenging data. The high-resolution characteristics lack the coarse-level data necessary for classification, which leads to disappointing early departure conclusions. This multi-scale dense network (MSDNet) uses two techniques to solve the issue at hand: 1) a multi-scale framework made up of a large number of sub-networks for producing coarse-level characteristics appropriate for categorization depending on attribute spatial information of different pixel density and size 2) interconnection to utilize initial and enhance model. Such a specially constructed framework significantly increases the overall effectiveness of the network's classifications.

The classifier inside coarse-scale systems at their coarsest level use dense connection features as a component of MSDNets, S, l utilises all the characteristics $[x_1^s, \ldots x_l^s]$. The model delivers the most current prediction in the anytime phase after propagating the input across the networks till the resource is exhausted. That after classification, a sample exits the networks f_k If the forecast confidence in the batching cost setting using the softmax probabilities maximum value—exceeds a predetermined cutoff point at testing time θ_k. Let that q is consistent across all

levels, allowing us to determine the likelihood that a sample can leave classification k as:

$$q_k = z(1-q)^{k-1}q$$ 3.34

3.5 Result Analysis

The various evaluation parameter was used for prediction which is described below. According to these factors, the outcomes are determined. A thorough assessment was presented by Wankhede, D. S.et al.,(2021) and compares the suggested MFCM-RSGWO-FRCNN to the previous CNN Abdel-Gawad et.al.,(2020) - Miao, J., et al.,(2020), Yogananda, C.G.B et al.,(2020)- Zaw, H., et al.,(2019), and VGG16 Kaur, G.et al.,(2020) techniques. It had been suggested Veeramuthu, A. et al.,(2022)- S. L. Bangare, et al.(2018) to use combined approaches to classify the brain tumor. This research used a core python programming approach.

Using a Core i7 processor running at its highest possible frequency of 3.5GHz and 8 GB of devoted DDR4 class memory under Windows 11 Home, the operating status of the suggested ways in the platform 3.8.0. To reach the desired outcome, the simulation must run for about five to ten minutes with a maximum of 100 iterations detailed result analysis shown in following table 3.1.

Table 3.1- *Result Analysis*

Method	Accuracy (%)	Sensitivity (%)	Specificity (%)	Time (sec)	Parameter	Layer
CNN-Inception-V3	92.01	91.96	89.2	20.34	24 million	43
CNN-AlexNet	92.96	91.96	89.1	73.97	60 million	13
VGG16	91.5	92.5	91	45.1	138 million	16
Proposed MFCM-RSGWO-FRCNN Model	93	93.12	93.43	10.99	2 million	48

3.5.1 Description of Available Datasets

The publically available Kaggle dataset, as well as the private dataset collected from TMC, were utilized as the basis of the construction of the suggested solution. It comprises 1000 MRI scans of brain tumor images. This available dataset relates to the expression of genes in glioma. Malignant brain tumor, which are the development of aberrant brain tissue, are what are known as malignant tumor. The 70% training data select randomly. The 30% testing data were used.

3.5.2 Simulation Output

Real-time brain images of patients with tumor and people without tumor are used to assess the effectiveness of the suggested its outcomes are evaluated to those of conventional methods FCM, two distinct real-time MRI brain images are used for identifying abnormalities in the brain.
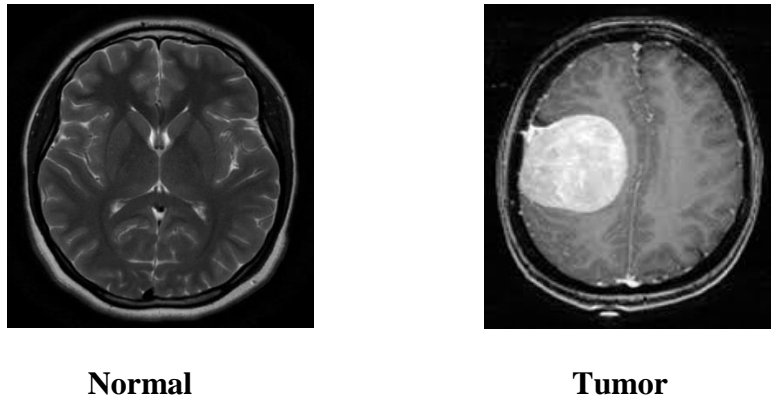
Normal   **Tumor**

Figure 3.3: Represent the Normal and Tumor Images

Source: TMC Data Shared Normal images

A representative MRI image of the brain from the dataset is shown in Figure 3.3. The publically available dataset was retrieved from Kaggle. The datasets contain two sets of brain MRI images; normal, and glioma. The dataset can be categorized into two units 70% is used for training, and 30% is used for testing.

(a)   (b)
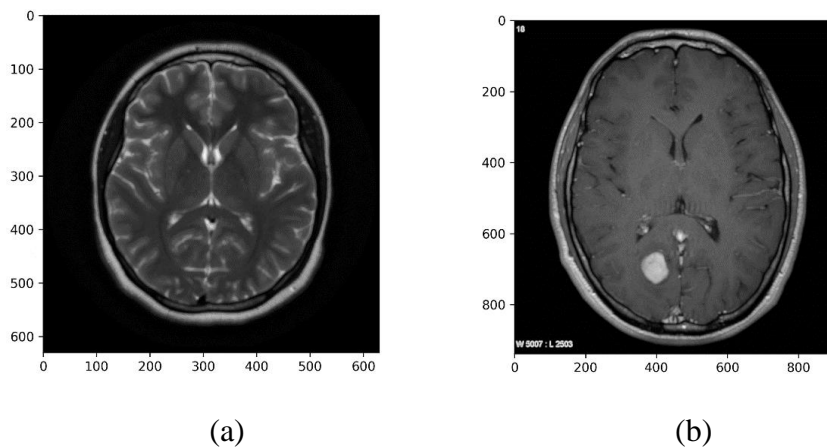
Figure 3.4: Filtered Images of Brain Tumor

The processed are shown in Figure 3.4. The crucial step is to examine images with a suitable brain tumor and determine are filtered using the histogram normalization technique.

102

(a)   (b)
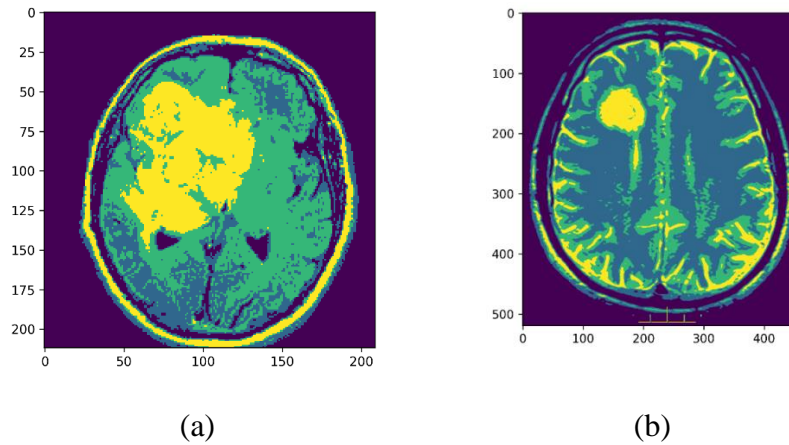
Figure 3.5: segmented Image of Brain Tumor

Figure 3.5 shows the segmented image of a brain tumor with various regions. The Green region (C1) shows the enhanced region. Blue region (C2) shows the necrotic. T1 shows the hypo-intensive region i.e, abnormal. C4 and C5 show the hyper intensive region with FLAIR.
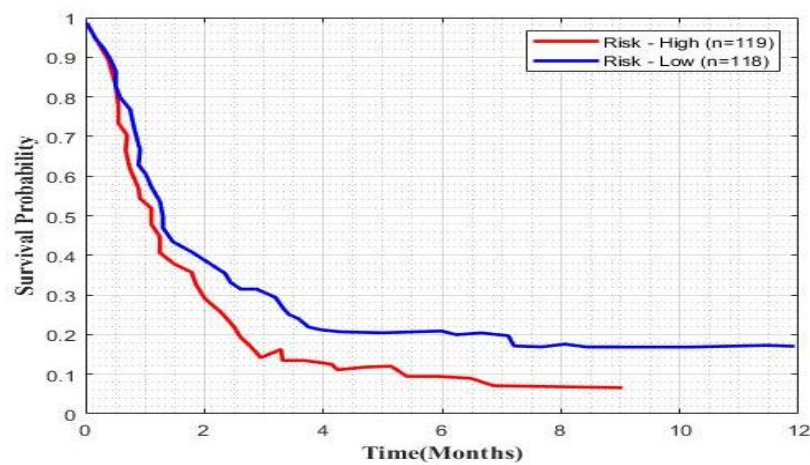
Figure 3.6: Overall Survival rate Probability of patients

The Time duration of survival rate of the various therapies are depicted in Figure 3.6 with respect to the age of patients. The results demonstrate that the risk profile succeeded well in determining the survival rate of Glioblastoma.

103
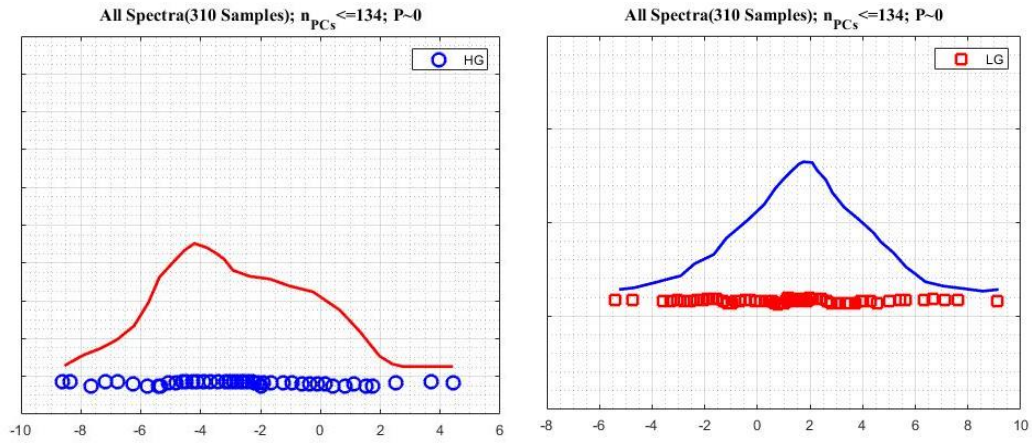
Figure 3.7: High-quality (HG) versus Low-quality (LG) specimens

Brain cancer types with high and low grades tumor are contrasted in Figure 3.7. The proposed method was utilized to show how high-grade and low-grade histological data were separated. There is a lot of as shown in Figure 3.7.

3.5.3 Performance Evaluation Parameter and Comparative Result Analysis

This research measured the various performance parameters used for predicting the survival rate from various dataset sizes which contain 50 to 1000 brain images.

3.5.3.1 Segmentation Time

Time measuring the duration of image segmentation for a pre-processed MRI brain image(S_t).

$$S_t = T_t - I_t \qquad\qquad 3.35$$
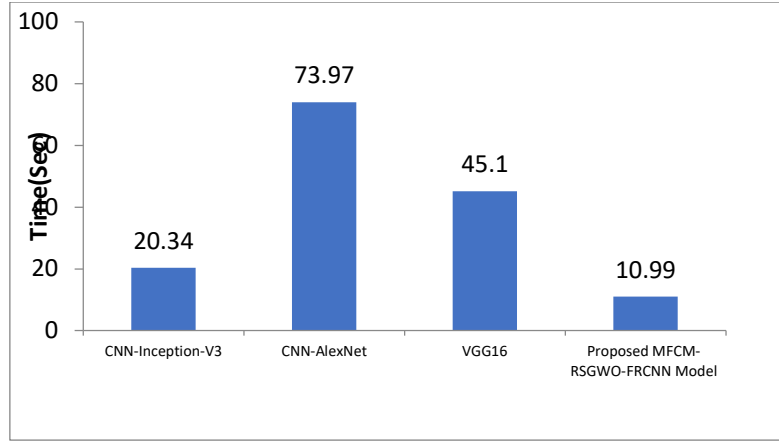
Figure 3.8: Bar represents the Comparative analysis of Segmentation Time

Figure 3.8 shows the total segmentation time findings from various MRI images with 50 to 1000 sizes of the brain image. It shows the segmentation time of the suggested method is marginally faster. The suggested method segments the images in 10.99 seconds, while the results of the existing method are 20.34,73.97 seconds, 45.1 seconds, and 62.78 seconds, respectively. The proposed strategy, which is illustrated in Figure 3.8, is ideal for precisely segmenting the tumor area.

3.5.3.2 Sensitivity Rate

Sensitivity is a metric for how well a tumor's damaged area can be found in the given MRI brain image. Whenever the outcome is affirmative, highly sensitive testing is much more useful. Equation 3.36 indicate the sensitivity.

$$S_n = \frac{T_{ed}}{T_{ed} + T_{ded}} \qquad 3.36$$

Where, T_{ed} shows the tumour is present and detected images, T_{ded} shows the tumour not present and not detected in MRI image.
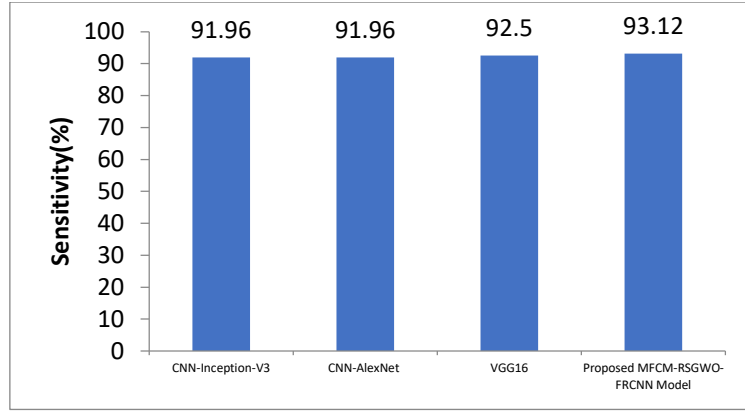
Figure 3.9: Bar represents the Comparative analysis of Sensitivity rate

Figure 3.9 depicted the overall sensitivity approaches for the whole dataset of MRI images which ranges from 50 to 1000. The proposed method generates an overall of 90% about any set of image data between 50 and 1000 image size. In comparison, the suggested DL technique performs significantly superior in terms of predictions and identification of the total survival rate of patients.

3.5.3.3 Specificity Rate

The ability to accurately spot the tumor-free zone on a collection of MRI dataset images is known as specificity rate. Maximum survival prediction rate findings lead to maximum specificity scores. Equation 3.37 indicates the specificity formula.

$$S_p = \frac{T_{ded}}{T_{ded} + T_{dep}} \qquad\qquad 3.37$$

Where, T_{dep} is the total number of MRI images that the tumour is not present but is detected.
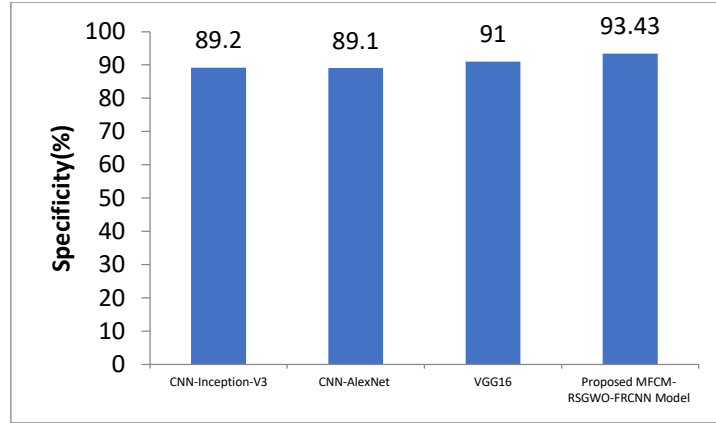
Figure 3.10: Bar represents the Comparative analysis of Specificity rate

Figure 3.10 shows the overall specificity, It is found that the proposed approach gives the maximum specificity as compared to existing algorithms. As a result, the suggested DL technique extracts improved non-tumor identification from the provided images.

3.5.3.4 Dice Score (Index)

Disc score is used to measure the overlap between two or more two images.

$$Dice\ Index = \frac{2\left|A_I \cap B_I\right|}{\left|A_I\right| + \left|B_I\right|} \qquad 3.38$$

Where, $A \in \{0,1\}$ is the extracted tumor area .The maximum disc score is represented by 1. The maximum disc score shows more overlap between the images with good performance.
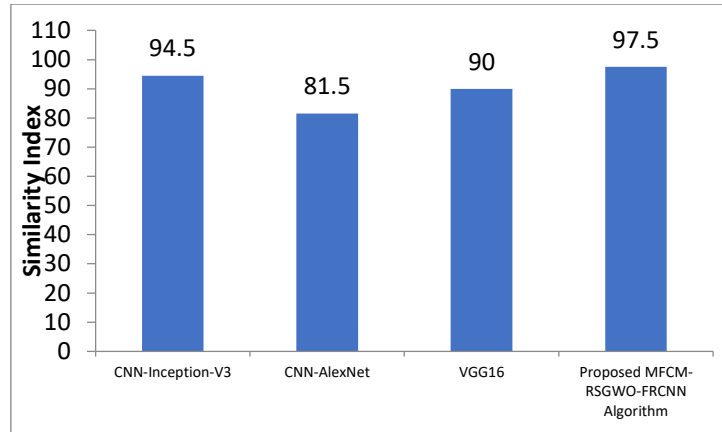
Figure 3.11: Bar represents the Comparative analysis of Dice Score

Figure 3.11 shows the Disc score of actual MRI images. Furthermore, the Dice score gauge segmentation results are used to measure the MRI Image dataset segmentation effectiveness.

3.5.3.5 Mean Square Error

The square in the forecasting system of the numerical data is which is a measurement of the fluctuation between the data. It is expressed in equation 3.39 and is widely regarded as an extraordinary error measure for mathematical data forecasting.

$$MSE = (EI_p - AI_p)^2 \qquad\qquad 3.39$$

Where E is the calculated value and A is the real value of MRI brain images

The MSE rate is 78 percent higher for dataset sizes ranging from 50 to 1000 as comparable algorithms like CNN-AlexNet and VGG16. By using the square procedure to evaluate a strategy's capacity to identify distinct sections, this metric increases the influence of the segmented image in the sample of brain image information.

3.5.3.6 Peak Signal to Noise Ratio

The PSNR is quantified in decibels (dB). The PSNR is measured using equation 3.40 as shown below.

$$PSNR = 10 \: log_{10} \frac{p^2}{(EI_p - AI_p)^2} \qquad\qquad 3.40$$

Where p is maximum pixel intensity present in MRI images.

The Peak-to-Signal-Noise ratio (PSNR) of various MRI brain images with the size of 50 to 1000 image pixels. The PSNR value is around 45% is the maximum as compared to an existing one.

3.5.3.7 Survival Prediction Rate

MRI brain images among all MRI brain images is known as the survival prediction rate. This metric is also known as the accuracy score of survival successfully predicted based on the classification of brain tumor. This can be measured and expressed in percentage, as shown below.

$$Ac_{pre} = \frac{NI_c}{TI_{MRI}} \qquad\qquad 3.41$$

Where, Ac_{pre} is the survival prediction rate or survival accuracy score, NI_c is the proportion.
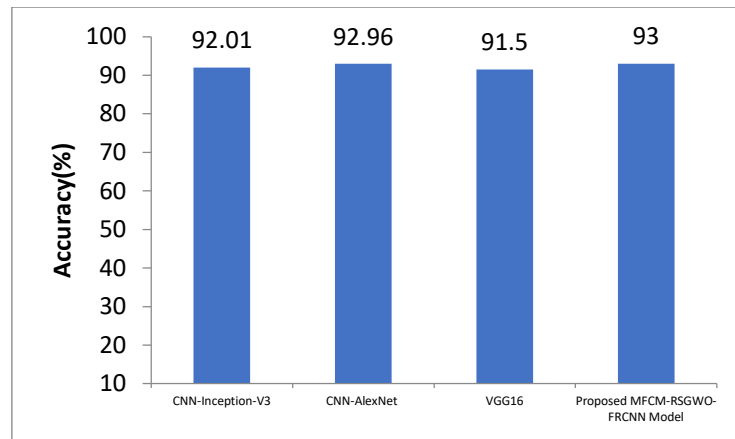
Figure 3.12: Bar represents the Comparative analysis of survival prediction rate

Figure 3.12 analysis of the standard benchmark MRI image dataset. As per the final experimental findings, the accuracy score of prediction is roughly 10% higher than the comparative methodologies for every different database. For example, the minimum size of the dataset is 50, and the proposed strategy yields 94.1%, compared to 72.67 and 80.1 for the approaches, respectively, from the existing methodologies. The proposed strategy gives an approximately 93.0% accuracy score in predicting the total survival rate of brain tumor for most other kinds of datasets as well.

Contribution of this Chapter

- This chapter proposed a model based on MFCM-RSGWO-FRCNN approach for the detection.

- The suggested method consists of four steps. The initial stage involves gathering the MRI brain data for utilization from a fixed website and preprocessing it to get rid of all the impurities. The MRI brain images also include several types of distortion, such as salted and speckle noise and Gaussian distortion. Furthermore, in certain instance, MRI images are

collected using different scanning devices, and imaging intensity is used to normalize the MRI images.

- As a result, preprocessing includes Pixel by statistical normalizing and denoising using filtering is to build the database by removing unwanted data and restoring missing features from MRI images.

- The MFCM classification technique is then used for segmentation utilizing radiomic characteristic data. Countless features may be retrieved from the segmented MRI brain images. The most important and instructive aspects from the retrieved important features.

- The categorization for overall survival rate estimation is then completed to features chosen in MRI brain images using a FR-CNN technique. As a result, the suggested classifier improves accuracy while requiring shorter training time and a faster converging rate.

- The proposed strategy gives an approximately 93.0% accuracy score in predicting the total survival rate of brain tumor for most other kinds of datasets as well.

CHAPTER 4

Recurrence risk prediction based on deep neural networks for brain glioblastoma multiform

4.1 Overview

As per the World Health Organization, the 722 to 80 age peoples in the US has the largest frequency of Glioblastoma, and it rises over time. The highly malignant astrocytic tumor exhibit fast cellular proliferation, necrotic, intravascular development, and structural variability as morphological features. Due to improvements in multimodal therapeutic options and MRI technologies, Glioblastoma patients have poor prediction thoroughly describe by Wu, W. et al.(2021). Sick people who don't obtain some therapy after being diagnosed pass away quickly, while those who get the best care often survive. Long-term survivability or just a few successful cures have now been documented by Li, H.,et al.,(2020). Ultimate mortality ratio estimated by Chato, L., & Latifi, S. (2021). Malignant tumor therefore has a poor prediction depending on the increased risk of tumor progression mentioned by Shim, K. Y. et al.,(2021). Following an average survival duration of 33 to 37.

4.1.1 Recurrent Glioblastoma Following Nivolumab and Bevacizumab

People with recurrent Glioblastoma have survival ratios after two years that range from 27% to 34% on existing therapeutic options 4-6, and survival rates for 5 yrs are fewer than 11%. New techniques are thus needed to enhance Glioblastoma treatment prognosis investigated by Priya, S. et al.,(2021). The main pathophysiology of GBM involves angiogenesis, which is characterized by increased production of vascular endothelium development factors. Several cutting-edge anti-angiogenesis methods

112

may hold promise for patients with recurrent Glioblastoma conveyed by Zuo, S.et al.,(2019). Patients with Glioblastoma had an improvement in PFS and good radiographic response times in 2010 mentioned by Hajianfar, G. et al. (2019). Due to the encouraging PFS outcomes, bevacizumab may not alter total survival in certain periods. Bevacizumab generated inconsistent results in respect of OS and PFS in large RCTs, in contrast to several similar anti-VEGF treatments as cediranib (a VEGF inhibitor), participants were also given analysed by Hashemzehi, R. et al.,(2020). Therefore, a meta-analysis incorporating VEGF and anti-VEGF is urgently needed mentioned by Lee, M. et al.,(2019) to examine the outcomes of gbm therapy for individuals with recurrent Glioblastoma.

4.1.2 Medical Image Modalities

Tumor grade, medication effectiveness evaluation, diagnostics, treatments, and other cerebral abnormalities are all important aspects of MRI. Many additional MR imaging methods have been developed to evaluate several biophysical characteristics of brain cells objectively discussed by Amin, J. et al(2018) - Özyurt, F. et al.,(2019). With a 92% efficiency and 86% specificity, Hsieh et al. proposed the logistic regression approach to effectively distinguish glioma from diffused lower-grade glioblastoma concluded by Thakur, T. et al., (2021). These are more approachable and resistive in the various analyses and acquiring procedures, but the data on the recurring tumor is lacking. In earlier studies, the results of patients who had their recurrent Glioblastoma tumor removed were evaluated subsequently Deepa, B et al.,(2021). In a minimum one of the trials, it was discovered that the amount of surgical intervention, the period between the first and second operations, baseline KPS grade, and aging were all

significantly related to Survival verify by Shim, Ka.et al.,(2020). It didn't offer any prior instructions while they thought about doing treatment on sick people.

4.2 Proposed RNN-GAN Model

People with gbm with grade IV tumor, suffer a short overall survival. Doctors are extremely interested in of recurring gbm tumors for treatment planning and accurate treatment. To forecast the diagnosis of an illness, a brain MRI study uses. As a result, helpful data is provided for customized therapy. Tumor shrinking is a possible relevant secondary aim if it correlates with increases in either patient's well-being or Survival. PFS and ORR are employed to quantify the postponement of tumor progression. These relationships have since been consistently demonstrated for other cancers and traditionally minimal stability is seen for glioma.
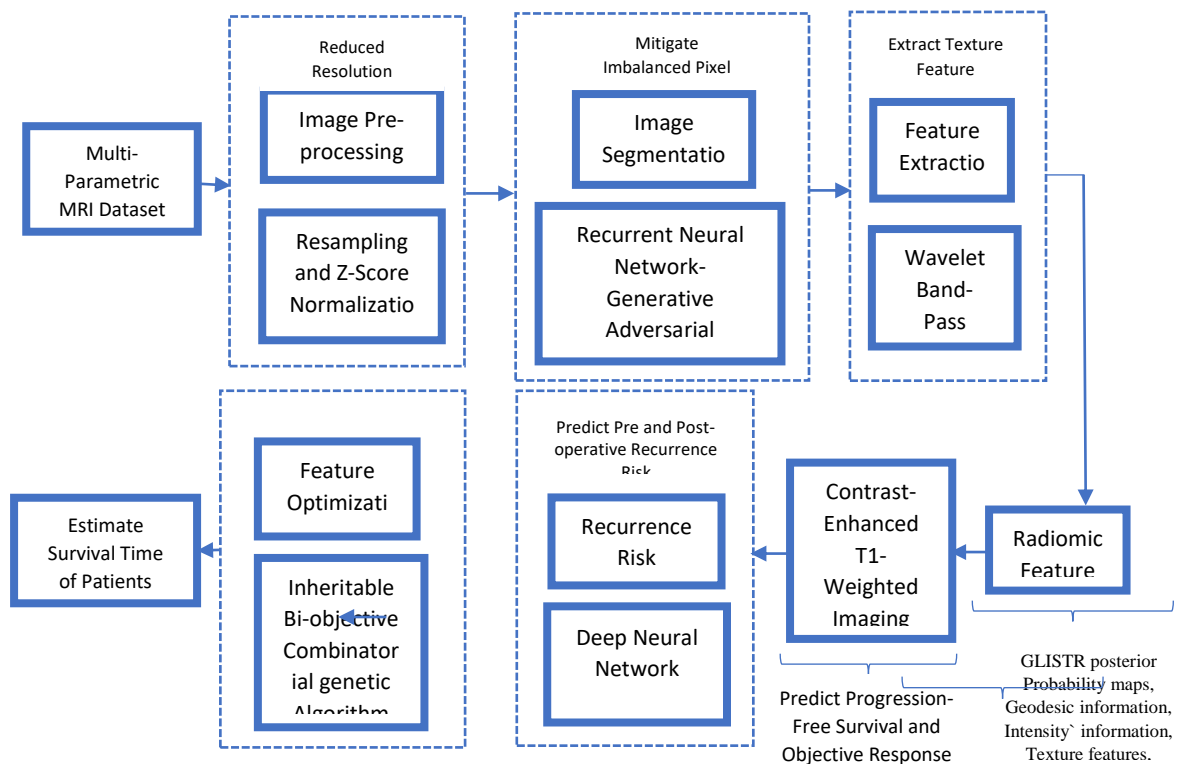
Figure 4.1: Architecture of Proposed RNN-GAN Model

The general structure of the suggested framework based on RNN-GAN is shown in Figure 4.1. Preprocessing, Z-score normalization, and spatial resampling are performed in step 1, followed by recurrent GAN techniques for tumor segmentation in step 2, radiomices texture based feature extraction (FE) is done based on wavelet band-pass filtering in step 3, and RF classifier was used to predicted recurrent glioblastoma in step 4.

4.2.1 Patient Population

There is no requirement for specific aware permission for this retrospective analysis, and it has been allowed by the regional Institutional Assessment Boards. Therefore, 80 patients in all were recruited for this study. Before beginning any sort of therapy or procedure, multiparametric MRI exams were carried out, except for Grade-I glioblastoma. The prediction deep models are constructed using an ML technique depending on the AUC and ROC of this network as determined by a 10-fold cross-validation. The effectiveness of the deep learning approach was contrasted with that of Bevacizumab and Nivolumab. Subsequently, 80 individuals were enlisted together with their medical characteristics.

4.2.1.1 Multi-Parametric MRI Dataset

For accurate medical medication selection, the characteristics from a multiparametric MRI-based radiomic feature analysis are used for forecasting, diagnosis, and identification assessment.

4.2.2 Pre-processing

Image Pre-processing is usually necessary following image capture to minimize physiological responses, such as breathing and head motions, as well as artifacts and biases in MRI data induced by MRI screening. It then contains image co-registration, bias field correction, intensity normalization, image pixel size re-sampling to lessen quality volatility, and skull reduction.

4.2.2.1 Resampling Image Pixel

Upsampling and pixel size quantization are necessary pre-processing processes in radiomics investigation, although it is unclear how pixel size and slice thickness affect radiomic features. Consequently, ICC was used to verify feature resilience:

$$ICC = \frac{MS_R - MS_E}{MS_R + (k-1)MS_E + \frac{k}{n}(MS_C - MS_E)} \qquad 4.1$$

Where n is total patients, MS_R is represents as MS_C, The ICC technique is used to evaluate the consistency and repeatability of numerical data in groups. It offers the advantage of enabling evaluations between more than two variable sets.

4.2.2.2 Z-Score Normalization

The Z-Score method includes removing the mean intensity of the area or whole images of concern, then dividing each pixel value by the associated standard deviation.

$$I_{z-score}(x) = \frac{I(x) - \mu_{zs}}{\sigma_{zs}} \qquad\qquad 4.2$$

Spatial data preprocessing is required during training in as to ensure that regions across MRI brain images have connections and comparable spatial arrangement, and it is important since CNNs often do not take into account the metadata related to brain images. A frequent spatial preprocessing technique in medical brain imaging is resampling.

4.2.2.3 Recurrent Generative Adversarial Network for Image Segmentation

This research presents the recurrent GAN approach for semantic segmentation of medical brain images. g is the GAN model which is based on traditional GAN

$$\min_{g} \max_{d} \; V(d,g) = E_y\left[\log d(y)\right] + E_z\left[\log\left(1 - d(g(z))\right)\right] \qquad 4.3$$

The discriminator utilizes the real data and the final output to determine if the predicted label is accurate or false, even though the final predicted segmentation is at the pixel levels.

$$L_{adv} \leftarrow \min_{g} \max_{d} \; V(d,g) = E_{x,y_{seg}}\left[\log d(x, y_{seg})\right] + E_{x,z}\left[\log\left(1 - d(x, g(x,z))\right)\right] \quad 4.4$$

In addition, the investigation employed a combined classification accuracy score by giving the less characterized set of pixels a higher value. The loss l_{acc} as given in equation 4.4 reduces unbalanced training data while elevating their significance throughout the learning process. Equation 4.5 is then used to calculate..

$$L_{RNN-GAN}(d,g) = L_{adv}(d,g) + L_{L1}(g) + L_{l_{acc}}(g) \qquad\qquad 4.5$$

To reduce the impact of uneven pixel labelling on medical brain images, Given that the mechanism takes the premise that all possible transition possibilities are equal, categorizing cross-entropy loss combined with adversarial loss provides an unbiased estimation for minimizing the risk. Complementary labels can produce more precise outcomes for a semantic segmentation challenge in addition to the usual losses.

As a result, when the MRI sequence is not specifically designed to identify tumor, two different lesions may seem practically similar and exact segmentation can be difficult.

4.2.2.4 Radiomic Feature Extraction

To further create the radiomics signature, additional components from both inferred and original MRI images are included. Additional Wavelet transform-based features have bigger significance coefficients regarding survival rate, which affects the radiomics signature model.

4.2.2.4.1 Contrast-Enhanced T1-Weighted MRI Imaging

The gold standard for detecting brain tumor is contrast-enhanced T1-weighted MRI scanning. It is straightforward to execute and accurately depicts the borders of typical brain tumor as well as dual-based lesions. T2-FLAIR imaging is widely employed in such circumstances because it differentiates abnormal signals from the normal brain parenchyma. Low-grade gliomas seldom ever show vasogenic edema, hence T2-FLAIR imaging is quite helpful for evaluating tumor size. All are hyperintense in T2-FLAIR sequences, however, high-grade gliomas provide a challenge for T2-FLAIR imaging because it cannot reliably discriminate between

infiltrating tumor and vasogenic edema. Enhanced imaging methods are routinely utilized to differentiate recurrent/residual tumor from post-treatment changes. The most often used enhanced imaging methods are MR spectroscopy, PWI, and DWI. Each of these can typically enable the radiologist to employ a careful synthesis after a tumor is appropriately differentiated from post-treatment modifications; thus, neither of these approaches has shown to be particularly precise. Drawn to identify the radiomic properties as the input volume. The 87 radiometric characteristics, comprising, were obtained from nine different MR sequences. Eleven different form characteristics were used in the investigation.

4.2.2.4.2 Wavelet Band-Pass Filtering

The scaled and translated functions $\psi_{m,n}(r)$, the wavelet transforms correlates to the disintegration $S(x)\varepsilon L^2(Q)$.

$$d_{m,n} = \frac{1}{\sqrt{2}} \int S(x)\psi * \frac{x-n}{m} dx \qquad\qquad 4.6$$

where the whole inverse function is expressed by $k \ \varepsilon \ Q^+$, $k \ \varepsilon \ Q^+$, and $*$. An experimental bandpass wavelet function's shifting and scaled variations, as well as low-pass scaling functions $R(z)$ shifted versions, a single-dimensional signal $y(z)$ is defined by the discrete wavelet transform (DWT):

$\psi(r)$ can be represented as:

$$\psi(r)=\begin{cases} 1 & 0 \leq r < \frac{1}{2} \\ -1 & \frac{1}{2} \leq r < 1 \\ 0 & otherwise \end{cases} \qquad\qquad 4.7$$

The Haar function $\psi_{m,n}$ is known as real line Q using the equation $\psi_{m,n}(-r) = 2^{\frac{m}{2}} \psi(2^m r - n)$, $r \varepsilon Q$ for each pair m,n of integers in Z.

The single-dimension DWT separates the MRI images into sub-images, and the three sub-bands offer data about this division and one offers an estimate. The brain MRI images produced via estimate will look similar to the original yet have varying sizes. The DWT separates a picture into horizontal and vertical components based on poor resolution. The high and low pass filters separate the picture into several sub-bands. When taking into account the DWT, the final result produced by estimation approach. When the approximate image is obtained, the process is paused, and the average outcome is calculated.

The convolution of the observed vibration signals by

$$s_b(t) = s(t) \times h_c(t) \qquad\qquad 4.8$$

Where $s_b(t)$ $f_L \sim f_H$. With changing, the filter's properties may be made suitable. Zero phase shift was carefully designed into the wavelet-based band-pass filter. The wavelet cluster as an electronic filter creates the analytic signal and simultaneously performs envelopes demodulation.

To guarantee that retrieving precision is represented for every approach, a protocol for feature extraction has been followed. This building shows the combination of all the basic parts.

4.2.2.4.3 Recurrence Risk Prediction

Glioblastoma tumor recurrence risk prediction is crucial because it raises patient survival ratios and decreases patient mortality. This problem is thought to be resolved by the effectiveness of the RF and DNN approaches.

4.2.2.4.3.1 Random Forest for Classification

Predicting the likelihood of a glioma tumor recurrence is essential. Depending on the outcome feature. It is believed that the success of the RF and DNN techniques will overcome this issue. To assess the importance of features and balance data in classification jobs, RF is a powerful approach. The RF technique is ideal for diverse datasets like these comprising patients with recurrent gbm since it resists overfitting due to the abundance of decision trees in the forest. All of such characteristics were initially assessed for their predictive power. The highest 128 attributes were used as input for the random forest method. The RF method was tested on the tested cohort using the learned RF techniques.

4.2.2.4.3.2 Deep Neural Network (DNN) Technique

All units in the layers are completely linked. The encoder has one or more data elements and a weight vectors X. The weighted sum of the outcomes for the preceding level h^{k-1} is utilized to determine the output h_j^k for the layer k comprising j units (especially $h^0 = x$).

$$g^k = W^k h^{k-1} + b^k, 1 \leq k \leq N \qquad 4.9$$

$$h^k = f\left(g^k\right) \qquad 4.10$$

The kth weight matrix between k^{th} layer and $(k-1)^{th}$ layer can be represented as W^k, Simultaneously, in the DNN structure, the softmax function for the output layer (N^{th} layer) is employed as an activation function and is specified as:

$$a^N = \frac{\exp\left(h^N\right)}{\sum_j \exp\left(h_j^N\right)}$$ 4.11

The weights is assigned to each layers of network based on the truncated normal distribution, as explained by

$$W \sim T\left[-\sqrt{\frac{2}{n_i + n_0}}, \sqrt{\frac{2}{n_i + n_0}}\right]$$ 4.12

n_i and n_o is the set of input/output unit. The deep learning approach fundamental architecture, that consists of numerous layers, is depicted in Figure 4.2.
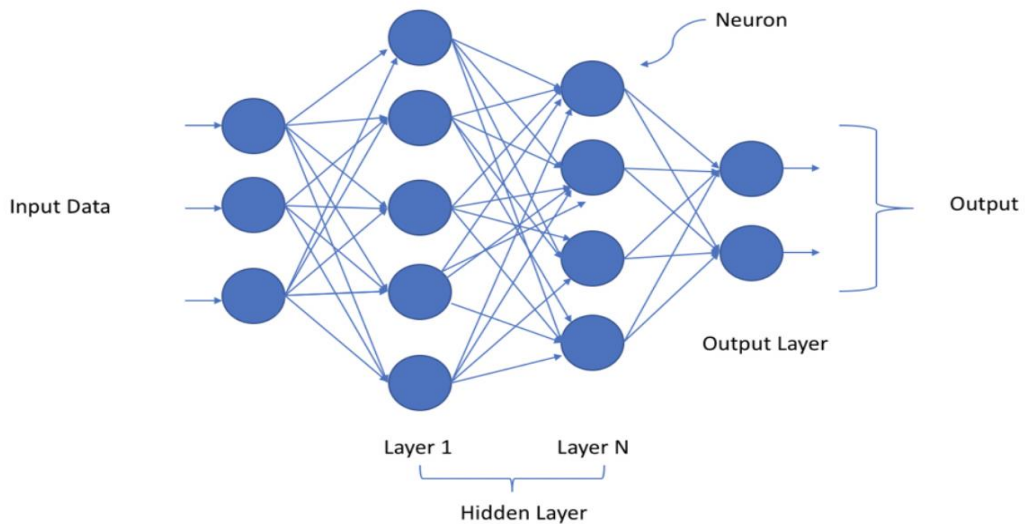

Figure 4.2: Layers of DNN

The gbm recurrence risk prediction job in this study is a binary classification problem, and the DNN model's objective function, also incorporates L2 regularization to help reduce the overfitting of the deep model. To minimize the loss function, the suggested DNN approach is described as follows:

$$L(y_t, \hat{y}_t) = -\frac{1}{N}\sum_{i=0}^{N}[y_t(i)\log \hat{y}_t(i) - (1 - y_t(i))\log(1 - \hat{y}_t(i))] + \frac{1}{2}\lambda\sum_{k=1}^{K}\sum_{j=1}^{n_k}\sum_{i=1}^{m_k}w_{ij}^{k\ 2} \qquad 4.13$$

Where, L is the errors among the labels' real values and the prediction results. $y_t(i)$ is the actual label for the ith class, $\hat{y}_t(i)$ is the predictive value to get the output layer. N is the batch size. $W^k = \{w_{ij}^k\}_{m_k \times n_k}$ is the kth weight matrix and K ($K=5$).

4.2.2.4.3.3 IBCGA

IBCGA is an adaptive approach for dealing with problems in optimization techniques that involve several factors. OED is also investigating how various influences affect the response parameter at the same time. The degree of an element influences its worth, and the OED is employed to discover the optimal level combination. An orthogonal array may compare the levels of items as a result of the analysis, which reduces the number of levels required proportionally. Every row in an orthogonal array shows the level of components in a certain combination, whereas the column shows which parts may be modified for each combination. The predominant impact of one factor on the response parameter is referred to as the major effect, and it is independent of the major effect of any other element. For example, an orthogonal design with p rows and $p-1$ columns having two levels (values of elements) is

designated as $L_P \left(2^{P-1} \right)$. The entity's major impact x having a level y is represented by

$$S_{xy} = \sum f_k . F_k, \quad k \ 1,\ldots,P \qquad 4.14$$

$$x = 1,\ldots,P-1 \qquad 4.15$$

$$y = 1,0 \qquad 4.16$$

Where, f_k represent the function that is used to measure the accuracy score from combined k and $F_k = 1$.

4.3 Result Analysis

The results of the recommended model, which uses a Deep Neural Network and Random Forest to accurately classify tumors, are shown in Table 4.1. A RF-DNN-based intelligent healthcare system is designed to accurately identify and classify brain cancers. The four categories that made up the publicly accessible Kaggle dataset included one no-tumor and three distinct types of tumors. Figure4.3 shows an example picture of a brain tumor, respectively.

Table 4.1- *Result Analysis*

Method	Accuracy (%)	Sensitivity (%)	Specificity (%)	Time (sec)	Parameter	Layer
CNN-Inception-V3	94.23	94	81.1	20.34	24 million	43
CNN-AlexNet	82	80	96	73.97	60 million	13
VGG16	95	95	96	45.1	138 million	16
Proposed RNN-GAN Model	95.11	97	98	9.45	7 million	20

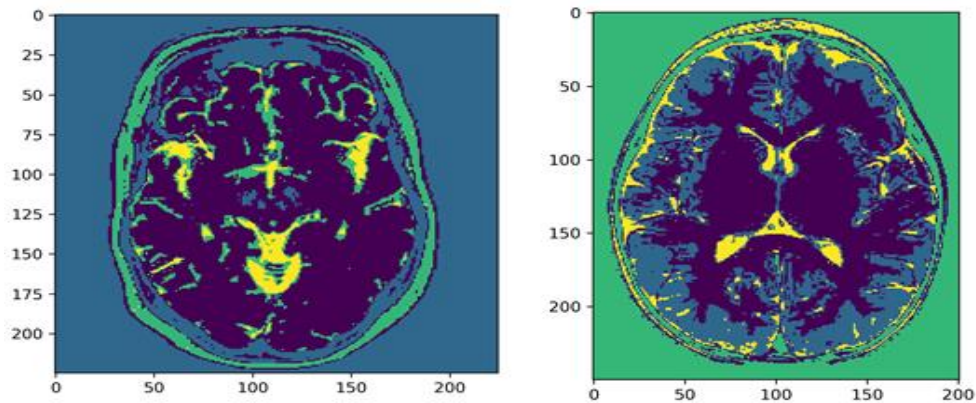**Figure. 4.3:** Sample Images for MRI Brain Tumour

The 10000 MRI brain tumor brain images were employed in the suggested model. The proposed deep learning approach comprises two distinct phases: training and testing. In the training phase, 81% of the input photos are selected from each class, and 19% are used in the testing phase. Miss rate (MR) and precision are used to gauge how effective the model is.

Table 4.2: *illustrates the simulation system configuration of the suggested task.*

System Configuration

OS	Windows 11 Pro
Memory	16 GB DDR4
Microprocessor	Intel Core i7 @ 2.7GHz
Simulation Time	10.190 seconds

The suggested method is then examined and put to the test. The suggested work runs on Windows 11 Pro and has a 16 GB DDR4 memory capacity. The simulation duration for the job is 10.190 seconds, and it also uses an Intel Core i7 @ 2.7GHz CPU.

The RNN-GAN model applied to brain tumor glioma analysis, the hyperparameter settings depend on both the generator and discriminator networks, as well as their training strategies. Following are the hyperparameter configuration of suggested model.

Learning Rate: 0.0001 (for both generator and discriminator)

Batch Size: 32

Epochs: 100 (or more depending on the convergence)

Optimizer: Adam optimizer

Number of Layers: 2

Units per Layer: 128 units for each LSTM/GRU layer

Dropout: 0.2 (to prevent overfitting)

Activation Function: ReLU activation for the hidden layers

Output Activation: Tanh activation (to scale the generated outputs)

4.3.1 Statistical Analysis

The PFS and OS forecasts were assessed using the Kaplan-Meier technique. The suggested approach was then computed for survival assessment that utilized the significance threshold.
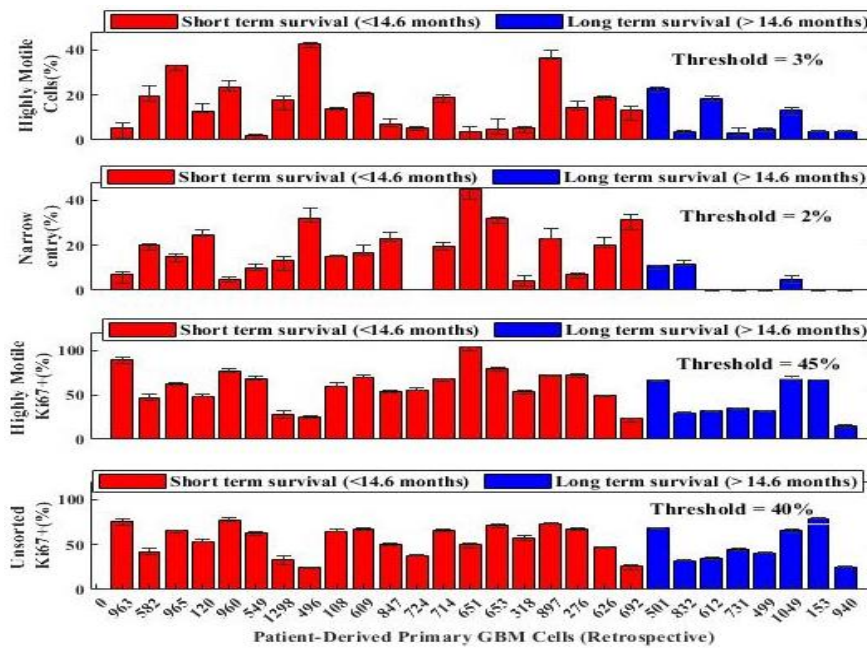
Figure. 4.4: Analysis of survival of RNN-GAN

Figure 4.4 shows the survival analysis of individuals with Glioblastoma. The patient derived from primary Glioma cells is then described, along with a prediction for both long- and short-term survivability. The survival study shows a short-term survival of fewer than 14.6 months and a long-term surviving of more than 14.6 months. As a result, the threshold values for the suggested approach are,

correspondingly, 3%, 2%, 45%, and 40% for limited entrance, various patients with long surviving, and less than short-term surviving.

ROC analysis was used for each brain imaging characteristic to classify both long- and short-term survivability. The two categories that performed the best were the size and texturing.

Figure. 4.5: Progression-Free Survival Score
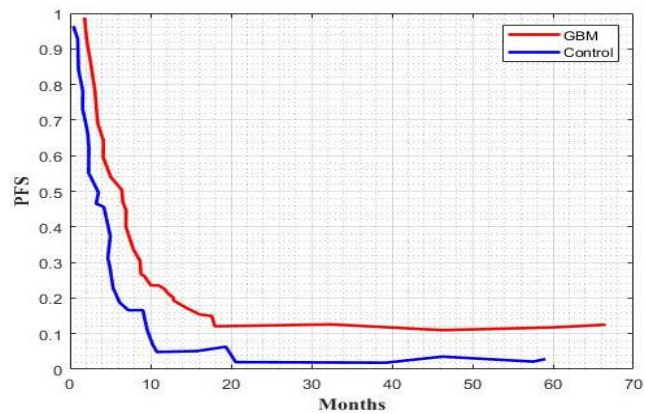
Figure 4.5 shows the Progression-Free Survival score of the proposed model. Progression-Free Survival is the time from randomization to the first sign of malignancy or the time till death from any cause. The Progression-Free Survival was then not markedly different between the Glioblastoma and the controls for various months.
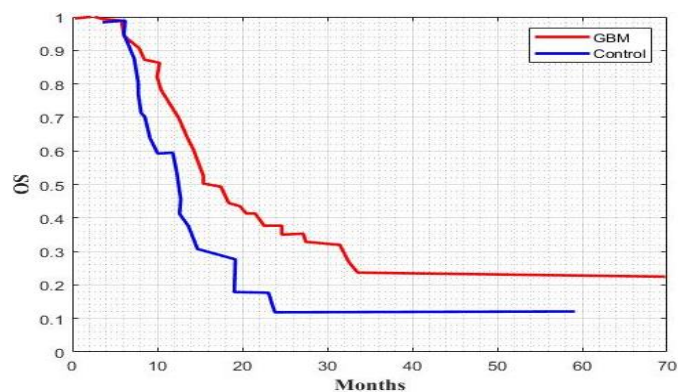

Figure. 4.6: Overall Survival Rate

128

The Overall Survival is predicted using the suggested approach as shown in Figure 4.6. The Overall Survival is assessed using the Kaplan-Meier technique; it was a primary result. The Overall Survival did not differ considerably from the Glioblastoma and the controls.
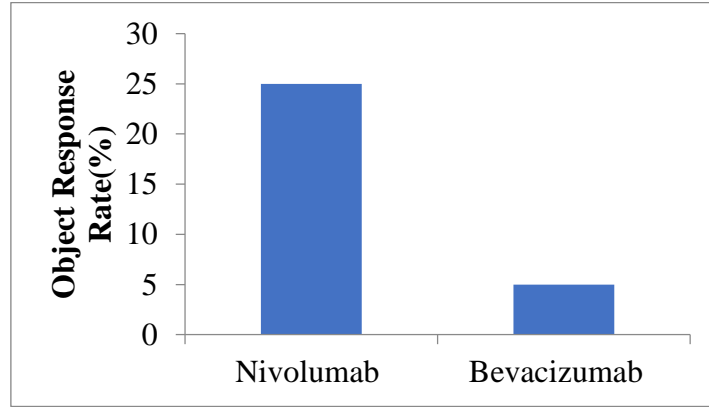
Figure. 4.7: Object Response Rate

Figure 4.7 illustrates the suggested approach to the objective response rate. As a result, it shows that individuals receiving nivolumab medication had a noticeably higher percentage of objective response than those receiving bevacizumab medication. This implies that nivolumab therapy was more effective than bevacizumab medication in terms of patient response.

4.3.2 Validation

The abnormal cell areas' segmentation outcomes were examined for manual segmentation based on the expertise of the radiologists. The Dice score was used to assess the spatial congruence between semi-automated and manual segmentation.

$$Dice_{\{tissue\}} = 2 \times \frac{A_{\{tissue NB\}} \bigcap A_{\{tissue man\}}}{A_{\{tissue NB\}} + A_{\{tissue man\}}} \qquad 4.17$$

Where $A_{\{tissue\_man\}}$ represents the region selectively segmented for the identical cell even by radiologists and $A_{\{tissue\_NB\}}$.
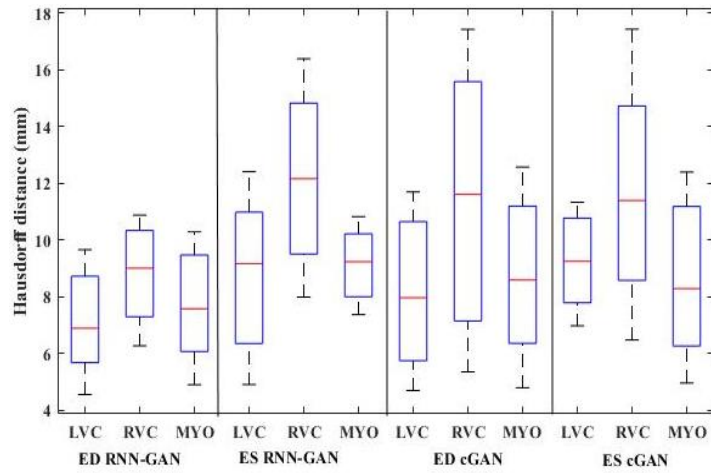
Figure. 4.8: Hausdorff Distance of the Proposed Work

The Hausdorff distance of the suggested model was shown in Figure 4.8. The Hausdorff distance is also computed to control the separation between segmentation borders.
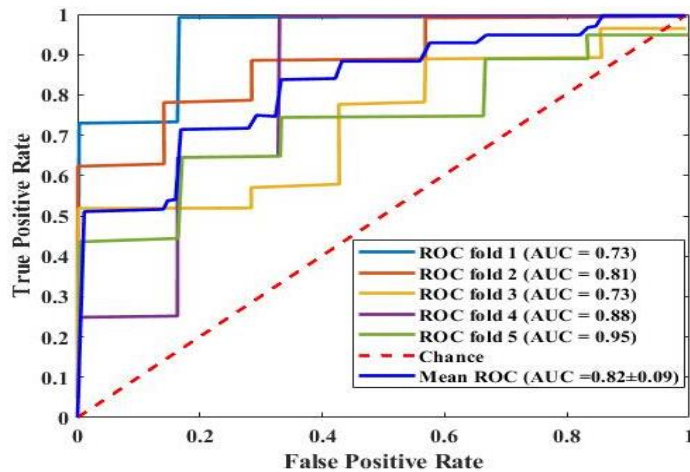
Figure. 4.9: Local Recurrence Graph of RNN-GAN

The deep learning model is recommended as a local recurrence graph, as illustrated in Figure 4.9. Furthermore, it showed the AUC as 0.73, 0.81, 0.73, 0.88,

and 0.95 and the ROC folding value as 1 to 5. The average AUC is thus 0.82, and the TPR steadily rises in tandem with the rising false positive ratio.
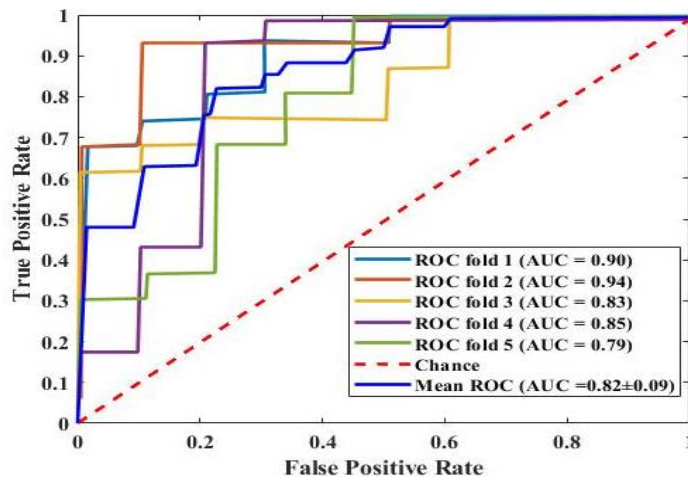
Figure. 4.10: Long term Recurrence of RNN-GAN

The long-term recurrence graph was shown in Figure 4.10. It also involves raising the FPR to raise the TPR. The AUC scores are then shown to be 0.90, 0.94, 0.83, 0.85, and 0.79, with the overall AUC value being 0.82.
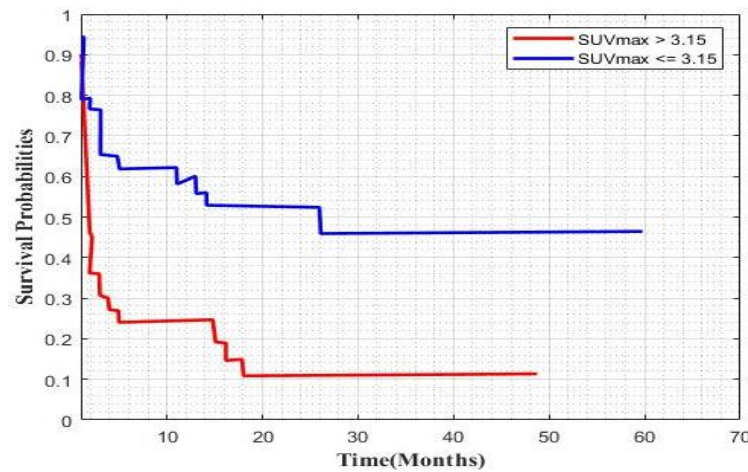
Figure. 4.11: Graph 1 Probability of Survival Rate of Patient

Figur 4.11 shows the effectiveness curve for the likelihood of survival. It also reflects the intake value that is standard. The Figure includes two graphs, one with a

maximal SUV of 3.15 or larger and the other with a maximal SUV of 3.15 or less. The maximal SUV is more than 3.15, and this produces a higher likelihood of survival rate than other SUVs.
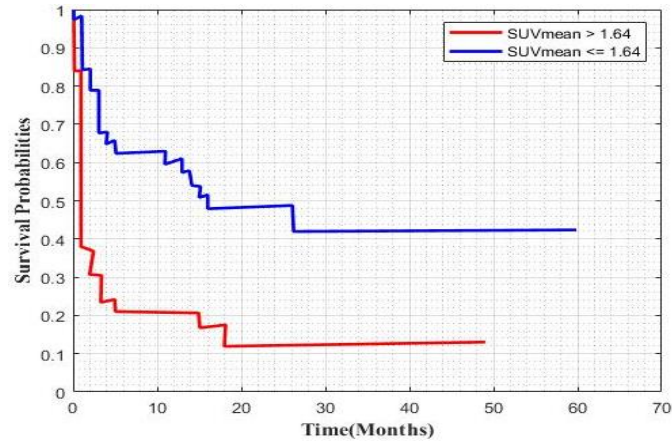
Figure 4.12 Graph 2 Probability of Survival Rate of Patient

The probability curve for the overall survival rate is shown in Figure 4.12. For various months, a total probability score greater than 1.64 indicates a higher likelihood of surviving than the other probabilities.
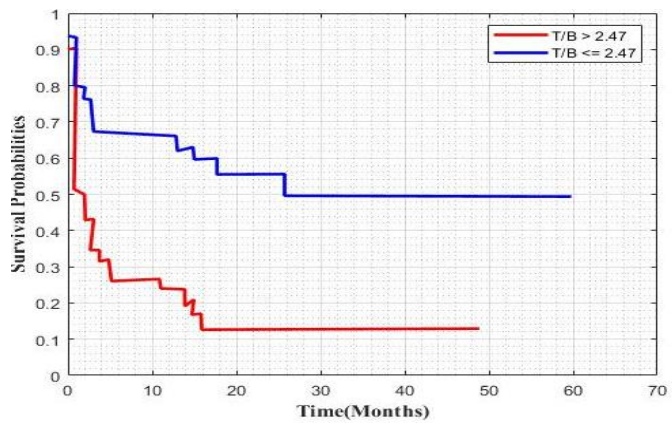
Figure 4.13: Graph 3 Probability of Survival Rate of Patient

The survival probability rate for various months is shown in Figure 4.13. As a result, there are two categories: one is for SUV values larger than 2.47 and the other is

for SUV values less than or equal to 2.47. The survival probability also drops since the proposed model shows the survival chance reduces with increasing months.
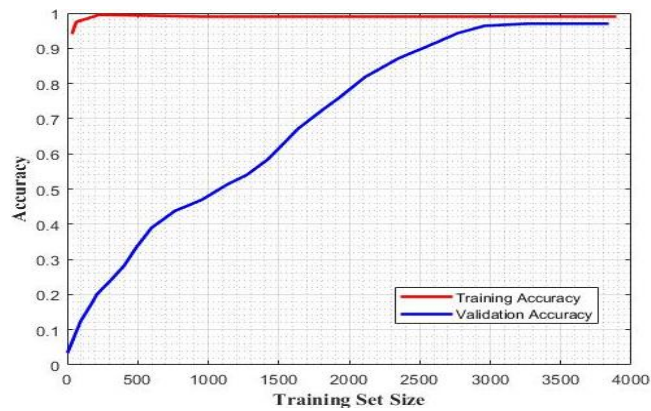
Figure 4.14: Training and Validation performance of RNN-GAN.

Figure 4.14 shows the training and validation performance accuracy score of RNN-GAN model. The proposed model training size ranges from 0 to 4000. As a result, it shows that the validation performance is steadily increasing while the training performance has a high value.
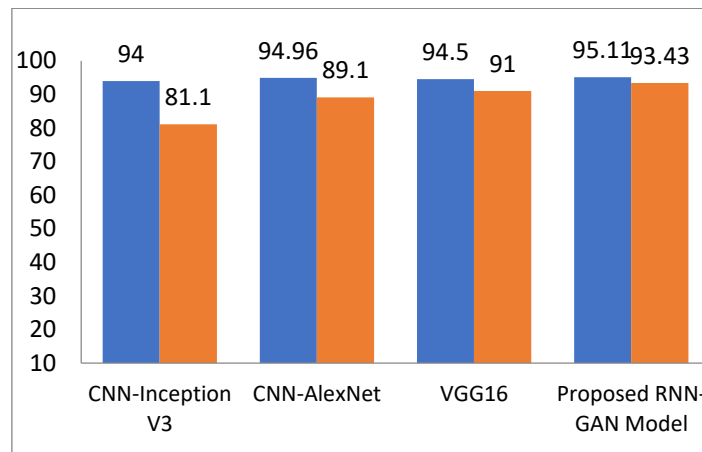
Figure 4.15: Bar represents the specificity and sensitivity score of RNN-GAN model with other deep learning models

The comparative analysis of suggested techniques with existing methods in terms of specificity and sensitivity score is shown in Figure 4.15. Moreover, the ability of aggregate MAqCI scores to accurately identify patients. As a result, both the score of specificity and the sensitivity of the recommended model are growing.
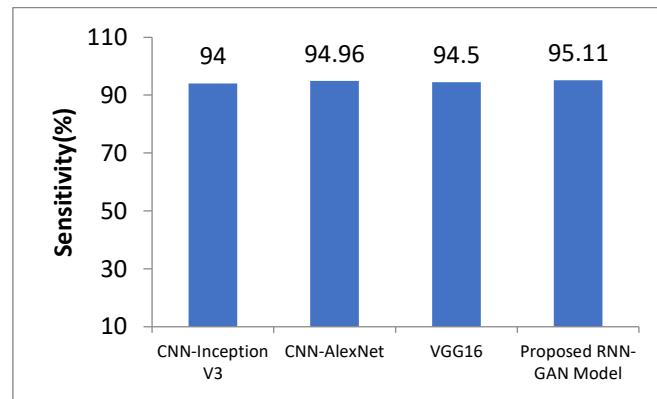
Figure 4.16: Comparative analysis of proposed model with other methods in terms of Sensitivity Score

Figure 4.16 shows the comparative result of RNN-GAN model with other deep learning models in terms of sensitivity score. The proposed method is then contrasted with the already-existing CNN-Inception-V3, CNN-AlexNet [26] and VGG-16 models. The RAN-GAN model outperforms the other deep learning techniques, outperforming the current CNN-Inception-V3 Model by 1.11%, CNN-AlexNet method by 0.15%, and the existing VGG-16 by 0.61%.
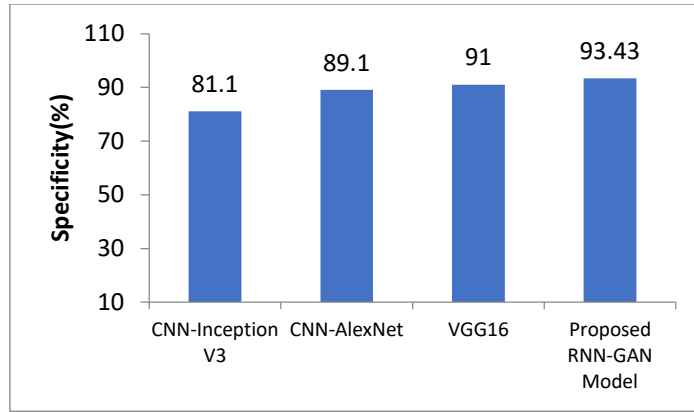
Figure 4.17: Bar represents the specificity score of RNN-GAN model with other deep learning models

Figure 4.17 illustrates the comparative result of RNN-GAN model with other deep learning models in terms of specificity. Furthermore, it shows that the CNN-Inception-V3, CNN-AlexNet [26] and VGG-16 models are evaluated to the provided model. The RNN-GAN model outperforms the CNN-Inception-V3 Model by 12%, CNN-AlexNet Model by about 4% and the VGG-16 by almost 2%.
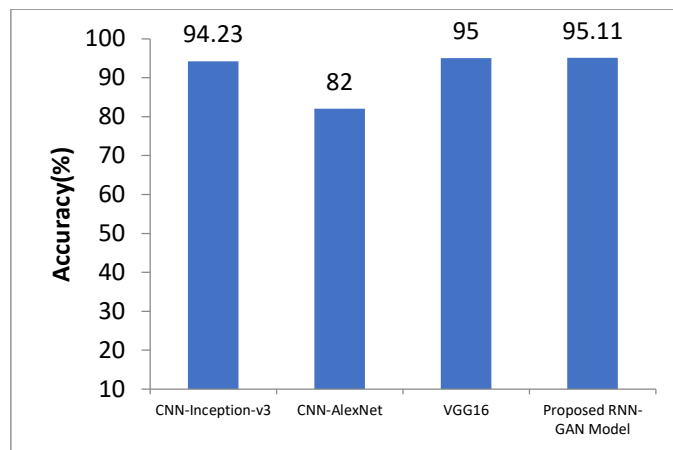
Figure 4.18: Bar represents the accuracy score of RNN-GAN model with other deep learning models

The accuracy score of RNN-GAN model with other deep learning models is shown in Figure 4.18. The CNN-Inception-V3, CNN-AlexNet and VGG-16 approaches are used to compare the final accuracy score with the proposed RNN-

GAN model. Therefore, the RNN-GAN model outperforms the current CNN-Inception-V3 approach by 0.88%, the CNN-AlexNet by 13%, and the VGG-16 by 0.11%
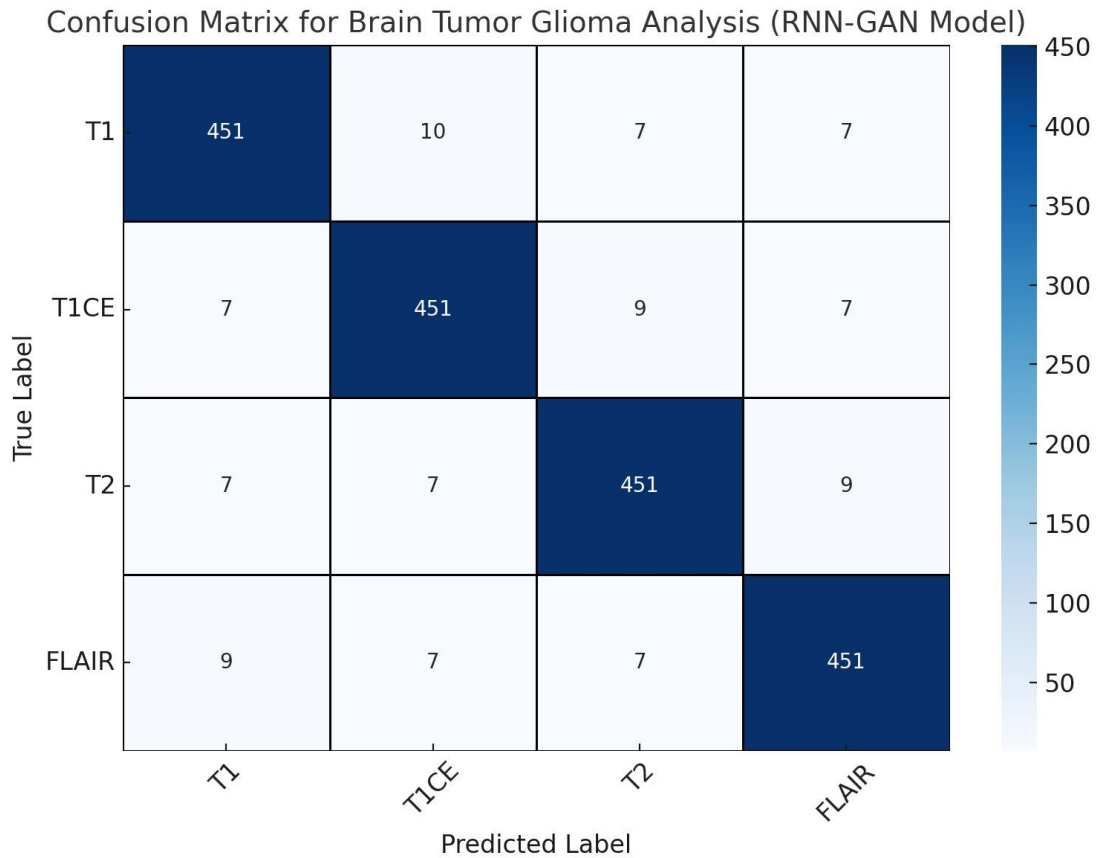
Figure 4.19: Confusion Matrix of Suggested Model

Figure 4.169 shows the confusion matrix for the RNN-GAN model on brain tumor glioma analysis demonstrates strong predictive performance, with high true positive rates for all four classes: T1, T1-Contrast, T2 and FLAIR, each correctly classified in 451 out of 475 instances. Misclassifications are relatively low and uniformly distributed, with off-diagonal values indicating minor confusion among the classes (7-10 samples being misclassified into other categories). The overall accuracy of 95.11% signifies that the model performs well in distinguishing between the different types of

brain tumor images, though there is still a small margin for reducing misclassification rates.

Contribution of this Chapter

- This chapter proposed RNN-GAN Model for detecting the glioblastoma brain tumor and also predicting the survival rate of patients. This model performs the several steps as;

- Preprocessing, Z-score normalization and spatial resampling are performed in step 1, followed by recurrent GAN techniques for tumor segmentation in step 2, radiomices texture-based feature extraction (FE) is done based on wavelet band-pass filtering in step 3, and RF classifier was used to predicted recurrent glioblastoma in step 4. This research sought to evaluate the efficacy of the preoperative and postoperative recurrent risks amongst glioma patients receiving a combination of bevacizumab and nivolumab therapy. Tumor regions of interest were segmented from T1 images that had undergone contrast enhancement. Utilizing a variety of textural features, the recurrence risk for GBM patients is predicted using the RF approach. The characteristics from MRIs were extracted using CE-T1W-MRI imaging information.

- Recurrence prognosis, survival rate, PFS, ORR, accuracy score, specificity, and sensitivity are the performances of the suggested research. The suggested approach is contrasted with the CNN-Inception-V3, CNN AlexNet and VGG16 forecasting techniques already in use.

- The specificity of the study is around 4% higher than the previous approaches, and the sensitivities of the suggested approach is almost 5% better. The efficiency of the suggested approach is 3% greater than the previous methodologies.

CHAPTER 5

Comparative Result Analysis

5.1 Overview

This study proposed two hybrid deep learning models for the prediction of glioblastoma brain tumors and also for predicting the survival rate of patients. This chapter discussed the comparative result analysis of both proposed models, MFCM RSGWO-FRCNN Model and RNN+GAN Model. According to the analysis of the final result of both models, select one of the best models for the prediction of brain tumors. This selected model is compared with the existing methods.

5.2 Comparative Analysis of Both Models

Table 5.1: *Comparative result analysis of the MFCM RSGWO-FRCNN Model with the RNN+GAN Model*

Parameters	MFCM RSGWO-FRCNN Model	RNN+GAN Model
Accuracy	93%	95.11%
Sensitivity	93.12%	95.11%
Specificity	93.43%	98%
Survival Rate	1.64 (16%)	2.47 (25%)
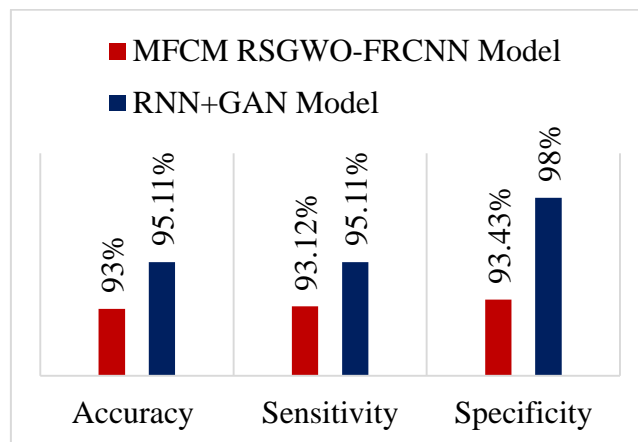
Figure 5.1: Bar represents the Comparative result analysis of MFCM RSGWO-FRCNN Model with RNN+GAN Model
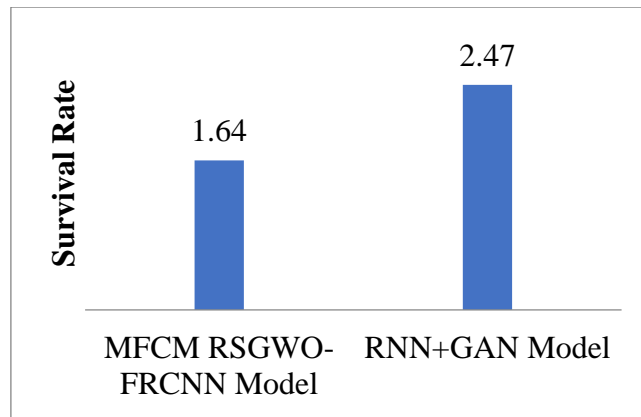
Figure 5.2: Survival rate Prediction of MFCM RSGWO-FRCNN Model with RNN+GAN

Model

Figure 5.1 and 5.2 shows the comparative analysis of the MFCM RSGWO-FRCNN Model with the RNN+GAN Model. It clearly shows that our second RNN+GAN Model gives a better result as compared to the first MFCM RSGWO-FRCNN Model. The RNN+GAN Model achieves a 95.11% accuracy score; Sensitivity is 95.11% and Specificity is 98%. The RNN+GAN Model increases the survival rate which is 2.47 (25%) after diagnosis and overall treatment of patients.

5.3 Comparative Analysis with Existing Methods

This section shows the comparative analysis of the RNN+GAN Model with previously existing methods. The proposed RNN+GAN Model is compared with some previous methods in terms of accuracy score. Table 5.2 shows the comparative result in terms of the accuracy score of the RNN+GAN Model with existing methods.

Table 5.2: *Comparative Accuracy score of RNN+GAN Model with Existing methods*

State-of-Art Methods	Accuracy Score in %	Parameter
Almalki Y.E. et. al. (2022)	95.3	4 million
N Varuna Shree et. al. (2018)	95.00	3 million
P. Gokila Brindha et. al. (2020)	71.51	50 million
S. Deepak et. al. (2020)	94.26	8 million
Jianming Ye et. al. (2021)	93.00	5 million
Khan et al. (2020)	89.00	70 million
Amena Mahmoud(2023)	95.10	5 million
Proposed RNN+GAN Model	95.11	7 million
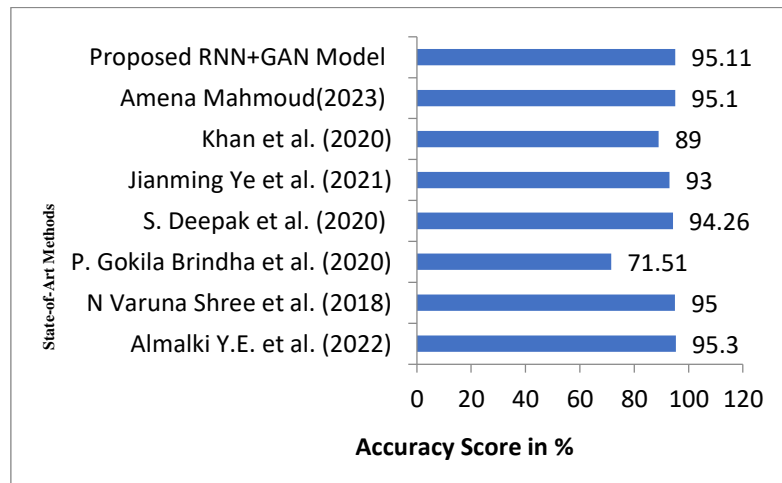
Figure 5.3: Bar represents the Comparative result of the Proposed RNN+GAN Model with existing methods

Table 5.3 *Comparative Analysis of Architecture with Existing CNN Architecture*

All Architecture	CNN-InceptionV3	CNN-Alexnet	CNN-VGG16	Proposed MFCM RSGWO-FRCNN Model	Proposed RNN-GAN Model
Layers	42-layers	13 layers	16 layers	48 layers	20 layers
Parameters	24 million	60 million	138 million	2 Million	7 Million
Image Size	224x224	224x224	224x224	224x224	224x224

CHAPTER 6

Conclusion and Future Scope

6.1 Conclusion

An awful and frequent form of brain tumor is glioma. For individualized treatments, an accurate pre-operative prediction for Glioblastoma patients is needed. Therefore, therapeutic management is essential to raising the survival rate or life expectancy of glioma patients. Healthcare professionals and investigators can employ image processing tools to identify bodily processes and issues before invasive procedures. The data from an MRI scanning is adequate for clinical assessment. The typical course of treatment for Glioblastoma is surgical removal and either radiotherapy or chemotherapy. The intrinsic variability of Glioblastoma causes a significant variation in total surviving rate and a broad range of diagnoses for the individual. The standard methods that have been tested up to this point have several drawbacks including complexity, the issue of data overfitting, similar to human flaws, and others.

This research proposed the two hybrid deep learning models for the prediction of glioblastoma brain tumors and also for predicting the survival rate of patients. In this chapter, we discussed the comparative result analysis of both proposed models MFCM RSGWO-FRCNN Model and the RNN+GAN Model. According to the analysis of the final result of both models, select one of the best models for the prediction of brain tumors. This selected model results are compared with the existing state-of-art methods.

In the first model, a dynamically Deep Learning technique for Glioblastoma brain cancer survival prediction rate was put out to address the aforementioned problems. Data preprocessing is the initial phase. The MRI brain images were improved by intensity normalization using histogram normalization, de-noising via bilateral filtering, and the removal of information contaminants. Probabilistic noise, salted and pepper distortion were also taken out. Secondly, radiomic feature segmentation was completed using the MFCM clustering approach. Then, Rough Set Theory-based Grey Wolf Optimization was used to choose the most important and instructive aspects from the obtained characteristics. Later, using FR-CNN, the overall survival predictions are categorized by selecting the important feature in MRI brain images.

The proposed MFCM-RSGWO-FRCNN approach is tested against state-of-art CNN-Inception-v3, CNN AlexNet and VGG16 approaches. Evaluation parameters like Accuracy, specificity, precision, sensitivity, PSNR, MSE, and Segmentation Time were used to examine the technique. The proposed MFCM-RSGWO-FRCNN has the advantages of less converging and the corresponding characteristics.

- The algorithm was successful to accurately predict the survival rate using classifications and required only a segmentation time of around 10 sec.

- With a lowered error rate of 2.3 percent in case of MSE compared to other approaches' 4.6 percent and 5 percent, it is significantly more efficient.

- The method generates a minimized noise ratio for the complete collection of photos for any different data sizes, as well as improved classification and forecasting performance of roughly 95%.

When compared to techniques like CNN-Inception-V3 , CNN AlexNet and VGG16, MFCM-RSGWO-effectiveness FRCNN's is able to forecast the right images in the data resource. The FCM, which was suggested to segments based on grouping, was shown to be less reliable than the MFCM-RSGWO-FRCNN. There are various methods to expand the suggested technique. The approach may start by performing a thorough type, time-based examination of the occurrence, distribution, and volume of the tumor. As a result, there are several issues that need to be resolved, such as the use of various validity indexes, heterogeneity measures, and comparing with different hybrid techniques for shortening segmentation duration.

In the second method hybrid deep learning model is designed to detect the glioblastoma tumor based on the recurrence risk. For the preprocessing, Z-score normalization, and spatial resampling are performed in step 1, followed by recurrent GAN techniques for tumor segmentation in step 2, radiomices texture-based feature extraction (FE) is done based on wavelet band-pass filtering in step 3, and RF classifier was used to predicted recurrent glioblastoma in step 4. This research sought to evaluate the efficacy of the preoperative and postoperative recurrent risks amongst glioma patients receiving a combination of bevacizumab and nivolumab therapy. Tumor regions of interest were segmented from T1 images that had undergone contrast enhancement. The radiomic feature-based MRI signals were derived from multi-parametric MRI data of sick people with glioblastoma to ascertain their connections with responses to OS and PFS. Utilizing a variety of textural features, the recurrence risk for GBM patients is predicted using the RF approach. The characteristics from MRIs were extracted using CE-T1W-MRI imaging information. Every stage is thoroughly explained in the next subtopics.

- Recurrence prognosis, survival rate, PFS, ORR, accuracy score, specificity, and sensitivity are the performances of the suggested research. The suggested approach is contrasted with the CNN-Inception-V3, CNN AlexNet and VGG16 forecasting techniques already in use.

- The specificity of the study is around 4% higher than the previous approaches, and the sensitivities of the suggested approach is almost 5% better. The efficiency of the suggested approach is 3% greater than the previous methodologies.

The probability of glioma recurring can therefore be effectively predicted using the suggested approach, and further research is needed to measure the specific immunological ecosystem of the brain during cancer settings.

After analysing both models, the second RNN+GAN Model gives a better result as compared to the first MFCM RSGWO-FRCNN Model. The RNN+GAN Model achieves a 95.11% accuracy score; Sensitivity is also 95.11% and Specificity is 98%. The RNN+GAN Model increases the survival rate which is 2.47% after diagnosis and overall treatment of patients.

6.2 Future Scope

1. The proposed segmentation algorithm focuses on two dimensional anatomical structures. It can also be extended to three dimensional volumetric structures.

2. As the intensity and orientation-based segmentation method is capable of extracting the features of the medical images accurately, it can also be applied to the fusion image.

3. As the online service is used for the detection of a brain cancer type, the research can be extended to other brain cancer types and locations also.

4. There is currently no publicly accessible dataset of large MRI sequences provided globally. To develop a huge capacity, open a test dataset, and testing the suggested techniques using the aid of the novel dataset to confirm their efficacy and continuously enhance it, efforts might be taken in the coming days to reach in touch with several other labs conducting relevant studies.

REFERENCES

1. Keerthana, A., B. Kavin Kumar, K. S. Akshaya, and S. Kamalraj. "Brain Tumour Detection Using Machine Learning Algorithm." In Journal of Physics: Conference Series, vol. 1937, no. 1, p. 012008. IOP Publishing, 2021. https://doi.org/10.1088/1742-6596/1937/1/0120087.

2. Abdel-Gawad, Ahmed H., Lobna A. Said, and Ahmed G. Radwan. "Optimized Edge Detection Technique for Brain Tumor Detection in MR Images." IEEE Access 8 (2020): 136243-136259. https://doi.org/10.1109/access.2020.3009898.

3. Almalki, Yassir Edrees, Muhammad Umair Ali, Waqas Ahmed, Karam Dad Kallu, Amad Zafar, Sharifa Khalid Alduraibi, Muhammad Irfan, Mohammad Abd Alkhalik Basha, Hassan A. Alshamrani, and Alaa Khalid Alduraibi. "Robust Gaussian and Nonlinear Hybrid Invariant Clustered Features Aided Approach for Speeded Brain Tumor Diagnosis." Life 12, no. 7 (2022): 1084. https://doi.org/10.3390/life12071084.

4. Amin, Javaria, Muhammad Sharif, Nadia Gul, Mudassar Raza, Muhammad Almas Anjum, Muhammad Wasif Nisar, and Syed Ahmad Chan Bukhari. "Brain Tumor Detection by Using Stacked Autoencoders in Deep Learning." Journal of Medical Systems 44 (2020): 1-12. https://doi.org/10.1007/s10916-019-1483-2.

5. Amin, Javeria, Muhammad Sharif, Mudassar Raza, and Mussarat Yasmin. "Detection of Brain Tumor Based on Features Fusion and Machine Learning." Journal of Ambient Intelligence and Humanized Computing (2024): 1-17. https://doi.org/10.1007/s12652-018-1092-9.

6. Amin, J., M. Sharif, M. Yasmin, and S. L. Fernandes. "A Distinctive Approach in Brain Tumor Detection and Classification Using MRI." Pattern Recognition Letters 139 (2020): 118-127.

7. Bae, Sohi, Yoon Seong Choi, Sung Soo Ahn, Jong Hee Chang, Seok-Gu Kang, Eui Hyun Kim, Se Hoon Kim, and Seung-Koo Lee. "Radiomic MRI Phenotyping of Glioblastoma: Improving Survival Prediction." Radiology 289, no. 3 (2018): 797-806. https://doi.org/10.31803/tg-20190712095507.

8. Baek, E. T., H. J. Yang, S. H. Kim, G. S. Lee, I. J. Oh, S. R. Kang, and J. J. Min. "Survival Time Prediction by Integrating Cox Proportional Hazards Network and Distribution Function Network." BMC Bioinformatics 22, no. 1 (2021): 1-15.

9. Bakas, S., M. Reyes, Int, and B. Menze. "Identifying the Best Machine Learning Algorithms for Brain Tumor Segmentation, Progression Assessment, and Overall Survival Prediction in the BRATS Challenge." arXiv (2018). https://arxiv.org/abs/1811.02629.

10. Bakas, S., M. Reyes, A. Jakab, S. Bauer, M. Rempfler, A. Crimi, R. T. Shinohara, C. Berger, S. Ha, M. Rozycki, M. Prastawa, E. Alberts, J. Lipkova, J. Freymann, J. Kirby, M. Bilello, H. M. Fathallah-Shaykh, R. Wiest, J. S. Kirschke, et al. "Identifying the Best Machine Learning Algorithms for Brain Tumor Segmentation, Progression Assessment, and Overall Survival Prediction in the BRATS Challenge." HAL (Le Centre Pour La Communication Scientifique Directe, 2018.

11. Beig, N., J. Patel, P. Prasanna, V. Hill, A. Gupta, R. Correa, K. Bera, S. Singh, S. Partovi, V. Varadan, M. Ahluwalia, A. Madabhushi, and P. C. Tiwari. "Radiogenomic Analysis of Hypoxia Pathway is Predictive of Overall Survival in Glioblastoma." Scientific Reports 8, no. 1 (2018). https://doi.org/10.1038/s41598-017-18310-0.

12. Bisdas, S., H. Shen, and S. Thust. "Texture Analysis and Support Vector Machine-Assisted Diffusional Kurtosis Imaging May Allow In Vivo Gliomas Grading and IDH-Mutation Status Prediction: A Preliminary Study." Scientific Reports 8 (2018).

13. Biswas, A., and M. S. Islam. "ANN-Based Brain Tumor Classification: Performance Analysis Using K-Means and FCM Clustering with Various Training Functions." In CRC Press eBooks, 83–102, 2021. https://doi.org/10.1201/9781003172772-6.

14. Brindha, P. G., M. Kavinraj, P. Manivasakam, and P. Prasanth. "Brain Tumor Detection from MRI Images Using Deep Learning Techniques." IOP Conference Series 1055, no. 1 (2021): 012115. https://doi.org/10.1088/1757-899x/1055/1/012115.

15. Carré, A., G. Klausner, M. Edjlali, M. Lerousseau, J. Briend-Diop, R. Sun, S. Ammari, S. Reuzé, E. A. Andres, T. Estienne, S. Niyoteka, E. Battistella, M. Vakalopoulou, F. Dhermain, N. Paragios, E. Deutsch, C. Oppenheim, J. Pallud, and C. Robert. "Standardization of Brain MR Images Across Machines and Protocols: Bridging the Gap for MRI-Based Radiomics." Scientific Reports 10, no. 1 (2020). https://doi.org/10.1038/s41598-020-69298-z.

16. Chaddad, A., S. Sabri, T. Niazi, and B. Abdulkarim. "Prediction of Survival with Multi-Scale Radiomic Analysis in Glioblastoma Patients." Medical & Biological Engineering & Computing 56, no. 12 (2018): 2287–2300. https://doi.org/10.1007/s11517-018-1858-4.

17. Chato, L., and S. Latifi. "Machine Learning and Radiomic Features to Predict Overall Survival Time for Glioblastoma Patients." Journal of Personalized Medicine 11, no. 12 (2021): 1336. https://doi.org/10.3390/jpm11121336.

18. Chen, G., Q. Li, F. Shi, I. Rekik, and Z. Pan. "RFDCR: Automated Brain Lesion Segmentation Using Cascaded Random Forests with Dense Conditional Random Fields." NeuroImage 211 (2020): 116620. https://doi.org/10.1016/j.neuroimage.2020.116620.

19. Chen, H., F. Lin, J. Zhang, X. Lv, J. Zhou, Z. Li, and Y. Chen. "Deep Learning Radiomics to Predict PTEN Mutation Status from Magnetic Resonance Imaging in Patients with Glioma." *Frontiers in Oncology* 11 (2021). https://doi.org/10.3389/fonc.2021.734433.

20. Cho, H., S. H. Lee, J. Kim, and H. Park. "Classification of the Glioma Grading Using Radiomics Analysis." PeerJ 6 (2018): e5982. https://doi.org/10.7717/peerj.5982.

21. Choi, K. H., S. H. Choi, and B. Jeong. "Prediction of IDH Genotype in Gliomas with Dynamic Susceptibility Contrast Perfusion MR Imaging Using an Explainable Recurrent Neural Network." Neuro-Oncology 21, no. 9 (2019): 1197–1209. https://doi.org/10.1093/neuonc/noz095.

22. Choi, Y. Y., S. Bae, J. H. Chang, S. M. Kang, H. Kim, J. H. Kim, T. H. Rim, S. H. Choi, R. Jain, and S. H. Lee. "Fully Automated Hybrid Approach to Predict the IDH Mutation Status of Gliomas via Deep Learning and Radiomics." Neuro-Oncology 23, no. 2 (2021): 304–313. https://doi.org/10.1093/neuonc/noaa177.

23. Deepa, B., M. G. Sumithra, R. Kumar, and M. Suriya. "Weiner Filter Based Hough Transform and Wavelet Feature Extraction with Neural Network for Classifying Brain Tumor." In International Conference on Inventive Computation Technologies, 2021. https://doi.org/10.1109/icict50816.2021.9358680.

24. Deepak, S., and P. M. Ameer. "Automated Categorization of Brain Tumor from MRI Using CNN Features and SVM." Journal of Ambient Intelligence and Humanized Computing 12, no. 8 (2021): 8357–8369. https://doi.org/10.1007/s12652-020-02568-w.

25. Divya, S., K. Padmapriya, and P. Ezhumalai. "A Preclinical Study on Radiomics-Driven Brain Tumor Prediction Using Deep Convolution Neural Network." Revista Geintec-Gestao Inovacao E Technologies 11, no. 2 (2021): 1481–1488.

26. Elshaikh, B. G., M. Garelnabi, H. Omer, A. Sulieman, B. Habeeballa, and R. A. Tabeidi. "Recognition of Brain Tumors in MRI Images Using Texture Analysis." Saudi Journal of Biological Sciences 28, no. 4 (2021): 2381–2387. https://doi.org/10.1016/j.sjbs.2021.01.035.

27.   Erickson, B. J., P. Korfiatis, and T. L. Kline. "Deep Learning in Radiology: Does One Size Fit All?" Journal of the American College of Radiology 15 (2018): 521–526.

28.   Fan, C., F. Xiao, and Y. Zhao. "A Short-Term Building Cooling Load Prediction Method Using Deep Learning Algorithms." Applied Energy 195 (2017): 222–233. https://doi.org/10.1016/j.apenergy.2017.03.064.

29.   Fang, B., Y. Li, H. Zhang, and J. C. Chan. "Hyperspectral Images Classification Based on Dense Convolutional Networks with Spectral-Wise Attention Mechanism." Remote Sensing 11, no. 2 (2019): 159. https://doi.org/10.3390/rs11020159.

30.   Feng, X., N. J. Tustison, S. H. Patel, and C. H. Meyer. "Brain Tumor Segmentation Using an Ensemble of 3-D U-Nets and Overall Survival Prediction Using Radiomic Features." Frontiers in Computational Neuroscience 14 (2020): 25.

31.   Fu, J., K. Singhrao, X. Zhong, Y. Gao, S. L. Qi, Y. Yang, D. Ruan, and J. S. Lewis. "An Automatic Deep Learning-Based Workflow for Glioblastoma Survival Prediction Using Preoperative Multimodal MR Images: A Feasibility Study." Advances in Radiation Oncology 6, no. 5 (2021): 100746. https://doi.org/10.1016/j.adro.2021.100746.

32.   Gaur, Loveleen, Mohan Bhandari, Tanvi Razdan, Saurav Mallik, and Zhongming Zhao. "Explanation-Driven Deep Learning Model for Prediction of Brain Tumor Status Using MRI Image Data." Frontiers in Genetics 13 (2022). https://doi.org/10.3389/fgene.2022.822666.

33.   Giger, M. L. "Machine Learning in Medical Imaging." Journal of the American College of Radiology 15 (2018): 512–520.

34.   Gu, X., Z. Shen, J. Xue, Y. Fan, and T. Ni. "Brain Tumor MR Image Classification Using Convolutional Dictionary Learning with Local Constraint." Frontiers in Neuroscience 15 (2021). https://doi.org/10.3389/fnins.2021.679847.

35. Gurbina, M., M. Lascu, and D. Lascu. "Tumor Detection and Classification of MRI Brain Image Using Different Wavelet Transforms and Support Vector Machines." In International Conference on Telecommunications, 2019. https://doi.org/10.1109/tsp.2019.8769040.

36. Khan, H. A., J. Wu, M. Mushtaq, and M. U. Mushtaq. "Brain Tumor Classification in MRI Image Using Convolutional Neural Network." Mathematical Biosciences and Engineering 17, no. 5 (2020): 6203–6216.

37. Haarburger, C., G. Müller-Franzes, L. Weninger, C. K. Kuhl, D. Truhn, and D. Merhof. "Radiomics Feature Reproducibility under Inter-Rater Variability in Segmentations of CT Images." Scientific Reports 10, no. 1 (2020). https://doi.org/10.1038/s41598-020-69534-6.

38. Hajianfar, G., et al. "Non-Invasive O6 Methylguanine-DNA Methyltransferase Status Prediction in Glioblastoma Multiforme Cancer Using Magnetic Resonance Imaging Radiomics Features: Univariate and Multivariate Radiogenomics Analysis." World Neurosurgery 132 (2019): e140–e161.

39. Han, Changhee, et al. "MADGAN: Unsupervised Medical Anomaly Detection GAN Using Multiple Adjacent Brain MRI Slice Reconstruction." BMC Bioinformatics 22, no. S2 (2021). https://doi.org/10.1186/s12859-020-03936-1.

40. Han, W., L. Q. Qin, C. P. Bay, X. R. Chen, K. M. Yu, N. Miskin, A. Li, X. P. Xu, and G. R. Young. "Deep Transfer Learning and Radiomics Feature Prediction of Survival of Patients with High-Grade Gliomas." American Journal of Neuroradiology 41, no. 1 (2020): 40–48. https://doi.org/10.3174/ajnr.a6365.

41. Hashemzehi, R., S. J. S. Mahdavi, M. Kheirabadi, and S. R. K. Tabbakh. "Detection of Brain Tumors from MRI Images Based on Deep Learning Using Hybrid Model CNN and NADE." Biocybernetics and Biomedical Engineering 40, no. 3 (2020): 1225–1232. https://doi.org/10.1016/j.bbe.2020.06.001.

42.   Hemanth, G., M. Janardhan, and L. Sujihelen. "Design and Implementing Brain Tumor Detection Using Machine Learning Approach." In 2019 3rd International Conference on Trends in Electronics and Informatics (ICOEI), 2019. https://doi.org/10.1109/icoei.2019.8862553.

43.   Hemanth, G., M. Janardhan, and L. Sujihelen. "Brain Tumor Detection and Tissue Classification Using Machine Learning." International Journal of Scientific Research in Engineering and Management 6, no. 6 (2022). https://doi.org/10.55041/ijsrem14197.

44.   Iqbal, S., M. S. Khan, T. Saba, Z. Mehmood, N. Javaid, T. Saba, and R. Abbasi. "Deep Learning Model Integrating Features and Novel Classifiers Fusion for Brain Tumor Segmentation." Microscopy Research and Technique 82, no. 8 (2019): 1302–1315. https://doi.org/10.1002/jemt.23281.

45.   Jakola, Asgeir S., Lars M. Sagberg, Sushil Gulati, and Ole Solheim. "Advancements in Predicting Outcomes in Patients with Glioma: A Surgical Perspective." Expert Review of Anticancer Therapy 20, no. 3 (2020): 167–177. https://doi.org/10.1080/14737140.2020.1735367.

46.   Jalalifar, Amir, Hany Soliman, Michael Ruschin, Arjun Sahgal, and Alireza Sadeghi-Naini. "A Brain Tumor Segmentation Framework Based on Outlier Detection Using One-Class Support Vector Machine." International Conference of the IEEE Engineering in Medicine and Biology Society, 2020. https://doi.org/10.1109/embc44109.2020.9176263.

47.   K, K. K., M. D. T., and S. K. Maheswaran. "An Efficient Method for Brain Tumor Detection Using Texture Features and SVM Classifier in MR Images." Asian Pacific Journal of Cancer Prevention 19, no. 10 (2018): 2789–2794. https://doi.org/10.22034/apjcp.2018.19.10.2789.

48.   Karayegen, Gokhan, and M. Faruk Aksahin. "Brain Tumor Prediction on MR Images with Semantic Segmentation by Using Deep Learning Network and 3D Imaging of Tumor Region." Biomedical Signal Processing and Control 66 (2021): 102458. https://doi.org/10.1016/j.bspc.2021.102458.

49. Kaur, Gurpreet, and Amandeep Oberoi. "Novel Approach for Brain Tumor Detection Based on Naïve Bayes Classification." In Springer eBooks, 451–462. 2020. https://doi.org/10.1007/978-981-32-9949-8_31.

50. Kayalibay, Berk, Gregor Jensen, and Paul van der Smagt. "CNN Based Segmentation of Medical Imaging Data." arXiv (2017). https://arxiv.org/abs/1701.03056.

51. Ke, Qiao, Jiangshe Zhang, Wei Wei, Robertas Damasevicius, and Marcin Wozniak. "Adaptive Independent Subspace Analysis of Brain Magnetic Resonance Imaging Data." IEEE Access 7 (2019): 12252–61. https://doi.org/10.1109/access.2019.2893496.

52. Khosravanian, Amir, Mojtaba Rahmanimanesh, Payman Keshavarzi, and Sajad R. K. Mozaffari. "Fast Level Set Method for Glioma Brain Tumor Segmentation Based on Superpixel Fuzzy Clustering and Lattice Boltzmann Method." Computer Methods and Programs in Biomedicine 198 (2021): 105809. https://doi.org/10.1016/j.cmpb.2020.105809.

53. Kim, Do Young, Hyemin Jang, Kyung Won Kim, Yunjin Shin, and Seong Ho Park. "Design Characteristics of Studies Reporting the Performance of Artificial Intelligence Algorithms for Diagnostic Analysis of Medical Images: Results from Recently Published Papers." Korean Journal of Radiology 20, no. 3 (2019): 405. https://doi.org/10.3348/kjr.2019.0025.

54. Kobayashi, Kazuki, Manabu Miyake, Masafumi Takahashi, and Ryuji Hamamoto. "Observing Deep Radiomics for the Classification of Glioma Grades." Scientific Reports 11, no. 1 (2021). https://doi.org/10.1038/s41598-021-90555-2.

55. Korte, Jan C., Geoffrey S. Ibbott, Nicholas Hardcastle, Tomas Kron, Jing Wang, Hussein Bahig, Beshoy Elgohari, et al. "Radiomics Feature Stability of Open-Source Software Evaluated on Apparent Diffusion Coefficient Maps in Head and Neck Cancer." Scientific Reports 11, no. 1 (2021). https://doi.org/10.1038/s41598-021-96600-4.

56.   Krishna, T., K. V. N. Sunitha, and Sunil Mishra. "Detection and Classification of Brain Tumor from MRI Medical Image Using Wavelet Transform and PSO-Based LLRBFNN Algorithm." International Journal of Computer Sciences and Engineering (2018). https://doi.org/10.26438/ijcse/v6i1.1823.

57.   Lee, Minsoo, Jongho Kim, So Won Kim, Hyun Woo Shin, Hyeon Yong You, Jong Cheol Choi, Hee Jong Seol, et al. "Prediction of IDH1 Mutation Status in Glioblastoma Using Machine Learning Technique Based on Quantitative Radiomic Data." World Neurosurgery 125 (2019): e688–e696. https://doi.org/10.1016/j.wneu.2019.01.157.

58.   Li, Hao, Yiying He, Lin Huang, Haoyu Luo, and Xiao Xiang Zhu. "The Nomogram Model Predicting Overall Survival and Guiding Clinical Decision in Patients with Glioblastoma Based on the SEER Database." Frontiers in Oncology 10 (2020). https://doi.org/10.3389/fonc.2020.01051.

59.   Li, Zhi, Hao Bai, Qi Sun, Qihua Liu, Lin Liu, Yun Zou, Yong Chen, Chen Liang, and Huaping Zheng. "Multiregional Radiomics Features from Multiparametric MRI for Prediction of MGMT Methylation Status in Glioblastoma Multiforme: A Multicentre Study." European Radiology 28, no. 9 (2018): 3640–3650. https://doi.org/10.1007/s00330-017-5302-1.

60.   Liu, Liyang, Huihui Zhang, Jian Wu, Zhixia Yu, Xiaoxia Chen, Islem Rekik, Qingshan Wang, Jianghong Lu, and Dinggang Shen. "Overall Survival Time Prediction for High-Grade Glioma Patients Based on Large-Scale Brain Functional Networks." Brain Imaging and Behavior 13, no. 5 (2019): 1333–1351. https://doi.org/10.1007/s11682-018-9949-2.

61.   Lotan, Eli, Rajan Jain, Narges Razavian, Gautam M. Fatterpekar, and Yvonne Lui. "State of the Art: Machine Learning Applications in Glioma Imaging." American Journal of Roentgenology 212, no. 1 (2019): 26–37. https://doi.org/10.2214/ajr.18.20218.

62.   Lu, Cheng-Feng, Feipei Hsu, Kuo-Liang Chang Hsieh, Yuan-Hao Kao, Shang-Jung Cheng, Ja Chen Hsu, Phei-Han Tsai, et al. "Machine Learning–Based Radiomics for Molecular Subtyping of Gliomas." Clinical Cancer Research 24, no. 18 (2018): 4429–4436. https://doi.org/10.1158/1078-0432.ccr-17-3445.

63.   Mahmoud, A., N.A. Awad, N. Alsubaie, S.I. Ansarullah, M.S. Alqahtani, M. Abbas, M. Usman, B.O. Soufiene, and A. Saber. "Advanced Deep Learning Approaches for Accurate Brain Tumor Classification in Medical Imaging." Symmetry 15 (2023): 571. https://doi.org/10.3390/sym15030571.

64.   Martinez, Elizabeth, Camilo Calderon, Hans Garcia, and Henry Arguello. "MRI Brain Tumor Segmentation Using a CNN over a Multi-Parametric Feature Extraction." In 2020 IEEE Colombian Conference on Applications of Computational Intelligence (IEEE ColCACI 2020), August 2020. https://doi.org/10.1109/colcaci50549.2020.9247926.

65.   Melam, Nagaraju. "Human Brain Tumor Detection Using Fast Bounding Box and Support Vector Machine." 2018.

66.   Miao, J., X. Zhou, and T. Huang. "Local Segmentation of Images Using an Improved Fuzzy C-Means Clustering Algorithm Based on Self-Adaptive Dictionary Learning." Applied Soft Computing 91 (2020): 106200. https://doi.org/10.1016/j.asoc.2020.106200.

67.   Mohsen, H., E.A. El-Dahshan, E.M. El-Horbaty, and A.M. Salem. "Classification Using Deep Learning Neural Networks for Brain Tumors." Future Computing and Informatics Journal 3, no. 1 (2017): 68–71. https://doi.org/10.1016/j.fcij.2017.12.001.

68.   Moradmand, H., S.M.R. Aghamiri, and R. Ghaderi. "Impact of Image Preprocessing Methods on Reproducibility of Radiomic Features in Multimodal Magnetic Resonance Imaging in Glioblastoma." Journal of Applied Clinical Medical Physics 21, no. 1 (2020): 179–90. https://doi.org/10.1002/acm2.12795.

69.   Murali, E., and K. Meena. "Brain Tumor Detection from MRI Using Adaptive Thresholding and Histogram-Based Techniques." Scalable Computing: Practice and Experience 21, no. 1 (2020): 3–10. https://doi.org/10.12694/scpe.v21i1.1600.

70.   Naser, M.A., and M.J. Deen. "Brain Tumor Segmentation and Grading of Lower-Grade Glioma Using Deep Learning in MRI Images." Computers in Biology and Medicine 121 (2020): 103758.

71.   Nogay, H.S., and H. Adeli. "Machine Learning (ML) for the Diagnosis of Autism Spectrum Disorder (ASD) Using Brain Imaging." Reviews in the Neurosciences 31, no. 8 (2020): 825–41. https://doi.org/10.1515/revneuro-2020-0043.

72.   Özyurt, F., E. Sert, E. Avci, and E. Dogantekin. "Brain Tumor Detection Based on Convolutional Neural Network with Neutrosophic Expert Maximum Fuzzy Sure Entropy." Measurement 147 (2019): 106830. https://doi.org/10.1016/j.measurement.2019.07.058..

73.   Panwar, S., M.V. Munot, S. Gawande, and P. Deshpande. "A Reliable and Efficient Approach for Diagnosis of Brain Tumor Using Transfer Learning." Biomedical and Pharmacology Journal 14, no. 1 (2021): 283–93. https://doi.org/10.13005/bpj/2124.

74.   Parthasarathy, G., L. Ramanathan, K. Anitha, and Y. Justindhas. "Predicting Source and Age of Brain Tumor Using Canny Edge Detection Algorithm and Threshold Technique." Asian Pacific Journal of Cancer Prevention 20, no. 5 (2019): 1409–14. https://doi.org/10.31557/apjcp.2019.20.5.1409.

75.   Patel, M., J. Zhan, K. Natarajan, R. Flintham, N. Davies, P. Sanghera, J.T. Grist, V. Duddalwar, A.C. Peet, and V. Sawlani. "Machine Learning-Based Radiomic Evaluation of Treatment Response Prediction in Glioblastoma." Clinical Radiology 76, no. 8 (2021): 628.e17–628.e27. https://doi.org/10.1016/j.crad.2021.03.019.

76.   Pei, L., L. Vidyaratne, M.M. Rahman, and K.M. Iftekharuddin. "Context-Aware Deep Learning for Brain Tumor Segmentation, Subtype Classification, and Survival Prediction Using Radiology Images." Scientific Reports 10, no. 1 (2020): 1–11.

77.   Priya, S., A. Agarwal, C. Ward, T. Locke, V. Monga, and G. Bathla. "Survival Prediction in Glioblastoma on Post-Contrast Magnetic Resonance Imaging Using Filtration-Based First-Order Texture Analysis: Comparison of Multiple Machine Learning Models." Rivista Di Neuroradiologia 34, no. 4 (2021): 355–62. https://doi.org/10.1177/1971400921990766.

78.   Qian, Z., L. Zhang, J. Hu, S. Chen, H. Chen, H. Shen, F. Zheng, Y. Zang, and X. Chen. "Machine Learning-Based Analysis of Magnetic Resonance Radiomics for the Classification of Gliosarcoma and Glioblastoma." Frontiers in Oncology 11 (2021). https://doi.org/10.3389/fonc.2021.699789.

79.   Rani, S., D. Ghai, S. Kumar, M.P. Kantipudi, A. Alharbi, and M.S. Ullah. "Efficient 3D AlexNet Architecture for Object Recognition Using Syntactic Patterns from Medical Images." Computational Intelligence and Neuroscience 2022 (2022): 1–19. https://doi.org/10.1155/2022/7882924.

80.   Ranjbarzadeh, R., and S.B. Saadi. "Automated Liver and Tumor Segmentation Based on Concave and Convex Points Using Fuzzy C-Means and Mean Shift Clustering." Measurement. https://doi.org/10.1016/j.measurement.2019.107086.

81.   Ranjbarzadeh, R., A.B. Kasgari, S.J. Ghoushchi, S. Anari, M. Naseri, and M. Bendechache. "Brain Tumor Segmentation Based on Deep Learning and an Attention Mechanism Using MRI Multi-Modalities Brain Images." Scientific Reports 11, no. 1 (2021). https://doi.org/10.1038/s41598-021-90428-8.

82.   Rathore, S., H. Akbari, J. Doshi, G. Shukla, M. Rozycki, M. Bilello, R.H. Lustig, and C. Davatzikos. "Radiomic Signature of Infiltration in Peritumoral Edema Predicts Subsequent Recurrence in Glioblastoma: Implications for

Personalized Radiotherapy Planning." Journal of Medical Imaging 5, no. 2 (2018): 1. https://doi.org/10.1117/1.jmi.5.2.021219.

83. Rathore, S., H. Akbari, M. Rozycki, K.G. Abdullah, M. Nasrallah, Z.A. Binder, R.V. Davuluri, R.H. Lustig, N. Dahmane, M. Bilello, D.M. O'Rourke, and C. Davatzikos. "Radiomic MRI Signature Reveals Three Distinct Subtypes of Glioblastoma with Different Clinical and Molecular Characteristics, Offering Prognostic Value Beyond IDH1." Scientific Reports 8, no. 1 (2018). https://doi.org/10.1038/s41598-018-22739-2.

84. Rosati, R., V. Kyrki, S. Silvestri, F. Marcheggiani, L. Tiano, and E. Frontoni. "Faster R-CNN Approach for Detection and Quantification of DNA Damage in Comet Assay Images." Computers in Biology and Medicine 123 (2020): 103912. https://doi.org/10.1016/j.compbiomed.2020.103912.

85. Bangare, S.L., G. Pradeepini, and S.T. Patil. "Implementation for Brain Tumor Detection and Three-Dimensional Visualization Model Development for Reconstruction." ARPN Journal of Engineering and Applied Sciences 13, no. 2 (2018): 467–73.

86. Saba, T., M.S. Khan, Z. Mehmood, U. Tariq, and N. Ayesha. "Microscopic Brain Tumor Detection and Classification Using 3D CNN and Feature Selection Architecture." Microscopy Research and Technique 84, no.

87. Sahaai, M.B., and G.R. Jothilakshmi. "Hierarchical Based Tumor Segmentation by Detection Using Deep Learning Approach." Journal of Physics: Conference Series 1921, no. 1 (2021): 012080. IOP Publishing.

88. Sharif, Muhammad, Javaid Amin, Muhammad Raza, Muhammad A. Anjum, Hammad Afzal, and Saqib A. Shad. "Brain Tumor Detection Based on Extreme Learning." Neural Computing and Applications 32, no. 20 (2020): 15975–87. https://doi.org/10.1007/s00521-019-04679.

89. Shboul, Zeina A., Mohammad Alam, Lakshitha Vidyaratne, Lei Pei, Mohamed I. Elbakary, and Khan M. Iftekharuddin. "Feature-Guided Deep Radiomics for Glioblastoma Patient Survival Prediction." Frontiers in Neuroscience 13 (2019): 966. https://doi.org/10.3389/fnins.2019.00966.

90. Shim, Ka Y., Sung Chung, Jae Jeong, Inpyeong Hwang, Chul-Kee Park, Tae Kim, Sung-Hye Park, Jae Won, Joo Ho Lee, Soon-Tae Lee, Roh-Eul Yoo, Koung K. Kang, Tae Yun, Ji-Hoon Kim, Chul-Ho Sohn, Kyu Choi, and Seung H. Choi. "Prediction of Recurrence Patterns in Glioblastoma Using DSC-MRI Radiomics-Based Deep Learning." Scientific Reports 11, no. 1 (2021). https://doi.org/10.1038/s41598-021-89218-z.

91. Shim, Ka, Sung Chung, Jae Jeong, Inpyeong Hwang, Chul-Kee Park, Tae Kim, Sung-Hye Park, Jae Won, Joo Ho Lee, Soon-Tae Lee, Roh-Eul Yoo, Koung K. Kang, Tae Yun, Ji-Hoon Kim, Chul-Ho Sohn, Kyu Choi, and Seung H. Choi. "Prediction of Recurrence Patterns in Glioblastoma Using DSC-MRI Radiomics-Based Deep Learning." Preprint, 2020. https://doi.org/10.21203/rs.3.rs-125593/v1.

92. Shree, N. V., and T. K. S. Kumar. "Identification and Classification of Brain Tumor MRI Images with Feature Extraction Using DWT and Probabilistic Neural Network." Brain Informatics 5, no. 1 (2018): 23–30. https://doi.org/10.1007/s40708-017-0075-5.

93. Sotoudeh, Hamed, Oghaz Shafaat, Joshua D. Bernstock, Matthew Brooks, Gergely A. Elsayed, Jason S. Chen, Pawel Szerip, Gabby Chagoya, Frank Gessler, Elham Sotoudeh, Abdullah Shafaat, and Gregory K. Friedman. "Artificial Intelligence in the Management of Glioma: Era of Personalized Medicine." Frontiers in Oncology 9 (2019): 768. https://doi.org/10.3389/fonc.2019.00768.

94. Sun, Li, Songtao Zhang, and Lin Luo. "Tumor Segmentation and Survival Prediction in Glioma with Deep Learning." In Lecture Notes in Computer Science, 83–93. 2018. https://doi.org/10.1007/978-3-030-11726-9_8.

95.   Sun, Li, Songtao Zhang, Hang Chen, and Lin Luo. "Brain Tumor Segmentation and Survival Prediction Using Multimodal MRI Scans with Deep Learning." Frontiers in Neuroscience 13 (2019). https://doi.org/10.3389/fnins.2019.00810.

96.   Suter, Yvonne, Urs Knecht, Mélanie Alão, Wesley Valenzuela, Edward Hewer, Philippe Schucht, Roland Wiest, and Michael Reyes. "Radiomics for Glioblastoma Survival Analysis in Pre-operative MRI: Exploring Feature Robustness, Class Boundaries, and Machine Learning Techniques." Cancer Imaging 20, no. 1 (2020). https://doi.org/10.1186/s40644-020-00329-8.

97.   Tandel, G. M., A. Balestrieri, T. Jujaray, N. N. Khanna, L. Saba, and Jasjit S. Suri. "Multiclass Magnetic Resonance Imaging Brain Tumor Classification Using Artificial Intelligence Paradigm." Computers in Biology and Medicine 122 (2020): 103804. https://doi.org/10.1016/j.compbiomed.2020.103804.

98.   Tandel, G. S., A. Tiwari, O. G. Kakde, N. Gupta, L. Saba, and J. S. Suri. "Role of Ensemble Deep Learning for Brain Tumor Classification in Multiple Magnetic Resonance Imaging Sequence Data." Diagnostics 13, no. 3 (2023): 481. https://doi.org/10.3390/diagnostics13030481.

99.   Tang, Z., Y. Xu, L. Jin, A. Aibaidula, J. Lu, Z. Jiao, J. Wu, H. Zhang, and D. Shen. "Deep Learning of Imaging Phenotype and Genotype for Predicting Overall Survival Time of Glioblastoma Patients." IEEE Transactions on Medical Imaging 39, no. 6 (2020): 2100–09.

100.   Thakur, T., I. Batra, M. Luthra, S. Vimal, G. Dhiman, A. S. Malik, and M. Shabaz. "Gene Expression-Assisted Cancer Prediction Techniques." Journal of Healthcare Engineering (2021). https://doi.org/10.1155/2021/4242646.

101.   Tian, Q., L. Yan, X. Zhang, Y. Hu, Y. Han, Z. Liu, H. Nan, Q. Sun, Y. Sun, Y. Yang, Y. Yu, J. Z. Zhang, B. Hu, G. Xiao, P. Chen, S. Tian, J. Xu, W. Wang, and G. B. Cui. "Radiomics Strategy for Glioma Grading Using Texture Features from Multiparametric MRI." Journal of Magnetic Resonance Imaging 48, no. 6 (2018): 1518–28. https://doi.org/10.1002/jmri.26010.

102. Veeramuthu, A., S. Meenakshi, G. Mathivanan, K. Kotecha, J. R. Saini, V. Vijayakumar, and G. Manogaran. "MRI Brain Tumor Image Classification Using a Combined Feature and Image-Based Classifier." Frontiers in Psychology 13 (2022). https://doi.org/10.3389/fpsyg.2022.848784.

103. Vijh, Shivani, Shubhangi Sharma, and Piyush Gaurav. "Brain Tumor Segmentation Using OTSU Embedded Adaptive Particle Swarm Optimization Method and Convolutional Neural Network." In Lecture Notes on Data Engineering and Communications Technologies, 171–94, 2020. https://doi.org/10.1007/978-3-030-25797-2_8.

104. Wankhede, D. S., and S. Rangasamy. "Review on Deep Learning Approach for Brain Tumor Glioma Analysis." Information Technology in Industry 9, no. 1 (2021): 395–408. https://doi.org/10.17762/itii.v9i1.144.

105. Wankhede, D. S., and S. Rangasamy. "Dynamic Architecture Based Deep Learning Approach for Glioblastoma Brain Tumor Survival Prediction." Neuroscience Informatics 2, no. 4 (2022): 100062. https://doi.org/10.1016/j.neuri.2022.100062.

106. Wijethilake, Nilupulee, Md Shariful Islam, and Hong Ren. "Radiogenomics Model for Overall Survival Prediction of Glioblastoma." Medical & Biological Engineering & Computing 58, no. 8 (2020): 1767–77. https://doi.org/10.1007/s11517-020-02179-9.

107. Wu, Jiewei, Yue Zhang, Weikai Huang, Li Lin, and Kai Wang. "Survival Prediction of Glioma Tumors Using Feature Selection and Linear Regression." In Intelligent Computing and Block Chain: First Bench Council International Federated Conferences, FICC 2020, Qingdao, China, October 30-November 3, 2020: Revised Selected Papers, vol. 1385, 85. Springer Nature, 2021.

108. Wu, Wenbin, Joseph L. Klockow, Miao Q. Zhang, Florence Lafortune, Emma Chang, Lei Jin, Yunqian Wu, and Heike E. Daldrup-Link. "Glioblastoma Multiforme (GBM): An Overview of Current Therapies and Mechanisms of Resistance." Pharmacological Research 171 (2021): 105780. https://doi.org/10.1016/j.phrs.2021.105780.

109. Xi, Y. B., F. Guo, and Z. L. Xu. "Radiomics Signature: A Potential Biomarker for the Prediction of MGMT Promoter Methylation in Glioblastoma." Journal of Magnetic Resonance Imaging 47 (2018): 1380–87.

110. Xia, W., B. Hu, H. Li, W. Shi, Y. Tang, Y. Yu, C. Geng, Q. Wu, L. Yang, Z. Yu, and D. Geng. "Deep Learning for Automatic Differential Diagnosis of Primary Central Nervous System Lymphoma and Glioblastoma: Multi-Parametric Magnetic Resonance Imaging Based Convolutional Neural Network Model." Journal of Magnetic Resonance Imaging (2021).

111. Yaqub, Muhammad, Jianfeng Feng, Muhammad Zia, Khizar Arshid, Kai Jia, Zia Ur Rehman, and Ameer Mehmood. "State-of-the-Art CNN Optimizer for Brain Tumor Segmentation in Magnetic Resonance Images." Brain Sciences 10, no. 7 (2020): 427. https://doi.org/10.3390/brainsci10070427.

112. Ye, Jian, Haijing Huang, Weijun Jiang, Xinxin Xu, Cheng Xie, Bin Lu, Xia Wang, and Xiaoxiang Lai. "Tumor Grade and Overall Survival Prediction of Gliomas Using Radiomics." Scientific Programming (2021).

113. Yogananda, Chinthapalli G. B., Bharat R. Shah, Mohammad Vejdani-Jahromi, Shubha S. Nalawade, Ganesh K. Murugesan, Faizan F. Yu, Marc C. Pinho, Brian C. Wagner, Kristin E. Emblem, Anders Bjørnerud, and Baowei Fei. "A Fully Automated Deep Learning Network for Brain Tumor Segmentation." Tomography 6, no. 2 (2020): 186–93.

114. Younis, Ahmad, Liao Qiang, Celestin O. Nyatega, Mubarak D. Adamu, and Haruna B. Kawuwa. "Brain Tumor Analysis Using Deep Learning and VGG-16 Ensembling Learning Approaches." Applied Sciences 12, no. 14 (2022): 7282. https://doi.org/10.3390/app12147282.

115. Zaw, Hein, Nirawat Maneerat, and Kenneth T. Win. "Brain Tumor Detection Based on Naïve Bayes Classification." In Proceedings of the 2019 5th International Conference on Engineering, Applied Sciences and Technology (ICEAST), 2019. https://doi.org/10.1109/iceast.2019.8802562.

116. Zhao, Junli, Zhaohui Meng, Li Wei, Chengyu Sun, Qiang Zou, and Rihong Su. "Supervised Brain Tumor Segmentation Based on Gradient and Context-Sensitive Features." Frontiers in Neuroscience 13 (2019). https://doi.org/10.3389/fnins.2019.00144.

117. Zhao, Yao, Yi Zhang, Ming Song, and Chao Liu. "Multi-view Semi-supervised 3D Whole Brain Segmentation with a Self-ensemble Network." In Lecture Notes in Computer Science, 256–65, 2019. https://doi.org/10.1007/978-3-030-32248-9_29.

118. Zuo, Shengtao, Xueying Zhang, and Liang Wang. "A RNA Sequencing-Based Six-Gene Signature for Survival Prediction in Patients with Glioblastoma." Scientific Reports 9, no. 1 (2019). https://doi.org/10.1038/s41598-019-39273-4.

LIST OF PUBLICATION

1. Wankhede, Disha Sushant, and Selvarani Rangasamy. "Review on Deep LearningApproach for Brain Tumor Glioma Analysis." In *Proceedings of the International Conference on Convergence of Smart Technologies (IC2ST-2021)*, January 9–10, 2021. *Journal of Information Technology in Industry*, vol. 9, no. 1, 2021, 395–408. Published online March 1, 2021. https://doi.org/10.17762/itii.v9i1.144.

2. Wankhede, Disha Sushant, and R. Selvarani. "Dynamic Architecture Based Deep Learning Approach for Glioblastoma Brain Tumor Survival Prediction." Neuroscience Informatics (2022): 100062. https://doi.org/10.1016/j.neuri.2022.100062.

3. Wankhede, Disha Sushant, Selvarani Rangasamy, and Chetan J. Shelke. "Risk Prediction of Brain Glioblastoma Multiforme Recurrence Using Deep Neural Networks." Journal of Algebraic Statistics 13, no. 3 (2022): 3894–3915. https://www.publishoa.com/index.php/journal/article/view/1198/1035.

4. Wankhede, Disha Sushant, and Chetan J. Shelke. "An Investigative Approach on the Prediction of Isocitrate Dehydrogenase (IDH1) Mutations and Co-deletion of 1p/19q in Glioma Brain Tumors." In 22nd International Conference on Intelligent Systems Design and Applications. ISDA 2022. Lecture Notes in Networks and Systems, vol. 715. Cham: Springer. https://doi.org/10.1007/978-3-031-35507-3_19.

5. Wankhede, Disha Sushant, Chetan J. Shelke, V. K. Shrivastava, R. Achary, and S. N. Mohanty. "Brain Tumor Detection and Classification Using Adjusted InceptionV3, AlexNet, VGG16, VGG19 with ResNet50-152 CNN Model." EAI Endorsed Transactions on Pervasive Health and Technology, June 2024. https://doi.org/10.4108/eetpht.10.6377

6. Wankhede, Disha Sushant. "Analysis and Prediction of Soil Nutrients pH, N, P, K for Crop Using Machine Learning Classifier: A Review." In International Conference on Mobile Computing and Sustainable Informatics. ICMCSI 2020.

EAI/Springer Innovations in Communication and Computing, edited by J. S. Raj. Cham: Springer, 2021. https://doi.org/10.1007/978-3-030-49795-8_10.

7.   Wankhede, Disha Sushant, and Chetan J. Shelke. "Improving Glioblastoma Multiforme Recurrence Prediction through Integrated Radiomics and Deep Learning Techniques." Panamerican Mathematical Journal 34, no. 1 (2024): 25–35.

8.   Wankhede, Disha Sushant, and Chetan J. Shelke. "An Experimental Study Using Deep Neural Networks to Predict the Recurrence Risk of Brain Tumor Glioblastoma Multiform." Journal of Electrical Systems 20, no. 1s (2024): 498–507. https://doi.org/10.52783/jes.793.

9.   Wankhede, Disha Sushant, and Chetan J. Shelke. "Enhanced Prediction of Glioma Brain Tumors Using Deep Learning Algorithm." AIAMMS2023 **(Accepted).**

10.   Wankhede, Disha Sushant, and Chetan J. Shelke. "An Enhanced Algorithm for Predicting IDH1 Mutations and 1p/19q Mitigation in Glioma Tumor." AIAMMS2023 **(Accepted).**

11.   Wankhede, Disha Sushant, and Chetan J. Shelke. "An Investigation on TCGA-LGG, TCIA MRI, Figure Share, Kaggle Datasets for Clinical Applications." **(Submitted).**

12. Mrs. Disha Sushant Wankhede, Dr. Chetan J. Shelke, "Brain Tumor Detection Device" Intellectual Property India, Patents, Mumbai, **Registration No. - 378301-001 02/03/2023**

13.   Mrs. Disha Sushant Wankhede, Dr. Chetan J. Shelke, "Device to Advance Brain Tumor detection and Monitoring" Intellectual Property India, Patents, Mumbai, **Registration No. - 396154-001 28/02/2024**

14.   Mrs. Disha Sushant Wankhede, Dr. Chetan J. Shelke, Glioma Brain tumor Classification and Segmentation using RS-GWO-MFCM-FRCNN. Copyright Office, Mumbai, **Registration no. SW-17671/2023**

15. Mrs. Disha Sushant Wankhede, Dr. Chetan J. Shelke, Glioma Brain Tumor Analysis: Unveiling Precise Classification and Segmentation through RS-GWOMFCM- FRCNN. Copyright Office, Mumbai, **Diary Number-21059/2023-CO/SW.**

BRAIN TUMOR GLIOMA ANALYSIS THROUGH COMPUTATIONAL INTELLIGENCE

Thesis submitted to Alliance University

for the Award of

DOCTOR OF PHILOSOPHY

by

MRS.DISHA SUSHANT WANKHEDE

Registration No.: 19030145CSE001

DEPARTMENT OF COMPUTER SCIENCE AND ENGINEERING

ALLIANCE COLLEGE OF ENGINEERING AND DESIGN

ALLIANCE UNIVERSITY

2024

RECOMMENDATION

An awful and frequent form of brain tumor is glioma. For individualized treatments, an accurate pre-operative prediction for Glioblastoma patients is needed. Therefore, therapeutic management is essential to raising the survival rate or life expectancy of glioma patients. Healthcare professionals and investigators can employ image processing tools to identify bodily processes and issues before invasive procedures. The data from an MRI scanning is adequate for clinical assessment. The typical course of treatment for Glioblastoma is surgical removal and either radiotherapy or chemotherapy. The intrinsic variability of Glioblastoma causes a significant variation in total surviving rate and a broad range of diagnoses for the individual. The standard methods that have been tested up to this point have several drawbacks including complexity, the issue of data overfitting, similar to human flaws, and others.

This research proposed the two hybrid deep learning models for the prediction of glioblastoma brain tumors and also for predicting the survival rate of patients. In this chapter, we discussed the comparative result analysis of both proposed models MFCM RSGWO-FRCNN Model and the RNN+GAN Model. According to the analysis of the final result of both models, select one of the best models for the prediction of brain tumors. This selected model results are compared with the existing state-of-art methods.

In the first model, a dynamically Deep Learning technique for Glioblastoma brain cancer survival prediction rate was put out to address the aforementioned problems. Data preprocessing is the initial phase. The MRI brain images were improved by intensity normalization using histogram normalization, de-noising via bilateral filtering, and the removal of information contaminants. Probabilistic noise, salted and pepper distortion were also taken out. Secondly, radiomic feature segmentation was completed using the MFCM clustering approach. Then, Rough Set Theory-based Grey Wolf Optimization was used to choose the most important and instructive aspects from the obtained characteristics. Later, using FR-CNN, the overall survival predictions are categorized by selecting the important feature in MRI brain images.

The proposed MFCM-RSGWO-FRCNN approach is tested against state-of-art CNN-Inception-v3, CNN AlexNet and VGG16 approaches. Evaluation parameters like Accuracy, specificity, precision, sensitivity, PSNR, MSE, and Segmentation Time were used to examine the technique. The proposed MFCM-RSGWO-FRCNN has the advantages of less converging and the corresponding characteristics.

- The algorithm was successful to accurately predict the survival rate using classifications and required only a segmentation time of around 10 sec.

- With a lowered error rate of 2.3 percent in case of MSE compared to other approaches' 4.6 percent and 5 percent, it is significantly more efficient.

- The method generates a minimized noise ratio for the complete collection of photos for any different data sizes, as well as improved classification and forecasting performance of roughly 95%.

When compared to techniques like CNN-Inception-V3 , CNN AlexNet and VGG16, MFCM-RSGWO-effectiveness FRCNN's is able to forecast the right images in the data resource. The FCM, which was suggested to segments based on grouping, was shown to be less reliable than the MFCM-RSGWO-FRCNN. There are various methods to expand the suggested technique. The approach may start by performing a thorough type, time-based examination of the occurrence, distribution, and volume of the tumor. As a result, there are several issues that need to be resolved, such as the use of various validity indexes, heterogeneity measures, and comparing with different hybrid techniques for shortening segmentation duration.

In the second method hybrid deep learning model is designed to detect the glioblastoma tumor based on the recurrence risk. For the preprocessing, Z-score normalization, and spatial resampling are performed in step 1, followed by recurrent GAN techniques for tumor segmentation in step 2, radiomices texture-based feature extraction (FE) is done based on wavelet band-pass filtering in step 3, and RF classifier was used to predicted recurrent glioblastoma in step 4. This research sought to evaluate the efficacy of the preoperative and postoperative recurrent risks amongst glioma patients receiving a combination of bevacizumab and nivolumab therapy. Tumor regions of interest were segmented from T1 images that had undergone contrast enhancement. The radiomic feature-based MRI signals were derived from multi-parametric MRI data of sick people with glioblastoma to ascertain their connections with responses to OS and PFS. Utilizing a variety of textural features, the recurrence risk for GBM patients is predicted using the RF approach. The characteristics from MRIs were extracted using CE-T1W-MRI imaging information. Every stage is thoroughly explained in the next subtopics.

- Recurrence prognosis, survival rate, PFS, ORR, accuracy score, specificity, and sensitivity are the performances of the suggested research. The suggested approach is contrasted with the CNN-Inception-V3, CNN AlexNet and VGG16 forecasting techniques already in use.

- The specificity of the study is around 4% higher than the previous approaches, and the sensitivities of the suggested approach is almost 5% better. The efficiency of the suggested approach is 3% greater than the previous methodologies.

The probability of glioma recurring can therefore be effectively predicted using the suggested approach, and further research is needed to measure the specific immunological ecosystem of the brain during cancer settings.

After analysing both models, the second RNN+GAN Model gives a better result as compared to the first MFCM RSGWO-FRCNN Model. The RNN+GAN Model achieves a 95.11% accuracy score; Sensitivity is also 95.11% and Specificity is 98%. The RNN+GAN Model increases the survival rate which is 2.47% after diagnosis and overall treatment of patients.

6.2 Future Scope

1. The proposed segmentation algorithm focuses on two dimensional anatomical structures. It can also be extended to three dimensional volumetric structures.

2. As the intensity and orientation-based segmentation method is capable of extracting the features of the medical images accurately, it can also be applied to the fusion image.

3. As the online service is used for the detection of a brain cancer type, the research can be extended to other brain cancer types and locations also.

4. There is currently no publicly accessible dataset of large MRI sequences provided globally. To develop a huge capacity, open a test dataset, and testing the suggested techniques using the aid of the novel dataset to confirm their efficacy and continuously enhance it, efforts might be taken in the coming days to reach in touch with several other labs conducting relevant studies.